(3)

AD-A257 702

WL-TR-92-7044

Numerical Solution and Algorithm Analysis for the Unsteady Navier-Stokes Equations on Dynamic Multiblock Grids Including Chemical Equilibrium

Volume II

J. M. Janus
C. F. Cox
A. Arabshahi
P. Cinella
D. L. Whitfield

Mississippi State University
P.O. Box 6176
Mississippi State MS 39762

DTIC
S ELECTE D
NOV 13 1992
B

OCTOBER 1992

FINAL REPORT FOR PERIOD JUNE 1989 - JUNE 1992

422660
92-29410
15800

WRIGHT LABORATORY, ARMAMENT DIRECTORATE
Air Force Materiel Command ▮ United States Air Force ▮ Eglin Air Force Base

NOTICE

This technical report has been reviewed and is approved for publication.

FOR THE COMMANDER

Robert F Donohue Jr

ROBERT F. DONOHUE, Jr.
Chief, Weapon Flight Mechanics Division

Even though this report may contain special release rights held by the controlling office, please do not request copies from the Wright Laboratory, Armament Directorate. If you qualify as a recipient, release approval will be obtained from the originating activity by DTIC. Address your request for additional copies to:

Defense Technical Information Center
Cameron Station
Alexandria VA 22304-6145

If your address has changed, if you wish to be removed from our mailing list, or if your organization no longer employs the addressee, please notify WL/MNAA, Eglin AFB FL 32542-5000, to help us maintain a current mailing list.

Do not return copies of this report unless contractual obligations or notice on a specific document requires that it be returned.

REPORT DOCUMENTATION PAGE

Form Approved
OMB No. 0704-0188

1. AGENCY USE ONLY *(Leave blank)*

2. REPORT DATE
October 1992

3. REPORT TYPE AND DATES COVERED
Final June 1989 - June 1992

4. TITLE AND SUBTITLE
Numerical Solution and Algorithm Analysis for the Unsteady Navier-Stokes Equations on Dynamic Multiblock Grids Including Chemical Equilibrium

5. FUNDING NUMBERS
C: F08635-89-C-0208
PE: 61102F
PR: 2307
TA: AW
WU: 15

6. AUTHOR(S)
J. M. Janus, C. F. Cox, A. Arabshahi, P. Cinella, and D. L. Whitfield

7. PERFORMING ORGANIZATION NAME(S) AND ADDRESS(ES)
Mississippi State University
P.O. Box 6176
Mississippi State MS 39762

8. PERFORMING ORGANIZATION REPORT NUMBER

9. SPONSORING/MONITORING AGENCY NAME(S) AND ADDRESS(ES)
Wright Laboratory, Armament Directorate
Weapon Flight Mechanics Division
Aerodynamics Branch (WL/MNAA)
Eglin AFB FL 32542-5000

10. SPONSORING/MONITORING AGENCY REPORT NUMBER
WL-TR-92-7044
Volume II

11. SUPPLEMENTARY NOTES
Due to the enormous backlog of work accumulated because of the DMR manpower reduction, and in the interest of getting this technology out to the users, **the text was not edited by TESCO, Inc.**

12a. DISTRIBUTION/AVAILABILITY STATEMENT
Approved for public release; distribution is unlimited.

12b. DISTRIBUTION CODE
A

13. ABSTRACT *(Maximum 200 words)*

This is a two volume final report for the research entitled Computation of Hypersonic Interference Flowfields. Volume I involves the numerical solution of the three-dimensional unsteady Euler and Navier-Stokes equations for a calorically perfect gas. This volume involves the development of techniques for the solution of three-dimensional inviscid and viscous hypersonic flows in chemical equilibrium. This research addresses the numerical formulation and solution of the equations as well as an analysis of the optimization of the numerical solution algorithm used to solve the equations. Selected results of numerous hypersonic flow computations--including computations of heat transfer to bodies with different nose shapes--are presented.

14. SUBJECT TERMS
Store Separation
Computational Fluid Dynamics
Navier-Stokes Equations
Euler Equations
Hypersonic Flow
Chemical Equilibrium

15. NUMBER OF PAGES

16. PRICE CODE

17. SECURITY CLASSIFICATION OF REPORT
Unclassified

18. SECURITY CLASSIFICATION OF THIS PAGE
Unclassified

19. SECURITY CLASSIFICATION OF ABSTRACT
Unclassified

20. LIMITATION OF ABSTRACT
UL

NSN 7540-01-280-5500

Standard Form 298 (Rev 2-89)
Prescribed by ANSI Std Z39-18
298-102

PREFACE

This program was conducted by Mississippi State University, P.O. Box 6176, Mississippi State MS 39762, under Contract No. F08635-89-C-0208 with the Wright Laboratory, Armament Directorate, Eglin Air Force Base FL 32542-5000. Dr. Dave M. Belk, WL/MNAA, managed the program for the Wright Laboratory. The principal investigators were Drs. J. Mark Janus and David L. Whitfield of Mississippi State University. The program was conducted from 12 June 1989 through 11 June 1992.

TABLE OF CONTENTS

TABLE OF CONTENTS (Concluded)

Appendix

LIST OF FIGURES

LIST OF FIGURES (Continued)

LIST OF FIGURES (Concluded)

LIST OF TABLES

LIST OF SYMBOLS

English Letters

α	speed of sound
X	species concentration
w	rate of production
t	time
$\vec{u}$	velocity vector
$\vec{n}$	unit normal vector
k_f, k_b	forward and backward reaction rates
K_c	equilibrium constant in concentration form
K_p	equilibrium constant in partial pressure form
$\mathcal{M}$	molecular mass
$\tilde{R}$	mixture gas constant
R	gas constant
Y	mass fraction
e	internal energy
e_o	total energy
c_v	specific heat at constant volume
$\tilde{c}_v$	frozen specific heat at constant volume
c_p	specific heat at constant pressure
$\tilde{c}_p$	frozen specific heat at constant pressure
h_f	heat of formulation
T	temperature
p	pressure
h	enthalpy
h_o	total enthalpy
s	entropy

LIST OF SYMBOLS (Continued)

g	Gibb's free energy
$\mathcal{N}$	mole number
N	number of species
NE	number of elemental species
NR	number of reactions
s_f	reference entropy
s^0	reference entropy at T = 0 K
h^0	reference enthalpy at T = 0 K
$\mathcal{K}$	thermal conductivity
Q	conservative variable vector
q	heat flux, primitive variable vector
F, F, H, S	inviscid flux vectors
F_v, G_v, H_v, S_v	viscous flux vectors
J	Jacobian of the coordinate transformation
k	generic curvilinear coordinate
I	identity matrix
$\overline{S}$, $\overline{S}_v$	generic inviscid and viscous flux Jacobian matrices
r	right eigenvector
l	left eigenvector
$\mathcal{R}$	standard Roe average
i, j, k	computational indices
u, v, w	Cartesian velocities
x, y, z	Cartesian coordinates
M	Mach number, dependent variable transformation matrix
P_k	right eigenvector matrix for primitive variables
T_k	right eigenvector matrix for conservative variables
K	split flux vector
$\overline{A}$	split flux Jacobian matrix

LIST OF SYMBOLS (Continued)

Pr	Prandtl number

Greek Letters

Δ	increment
δ	central difference operator
$\tilde{\mathfrak{B}}_k$	relative contravariant velocity
$\tilde{\theta}_k$	absolute contravariant velocity
ϱ	density
Θ_v	characteristic vibrational temperature
μ	viscosity
ν', ν''	stoichiometric coefficients
$\overline{\Omega}$	collision cross-section
ξ	degree of advancement
ξ, η, ς	curvilinear coordinates
λ	eigenvalues
$\varkappa$	flux Jacobian matrix with respect to primitive variables
Γ	isentropic index
γ	ration of specific heats
$\tilde{\gamma}$	ratio of frozen specific heats
$\bar{\gamma}$	ratio of enthalpy and internal energy derivatives with respect to temperature at constant density
τ	time; shear stress
τ_{FD}, τ_{CR}	characteristic fluid dynamic and chemical reaction time

Symbols

∇	gradient
$< >$	arithmetic average
$[\![\ ]\!]$	jump

LIST OF SYMBOLS (Concluded)

Subscripts

l	laminar, left
r	reference, right
t	turbulent
∞	freestream quantity
0	initial quantity

Superscripts

n	time step
—	integral average
$\wedge$	averaged quantity
+	corresponding to positive eigenvalues
-	corresponding to negative eigenvalues

SECTION I

INTRODUCTION

Recent interest in developing high-speed commercial transports, as well as more advanced reentry vehicles, has lead to a resurgence of research into hypersonic aerodynamics. Simulating this flow regime requires the modeling of the chemical activity that characterizes it. Several researchers have developed successful finite-rate chemistry codes (see Candler and MacCormack [Reference 1], and Walters et al. [Reference 2]). However, finite-rate chemistry is both complicated and expensive. In addition to the requirement that the reaction paths be known (a highly non-trivial task in itself), finite-rate chemistry requires the substitution of a usually large number of species continuity equations in place of the global mass conservation equation. Also, for near equilibrium flows, the finite-rate equations become extremely stiff. Considering the difficulties associated with finite-rate chemistry, flow simulations using the local chemical equilibrium assumption become very attractive.

In recent years, the numerical solution of chemical equilibrium problems has been investigated by several researchers. Liu and Vinokur [Reference 3] give an excellent review of algorithms for the determination of properties for an equilibrium gas mixture. Meintjes and Morgan [Reference 4] present an interesting formulation based on defining all the necessary reactions in terms of element variables.

Many researchers have developed flow solvers based upon curve fits for the equilibrium properties [Reference 5–9]. However, it needs to be stressed that formulations based upon curve fits, while competitive in terms of CPU time, are limited to a specific mixture composition for each tabulation [Reference 10]. The study of arbitrary mixtures requires the creation of new tabulations for each mixture of interest.

Other researchers have explored the capabilities of a flow solver based on the local chemical equilibrium behavior of a given gas mixture. Finite-rate and chemical equilibrium computations for blunt-body flow, using a 5-species air model, were compared by Désidéri, Glinsky and Hettena [Reference 11]. Davy, Lombard and Green [Reference 12] present viscous computations which simulate an entry into the atmosphere of Jupiter, and Wang and Chen [Reference 13] present rocket engine nozzle computations using hydrogen/air mixtures. However, the flow solvers used in the above studies are incapable of handling arbitrary gas mixtures, and the codes would have to be rewritten for a different gas mixture of interest.

The approach taken in this study involves the coupling of a "Black Box" chemical equilibrium solver with a three-dimensional, Thin Layer Navier-Stokes flow solver that has been modified to include real gas effects. The Black Box computes the equilibrium composition and temperature of gas mixtures at constant density and internal energy, and provides the flow solver with the necessary thermodynamic and transport properties. The modifications to the flow solver are minor, although they include the implementation of a newly derived approximate Riemann solver of the Roe type. A key advantage of this "real gas" flow solver is the capability to handle arbitrary mixtures of thermally perfect gases in local chemical equilibrium.

The subject matter of the present study is divided into two parts. Part one concerns the development and testing of the Black Box and is covered by Sections II through V. The modification of a perfect gas flow solver to include real gas effects and its subsequent application comprise the second part of this report, which is covered in Sections VI through VIII.

The mathematical foundations and governing equations for the determination of the equilibrium composition and thermodynamic properties of a homogeneous mixture of thermally perfect gases are developed in Section II. Two different solution procedures are proposed, and a third discussed briefly. In Section III, practical models for the description of the thermochemical properties are discussed. Included are various options for the thermodynamic model, equilibrium constant, chemistry model, and transport properties. In Section IV, numerical procedures for the solution of the governing equations developed in Section II are given. Results from the numerical testing of the Black Box chemical equilibrium solver are presented in Section V. Several chemistry models and various compositions are utilized, and efficiency and robustness studies are performed.

The governing equations for three-dimensional, viscous, heat-conducting flows written for a time-dependent, generalized coordinate system are presented in Section VI. In Section VII, the numerical methods for the solution of the gasdynamic equations are presented. Real gas formulations are developed for the Steger–Warming flux-vector splitting scheme and split flux Jacobians, as well as a newly derived approximate Riemann solver of the Roe-type. These algorithms are cast in a manner compatible with their perfect gas counterparts. Applications of the chemical equilibrium flow solver are given in Section VIII, along with comparisons with perfect gas solutions.

SECTION II

MATHEMATICAL FORMULATION: BLACK BOX

1. CHEMICAL EQUILIBRIUM

In order to classify the chemical activity that characterizes high-speed, high-temperature flows, an order of magnitude analysis is usually made of the reaction time versus the fluid dynamic time. Specifically, considering a single control volume in the flow domain, the fluid dynamic time τ_{FD} can be defined to be the time it takes for a fluid particle to traverse this space. The reaction time τ_{CR} may be taken as the time required to partially complete a chemical reaction. There are three cases that occur,

$$\tau_{FD} \begin{cases} << \tau_{CR} , \\ \approx \tau_{CR} , \\ >> \tau_{CR} . \end{cases} \tag{1}$$

The first case corresponds to frozen flow, in which the reaction has no time to occur. The second case is the most general in which the reaction may or may not have time to complete, and is classified as finite-rate chemistry. For the last case, the reaction has infinite time to occur and thus will reach its equilibrium composition. Physically, frozen and equilibrium chemistry represent the limiting cases for the real-life situation: finite-rate chemistry. Furthermore, if the last case is applicable at each volume in the flowfield and for all reactions occurring within the flow, then the flowfield can be assumed to be in local chemical equilibrium.

In the following development, a gas mixture composed of N chemical species, in which there are NE elemental species, will be considered. A general formulation of the chemical equations for NR reactions involving the N species X_i can be written

$$\begin{aligned} \nu'_{1,r} X_1 + \nu'_{2,r} X_2 + \dots + \nu'_{N,r} X_N &\leftrightarrows \\ \nu''_{1,r} X_1 + \nu''_{2,r} X_2 + \dots + \nu''_{N,r} X_N, &\quad r = 1,\dots,NR, \end{aligned} \tag{2}$$

where $\nu'_{i,r}$, $\nu''_{i,r}$ are the stoichiometric coefficients of species i in reaction r for the reactants and products respectively.

Considering a reactive flow involving the above mentioned gas mixture, the governing fluid dynamic equations can be derived following Vincenti and Kruger [Reference 14]. In particular, the species continuity equations written in integral form for a control volume V bounded by a control surface S are

$$\frac{\partial}{\partial t}\int\int\int_V \varrho_i dV + \oint_S \varrho_i(\vec{u}_i - \vec{u}_s)\cdot\vec{n}dS = \int\int\int_V w_i dV\ , \qquad i = 1,\ldots,N, \tag{3}$$

where ϱ_i is the species density, $\vec{u}_i$ is the species velocity, $\vec{u}_s$ is the surface velocity and $\vec{n}$ is the unit vector normal to the control surface. The terms in the above equation represent, from left to right, unsteady contributions integrated over the volume, inviscid and viscous fluxes integrated over the surface, and a source term due to chemical reactions integrated over the volume.

The source term w_i in Equation (3) represents the rate of production of species i and can be written as

$$\begin{aligned} w_i = {} & \mathcal{M}_i \sum_{r=1}^{NR}(\nu''_{i,r} - \nu'_{i,r})\cdot \\ & \left[k_{f,r}\prod_{l=1}^{N}\left(\frac{\varrho_l}{\mathcal{M}_l}\right)^{\nu'_{l,r}} - k_{b,r}\prod_{l=1}^{N}\left(\frac{\varrho_l}{\mathcal{M}_l}\right)^{\nu''_{l,r}}\right], \qquad i = 1,\ldots,N, \end{aligned} \tag{4}$$

where $\mathcal{M}_i$ is the molecular mass of species i and $k_{f,r}$, $k_{b,r}$ are the forward and backward reaction rates for reaction r, respectively. These reaction rates are related by

$$k_{f,r} = k_{b,r}K_{c,r}\ , \tag{5}$$

where the equilibrium constant $K_{c,r}$ is introduced, which is a known function of the thermodynamic state. Substituting the preceding relation into Equation (4), the rate of production can be rewritten in the following form

$$\begin{aligned} w_i = {} & \mathcal{M}_i \sum_{r=1}^{NR}(\nu''_{i,r} - \nu'_{i,r})k_{b,r}\cdot \\ & \left[K_{c,r}\prod_{l=1}^{N}\left(\frac{\varrho_l}{\mathcal{M}_l}\right)^{\nu'_{l,r}} - \prod_{l=1}^{N}\left(\frac{\varrho_l}{\mathcal{M}_l}\right)^{\nu''_{l,r}}\right], \qquad i = 1,\ldots,N, \end{aligned} \tag{6}$$

where at chemical equilibrium the term in brackets is identically zero because it reduces to the Law of Mass Action

$$K_{c,r} = \frac{\prod_{l=1}^{N}\left(\frac{\varrho_l}{\mathcal{M}_l}\right)^{\nu'_{l,r}}}{\prod_{l=1}^{N}\left(\frac{\varrho_l}{\mathcal{M}_l}\right)^{\nu''_{l,r}}}\ , \qquad r = 1,\ldots,NR, \tag{7}$$

which is valid for equilibrium chemistry.

The limiting cases of equilibrium and frozen chemistry should be readily apparent in Equation (6). Frozen chemistry corresponds to the backward reaction rate going to zero, which results in the rate of production terms going to zero and dropping from the species continuity equation. In this case it can be shown that there will be no change in the species mass fractions if diffusion is neglected. On the other hand, equilibrium chemistry corresponds to the backward reaction rates approaching infinity. In this case the bracketed terms in Equation (6) go to zero and the rate of production terms will reach a finite limit value which will balance out the unsteady, inviscid and viscous contributions to the species continuity equations, Equation (3).

2. EQUATIONS OF STATE

A very important assumption in the following development is that the effect of intermolecular forces in the gas mixture is negligible. As a result, the individual gases comprising the mixture will behave as thermally perfect gases. Moreover, the assumption of local chemical equilibrium implies that the thermodynamic state at any given time and any point in space need be defined as a function of only two state variables. For reasons that will become apparent later, the density ϱ and temperature T were chosen as the two fundamental state variables.

For a mixture composed of N species, the total density ϱ and the mass fractions Y_i are given by the relations

$$\varrho = \sum_{i=1}^{N} \varrho_i \,, \qquad Y_i = \frac{\varrho_i}{\varrho} \,. \tag{8}$$

Using the standard mixing rule, the mixture gas constant $\tilde{R}$ is defined from the known species properties

$$\tilde{R} = \sum_{i=1}^{N} Y_i R_i \,, \tag{9}$$

where R_i is the gas constant for species i. Similarly, the total internal energy of a mixture can be given as the sum of the species contributions, which results in the caloric equation of state

$$e = \sum_{i=1}^{N} Y_i e_i = \sum_{i=1}^{N} Y_i \left[\int_{T_{ref}}^{T} c_{v_i}(\tau)\, d\tau + h_{f_i} \right] \,, \tag{10}$$

where c_{v_i} is the species specific heat at constant volume and h_{f_i} is the species heat of formation at reference temperature T_{ref}.

Since the mixture is composed of thermally perfect gases, the thermal equation of state will be given by Dalton's Law

$$p = \sum_{i=1}^{N} \varrho_i R_i T = \varrho \tilde{R} T \ , \tag{11}$$

where the total mixture pressure is the sum of the partial pressures. The thermal equation of state is indirectly related to the caloric equation of state Equation (10) via temperature. Thus for a given chemical composition the temperature must be obtained from either the caloric or the thermal equation of state depending on whether internal energy or pressure is known.

The mixture specific heats can be derived as functions of density and temperature derivatives of the mass fractions. The specific heat at constant volume is defined to be

$$c_v \equiv \left(\frac{\partial e}{\partial T}\right)_v = \sum_{i=1}^{N} Y_i \left(\frac{\partial e_i}{\partial T}\right)_\varrho + \sum_{i=1}^{N} e_i \left(\frac{\partial Y_i}{\partial T}\right)_\varrho \ . \tag{12}$$

Recognizing that the first partial is nothing more than the species specific heat at constant volume, the relation will reduce to

$$c_v = \tilde{c}_v + \sum_{i=1}^{N} e_i \left(\frac{\partial Y_i}{\partial T}\right)_\varrho \ , \tag{13}$$

where the frozen specific heat at constant volume

$$\tilde{c}_v = \sum_{i=1}^{N} Y_i c_{v_i} \ , \tag{14}$$

has been introduced. The mixture specific heat at constant pressure can be defined as

$$c_p \equiv \left(\frac{\partial h}{\partial T}\right)_p = \left(\frac{\partial h}{\partial T}\right)_\varrho + \left(\frac{\partial h}{\partial \varrho}\right)_T \left(\frac{\partial \varrho}{\partial T}\right)_p \ , \tag{15}$$

where the mixture enthalpy $h = e + \tilde{R}T$ has been introduced, which can be given as the sum of the species contributions

$$h = \sum_{i=1}^{N} Y_i h_i \ , \tag{16}$$

using the standard mixture rule. The enthalpy derivatives are then obtained as

$$\left(\frac{\partial h}{\partial \varrho}\right)_T = \sum_{i=1}^{N} h_i \left(\frac{\partial Y_i}{\partial \varrho}\right)_T \ , \tag{17}$$

and

$$\left(\frac{\partial h}{\partial T}\right)_\varrho = \tilde{c}_p + \sum_{i=1}^{N} h_i \left(\frac{\partial Y_i}{\partial T}\right)_\varrho \ , \tag{18}$$

where the frozen specific heat at constant pressure has been introduced

$$\tilde{c}_p = \sum_{i=1}^{N} Y_i c_{p_i} \ . \tag{19}$$

The partial derivative of density with respect to temperature at constant pressure can be obtained from the differential form of the thermal equation of state, Equation (11), as

$$\left(\frac{\partial \varrho}{\partial T}\right)_p = -\frac{\varrho}{T} \frac{\tilde{R} + T \sum_{i=1}^{N} R_i \left(\frac{\partial Y_i}{\partial T}\right)_\varrho}{\tilde{R} + \varrho \sum_{i=1}^{N} R_i \left(\frac{\partial Y_i}{\partial \varrho}\right)_T} \ , \tag{20}$$

Finally, substitution of Equations (17-20) into Equation (15) gives the mixture specific heat at constant pressure

$$c_p = c_v + \frac{\tilde{R} + T \sum_{i=1}^{N} R_i \left(\frac{\partial Y_i}{\partial T}\right)_\varrho}{\tilde{R} + \varrho \sum_{i=1}^{N} R_i \left(\frac{\partial Y_i}{\partial \varrho}\right)_T} \left[\tilde{R} - \frac{\varrho}{T} \sum_{i=1}^{N} e_i \left(\frac{\partial Y_i}{\partial \varrho}\right)_T\right] \ . \tag{21}$$

3. SPEED OF SOUND

A key thermodynamic property for high-speed flows is the speed of sound, which is defined as

$$a^2 = \left(\frac{\partial p}{\partial \varrho}\right)_s \ . \tag{22}$$

For a thermodynamic system in chemical equilibrium, the combined First and Second Laws of Thermodynamics can be written as

$$T ds = de - \frac{p}{\varrho^2} d\varrho \ . \tag{23}$$

Using the above relation, the equation for the speed of sound Equation (22) can be rewritten in the following form

$$a^2 = \left(\frac{\partial p}{\partial \varrho}\right)_e + \frac{p}{\varrho^2}\left(\frac{\partial p}{\partial e}\right)_\varrho \ . \tag{24}$$

Using the differential forms of the caloric and thermal equations of state, Equations (10) and (11) respectively, and Equation (23), the pressure partial derivatives are found to be

$$\left(\frac{\partial p}{\partial \rho}\right)_e = T\left[\tilde{R} + \rho\sum_{i=1}^{N} R_i\left(\frac{\partial Y_i}{\partial \rho}\right)_T\right] - \frac{\rho}{c_v}\left[\tilde{R} + T\sum_{i=1}^{N} R_i\left(\frac{\partial Y_i}{\partial T}\right)_\rho\right]\sum_{i=1}^{N} e_i\left(\frac{\partial Y_i}{\partial \rho}\right)_T , \tag{25}$$

and

$$\left(\frac{\partial p}{\partial e}\right)_\rho = \frac{\rho}{c_v}\left[\tilde{R} + T\sum_{i=1}^{N} R_i\left(\frac{\partial Y_i}{\partial T}\right)_\rho\right] . \tag{26}$$

Substituting Equations (25) and (26) into Equation (24), the equation for the speed of sound can be put into a more familiar form

$$a^2 = \Gamma\,\frac{p}{\rho} , \tag{27}$$

where the isentropic index Γ is defined to be

$$\Gamma = \bar{\gamma} + \frac{\rho}{\tilde{R}T}\sum_{i=1}^{N}\left(\frac{\partial Y_i}{\partial \rho}\right)_T\left[R_i T - (\bar{\gamma} - 1)e_i\right] . \tag{28}$$

In the above equation, the ratio of the partial derivative of enthalpy with respect to temperature at constant density to the partial derivative of energy with respect to temperature at constant density has been introduced

$$\bar{\gamma} = \left(\frac{\partial h/\partial T}{\partial e/\partial T}\right)_\rho = 1 + \frac{\tilde{R} + T\sum_{i=1}^{N} R_i\left(\frac{\partial Y_i}{\partial T}\right)_\rho}{c_v} . \tag{29}$$

Although the above equation for the speed of sound is seemingly simple, it should be readily apparent that the isentropic index is a complex function of density and temperature.

In general, there are at least four different "gammas" that can be defined for an equilibrium gas: the two mentioned already, the ratio of specific heats $\gamma = c_p/c_v$, and the ratio of frozen specific heats $\tilde{\gamma} = \tilde{c}_p/\tilde{c}_v$. Although generally their values are different, all four of these "gammas" will reduce to the same value for frozen flows, of which perfect gas is a subset. More details on the derivation of the equilibrium sound speed are given in Appendix A.

4. SOLUTION TECHNIQUES

As stated previously, chemical equilibrium is achieved when the reaction rates go to infinity. Thus the species rate of production terms reach a limiting value and do so while keeping two state properties constant. Examination of the species continuity equations, Equation (3), shows that changes in these production terms occur at constant specific volume and thus constant density. From the combined First and Second Laws of Thermodynamics, Equation (23), it can be seen that for a reversible process occurring at constant density, the internal energy will also remain constant. Therefore, evaluation of the equilibrium system will occur at constant density and internal energy.

Two different formulations for the solution of the chemical equilibrium state at constant density and internal energy have been developed and will be discussed in detail in the following subsections. The first is the Mass Constraint Technique, which uses a modified form of the laws of mass action, plus elemental mass constraints and an energy equation. The resulting system of equations can be reduced through the use of the concept of degree of advancement for a chemical reaction. This reduction is the foundation of the second formulation, which will be named the Degree of Advancement Technique. Additionally, a third formulation, based on the work of Meintjes and Morgan [Reference 4], was attempted. However, preliminary tests indicated that this formulation was not suitable for calculations where temperature is not constant.

In addition to the previous formulations, the first method has been modified in order to solve chemical equilibrium problems at constant pressure and temperature, and constant pressure and density. The importance of these modifications will become apparent later, when the boundary conditions for the flow solver will be described.

a. MASS CONSTRAINT TECHNIQUE

The chemical equilibrium state can be determined through the solution of an algebraic set of $N + 1$ equations, comprising N–NE laws of mass action, NE elemental species mass constraints and an energy equation, for $N + 1$ unknowns, N species densities and temperature. In this development, the governing equations are written in a form compatible with finite–rate chemistry.

As stated previously, the limiting case of chemical equilibrium corresponds to backward reaction rates going to infinity, and the bracketed terms in Equation (6) going to zero since they reduce to the laws of mass action. In order to avoid the difficulties associated with the determination of the limit values, the backward reaction rates are assumed to have a finite value, unity, and the rates of productions are set equal to zero. This gives a modified form of the laws of mass action that remains compatible to the finite–rate form expressed in Equation (6) while still satisfying the chemical equilibrium state. These modified laws of mass action are written as

$$w_i\ (\varrho_j, T) = \mathcal{M}_i \sum_{r=1}^{NR} (\nu''_{i,r} - \nu'_{i,r}) \left[K_{c,r} \prod_{j=1}^{N} \left(\frac{\varrho_j}{\mathcal{M}_j} \right)^{\nu'_{j,r}} - \prod_{j=1}^{N} \left(\frac{\varrho_j}{\mathcal{M}_j} \right)^{\nu''_{j,r}} \right] = 0\ , \qquad (30)$$

$$i = 1, \ldots, N - NE,$$

where the index i now covers only the nonelemental species instead of the entire range.

The elemental mass conservation equations represent the fact that, in the absence of nuclear reactions, mass is neither created nor destroyed, and are written as

$$w_{N-NE+i}(\varrho_j) = \sum_{j=1}^{N} \frac{a_{i,j}}{\mathcal{M}_j} \frac{\varrho_j}{\varrho} - \left[\sum_{j=1}^{N} \frac{a_{i,j}}{\mathcal{M}_j} \frac{\varrho_j}{\varrho} \right]_{t=0} = 0, \qquad i = 1, \ldots, NE, \qquad (31)$$

where $a_{i,j}$ is the number of particles of element i present in species j. The second term on the left hand side represents the initial values at the beginning of the computation. The NE elemental species need not be true elements themselves, but they must contain the element that they represent. An example would be the use of carbon monoxide CO as the elemental species for either the element carbon C or the element oxygen O.

In order to complete the system, an equation relating the unknown temperature to the known state properties is needed. This is accomplished with the caloric equation of state, Equation (10), written in terms of the total energy per unit volume

$$d(\varrho_j, T) = \varrho e_0 - \sum_{j=1}^{N} \varrho_j \left[\int_{T_{ref}}^{T} c_{v_j}(\tau) d\tau + h_{f_j} \right] - \varrho \frac{u_0^2}{2} = 0\ , \qquad (32)$$

where density ϱ, total energy per unit volume ϱe_0, and velocity u_0 are known quantities that are readily available from any flow solver written in conservation form. The species specific heats at constant volume c_{v_j} are functions of temperature and are provided by the thermodynamic models, which will be discussed in Section III.

b. DEGREE OF ADVANCEMENT TECHNIQUE

The use of the concept of degree of advancement for a chemical reaction provides an alternative formulation to the Mass Constraint Technique. This alternative formulation, titled the Degree of Advancement Technique, can provide a significant advantage over the previous formulation. The advantage comes from reducing the system of N+1 equations to as little as N-NE+1 equations by substituting degrees of advancements for the species densities.

For a single reaction of the form given by Equation (2), the ratio of the infinitesimal changes in the number of moles for each species is proportional to the ratio of the differences between the product and reactant stoichiometric coefficients of those species. This relationship is written as

$$d\mathcal{N}_1 : d\mathcal{N}_2 : \ldots : d\mathcal{N}_N = (v_1'' - v_1') : (v_2'' - v_2') : \ldots : (v_N'' - v_N') \ , \tag{33}$$

where $\mathcal{N}_j$ is the mole number for the species j. An example of this relationship can be given for the simple combustion reaction

$$2H_2 + O_2 \leftrightarrows 2H_2O \ , \tag{34}$$

where Equation (33) will read

$$d\mathcal{N}_{H_2} : d\mathcal{N}_{O_2} : d\mathcal{N}_{H_2O} = (-\ 2) : (-\ 1) : (+\ 2) \ . \tag{35}$$

Introducing an infinitesimal constant of proportionality and recognizing that $d\mathcal{N}_j = dY_j/\mathcal{M}_j$, where $Y_j = \varrho_j/\varrho$ is the species mass fraction, these ratios can be rewritten as

$$\frac{dY_1}{\mathcal{M}_1(v_1'' - v_1')} = \frac{dY_2}{\mathcal{M}_2(v_2'' - v_2')} = \ldots = \frac{dY_N}{\mathcal{M}_N(v_N'' - v_N')} = d\xi \ , \tag{36}$$

where ξ is the degree of advancement for the reaction. Extending this approach to multiple, coupled reactions, the degree of advancement ξ_r for reaction r can be defined by the differential relation

$$\frac{\partial Y_j}{\partial \xi_r} = \mathcal{M}_j(v_{j,r}'' - v_{j,r}') \ , \qquad j = 1,\ldots,N, \qquad r = 1,\ldots,NR \ . \tag{37}$$

Noting that density is kept constant, the system of NR equations for a species j can be solved to give the species density as a function of the NR degrees of advancement

$$\varrho_j = (\varrho_j)_{t=0} + \mathcal{M}_j\ \varrho \sum_{r=1}^{NR} (v_{j,r}'' - v_{j,r}')\xi_r \ , \qquad j = 1,\ldots,N, \tag{38}$$

where the initial condition $(\xi_r)_{t=0} = 0$ has been applied.

Using the above transformation relation, Equation (38), the laws of mass action as well as the energy equation can be rewritten in terms of the degrees of advancement. Furthermore, substituting Equation (38) into the mass constraint equations Equation (31), as follows

$$\sum_{j=1}^{N} \frac{a_{i,j}}{\mathcal{M}_j}\left[(Y_j)_{t=0} + \mathcal{M}_j \sum_{r=1}^{NR}(v_{j,r}'' - v_{j,r}')\xi_r\right] = \left[\sum_{j=1}^{N}\frac{a_{i,j}\ \varrho_j}{\mathcal{M}_j\ \varrho}\right]_{t=0} , \tag{39}$$

$$i = 1,\ldots,NE,$$

results, after some manipulation, into the expression

$$\sum_{r=1}^{NR}\left[\sum_{j=1}^{N} a_{i,j}(\nu''_{j,r} - \nu'_{j,r})\right]\xi_r = 0, \qquad i = 1,\ldots,NE\,. \tag{40}$$

It is easily verified that the bracketed terms go to zero identically since reaction r must be stoichiometrically balanced with respect to element i. To illustrate this, consider again the example of the simple combustion reaction consisting of the three species H_2, O_2 and H_2O. The elemental species are selected as H_2 and O_2 and represent the two elements, atomic hydrogen H and oxygen O, respectively. Expanding the bracketed terms for each element gives

$$2(0 - 2) + 0(0 - 1) + 2(2 - 0) \equiv 0, \qquad \text{Element} = \text{H}, \tag{41}$$

$$0(0 - 2) + 2(0 - 1) + 1(2 - 0) \equiv 0, \qquad \text{Element} = \text{O}\,. \tag{42}$$

Thus the mass constraints are implicitly satisfied and are eliminated from the governing equations because the degrees of advancement will stoichiometrically balance the individual reactions. The resulting system of equations consists of NR laws of mass action and an energy equation, with the unknowns being the degrees of advancement and temperature. The maximum advantage over the Mass Constraint Technique is obtained when the number of reactions is equal to the minimum number of necessary reactions, $NR = N - NE$.

c. SYSTEMS AS FUNCTIONS OF ALTERNATE STATE PROPERTIES

In the previous sections the caloric equation of state was employed to find the chemical composition of the gas mixture. This choice works well for control volumes in the flow field, since the two known state variables are density and internal energy. However, either or both of these state variables may not be available at the boundaries if certain boundary conditions are to be enforced. For example, the known state variables for specified pressure and temperature gradient boundary conditions are pressure and temperature. Another example is subsonic characteristic variable boundary conditions whereby pressure and density are known. Consequently, the determination of the equilibrium composition at boundary points has to be handled separately. When pressure is a known property, as in both of the above mentioned examples, the thermal equation of state, Equation (11), can be employed instead of the caloric equation of state. The other equations in the system remain unchanged. However, while the unknowns are still species densities and temperature for the first example, ($p - \varrho$ case), they become the species densities and total density for the second example, ($p - T$ case).

5. THERMODYNAMIC PROPERTIES

The next step following the determination of the equilibrium composition is the evaluation of any thermodynamic properties of interest, which include pressure, speed of sound, and isentropic index Γ (commonly used in flux-split numerical schemes).

Evaluation of some of these properties requires knowledge of partial derivatives of the mass fractions with respect to density and temperature, as can be seen from the expression for the speed of sound, Equations (27–29). These derivatives can be expressed as functions of the partial derivatives of the species densities, and are given as

$$\frac{\partial Y_i}{\partial \varrho} = \frac{1}{\varrho}\left[\frac{\partial \varrho_i}{\partial \varrho} - \frac{\varrho_i}{\varrho}\right] , \tag{43}$$

$$\frac{\partial Y_i}{\partial T} = \frac{1}{\varrho}\frac{\partial \varrho_i}{\partial T} . \tag{44}$$

The derivatives of the species densities can be obtained using the Implicit Function Theorem. Specifically, the first set of N equations in the Mass Constraint Technique implicitly define N functions of density and temperature

$$w_i[\varrho_1(\varrho, T), \varrho_2(\varrho, T), ..., \varrho_N(\varrho, T)] = 0 , \qquad i = 1, ..., N , \tag{45}$$

where the species densities are the N functions, $\varrho_j = \varrho_j(\varrho, T)$. The Implicit Function Theorem states that the derivatives of the N functions with respect to density and temperature are given by the solution of $dw_i = 0$ provided that the partial derivatives of w_i exist and are continuous, and the determinant of matrix $A = \partial w_i/\partial \varrho_j$ is not zero. Thus the derivatives of the species densities with respect to density and temperature are obtained through the solution of the following systems

$$A\left(\frac{\partial \varrho_j}{\partial \varrho}\right) = - B , \tag{46}$$

$$A\left(\frac{\partial \varrho_j}{\partial T}\right) = - C , \tag{47}$$

where $B = \partial w_i/\partial \varrho$ and $C = \partial w_i/\partial T$.

This procedure can be similarly applied to the Degree of Advancement Technique, where the functions are now $N - NE$ degrees of advancements, $\xi_r = \xi_r(\varrho, T)$. The linear systems are now

$$A\left(\frac{\partial \xi_r}{\partial \varrho}\right) = -B\,, \tag{48}$$

$$A\left(\frac{\partial \xi_r}{\partial T}\right) = -C\,, \tag{49}$$

where matrix $A = \partial w_i/\partial \xi_r$, and the right-hand sides of both systems remain the same. Using the differential form of the transformation relation, Equation (37), the partial derivatives of the mass fractions can be given in terms of the partial derivatives of the degrees of advancement, as follows

$$\frac{\partial Y_i}{\partial \varrho} = \sum_{r=1}^{N-NE} \mathcal{M}_i(\nu''_{i,r} - \nu'_{i,r})\left(\frac{\partial \xi_r}{\partial \varrho}\right) \tag{50}$$

$$\frac{\partial Y_i}{\partial T} = \sum_{r=1}^{N-NE} \mathcal{M}_i(\nu''_{i,r} - \nu'_{i,r})\left(\frac{\partial \xi_r}{\partial T}\right) \tag{51}$$

SECTION III

PRACTICAL MODELS

The mathematical foundation of local chemical equilibrium has been given in the previous section for an arbitrary mixture of thermally perfect gases. No restrictive assumptions have been placed on the functional form of the species internal energy, with the exception that each component is considered to behave as a thermally perfect gas. Similarly, the equilibrium constant, the chemical system and the other related properties have been given in general form. Therefore, virtually any practical model can be utilized in conjunction with the present formulation. The specific models developed and used in the "Black Box" for the species internal energy, the equilibrium constant, the chemical system and the transport properties are given in the following.

1. INTERNAL ENERGY

There are two thermodynamic models available for use in the Black Box. The first is an equilibrium statistical mechanics model and will be referred to as the Vibrational Model. The second model is based on polynomial curvefits and will be termed the Curvefit Model.

a. VIBRATIONAL MODEL

From statistical mechanics, the internal energy can be taken as the sum of the translational, rotational, vibrational and electronic contributions [Reference 14]. Neglecting the electronic contributions and considering the translational and rotational contributions at their fully excited values the equation for the species internal energy will read

$$e_i = n_i R_i T + \sum_{v=1}^{NVT_i} \frac{R_s \Theta_{v,i}}{e^{\Theta_{v,i}/T} - 1} + h_{f_i} , \qquad i = 1,\ldots,N , \tag{52}$$

where the vibrational contributions are modeled as simple harmonic oscillators. In the above, $\Theta_{v,i}$ are the characteristic temperatures for vibration and the summation represents the fact that for polyatomic molecules there will be more than one vibrational temperature. The number of vibrational temperatures for species i is defined to be NVT_i. In Equation (52), the first term represents the translational and rotational contributions. The parameter n_i will have a value of 3/2 for a monatomic gas, 5/2 for a diatomic or linear polyatomic gas and 6/2 for a nonlinear polyatomic gas. The characteristic vibrational temperatures are obtained from the JANAF tables [Reference 22].

b. CURVEFIT MODEL

The Curvefit Model uses fourth-order polynomials to curvefit the species specific heat at constant volume

$$c_{v_i} = a_{1,i} + a_{2,i}\,T + a_{3,i}\,T^2 + a_{4,i}\,T^3 + a_{5,i}\,T^4 , \qquad (53)$$

where the internal energy is given by

$$e_i = a_{6,i} + \int_{T_{ref}}^{T} c_{v_i}(\tau)d\tau , \qquad i = 1,\ldots,N . \qquad (54)$$

There are several curvefit formulations available in the literature. McBride et al [Reference 15]. give curvefits for molecules involving the first 18 elements, which are applicable up to 6000 K. This range was extended to 15,000 K for carbon, hydrogen, nitrogen and oxygen systems by Esch et al [Reference 16]. Gupta et al [Reference 17]. provide improved curvefits, applicable up to 30,000 K for an 11-species air model. In the Black Box, the first set of curvefits is used for argon systems, the second set for carbon and hydrogen systems, and the latter curvefits are utilized for the eleven species air model they were intended for.

2. EQUILIBRIUM CONSTANT

The equilibrium constants define the equilibrium composition of the mixture and are functions of temperature. The Black Box incorporates two models for their determination. In the first one, experimental values are curvefitted employing an Armehius-type functional form. The second model derives the equilibrium constant from the species Gibb's free energy, following the example of Liepmann and Roshko [Reference 18].

a. CURVEFIT K_c

The first model is based on curvefits compatible with Arrenhius type chemistry

$$K_{c,r} = C_c T^{\eta_c} e^{-\theta/T} , \qquad r = 1,\ldots,NR , \qquad (55)$$

where the constants can be found in Vincenti and Kruger [Reference 14] for a 7-species air model and Kang and Dunn [Reference 19] for an 11-species air model. The major advantage of the Curvefit K_c is the use of accurate empirical data for the determination of the equilibrium constant. However, this leads to a disadvantage in that the empirical data may not be available.

b. CONSISTENT K_C

The second model is based on the minimization of Gibb's free energy at constant pressure and temperature. Thus the equilibrium constant can be obtained indirectly from the thermodynamic model and therefore is not limited to the availability of experimental data. This model, termed the Consistent K_C Model, is very general and depends only on the availability of certain reference values which are much easier to obtain than the curvefits mentioned previously. However, any errors introduced by assumptions and simplifications made in the thermodynamic model are inherited by the equilibrium constant.

Gibbs's free energy for a species can be written as

$$\begin{aligned} g_i &= h_i - Ts_i \,, \\ &= \int_{T_{ref}}^{T} c_{p_i}(\tau)d\tau + h_{f_i} - T\int_{T_{ref}}^{T} \frac{c_{p_i}(\tau)d\tau}{\tau} + R_i T \ln\left(\frac{p_i}{p_{f_i}}\right) - Ts_{f_i} \,, \end{aligned} \tag{56}$$

where the equation for species entropy and enthalpy have been utilized. In the above, s_{f_i} and h_{f_i} are the reference entropy and enthalpy taken at the reference temperature T_{ref} and pressure p_{f_i}. Using the standard mixture rule, the total Gibb's free energy for the mixture is then

$$\begin{aligned} g = {} & \sum_{i=1}^{N} \frac{\varrho_i}{\varrho} \int_{T_{ref}}^{T} c_{p_i}(\tau)d\tau - T\sum_{i=1}^{N} \frac{\varrho_i}{\varrho} \int_{T_{ref}}^{T} \frac{c_{p_i}(\tau)d\tau}{\tau} + \sum_{i=1}^{N} \frac{\varrho_i}{\varrho} h_{f_i} \\ & + \sum_{i=1}^{N} \frac{\varrho_i R_i T}{\varrho} \ln\left(\frac{p_i}{p_{f_i}}\right) - T\sum_{i=1}^{N} \frac{\varrho_i}{\varrho} s_{f_i} \,. \end{aligned} \tag{57}$$

Gibb's free energy can be written as a function of pressure, temperature and the degrees of advancement, $g = g(p, T, \xi_r)$. Chemical equilibrium occurs at the point where the Gibb's free energy is a minimum under constant pressure and temperature. Minimizing the above equation for reaction r at constant pressure and temperature, $\partial g/\partial \xi_r = 0$, utilizing the differential form of the transformation relation Equation (37), and taking the exponential of both sides, results in the expression

$$\prod_{s=1}^{N} (p_s)^{(\nu''_{s,r} - \nu'_{s,r})} = \prod_{s=1}^{N} (p_{f_s})^{(\nu''_{s,r} - \nu'_{s,r})} \exp\left[-\sum_{s=1}^{N} \frac{\omega_s(T)}{R_s T} (\nu''_{s,r} - \nu'_{s,r}) \right] = K_{p,r} \,, \tag{58}$$

where

$$\omega_s = g_s - R_s T \ln\left(\frac{p_s}{p_{f_s}}\right) = \int_{T_{ref}}^{T} c_{p_s}(\tau)d\tau - T\int_{T_{ref}}^{T} \frac{c_{p_s}(\tau)d\tau}{\tau} + h_{f_s} - Ts_{f_s} \,. \tag{59}$$

The previous formula is the Law of Mass Action written in terms of the partial pressures. Expressing the constant in terms of the concentrations and assuming that the reference pressure is the same for all species ($p_{f_s} = p_{ref}$), the following relation for the equilibrium constant is obtained

$$K_{c,r} = \left(\frac{p_{ref}}{\tilde{R}T}\right)^{\sum_{s=1}^{N}(\nu''_{s,r} - \nu'_{s,r})} \exp\left[-\sum_{s=1}^{N} \Omega_s(T)\ (\nu''_{s,r} - \nu'_{s,r})\right] , \qquad (60)$$

where

$$\Omega_s(T) = \frac{\omega_s(T)}{R_s T} . \qquad (61)$$

The term ω_s given in Equation is determined by the thermodynamic model employed. In the final form, the term Ω_s will be given for the Curvefit Model as follows

$$\Omega_s(T) = a_{1,s}(1 - \ln T) - a_{2,s}\frac{T}{2} - a_{3,s}\frac{T^2}{6} - a_{4,s}\frac{T^3}{12} - a_{5,s}\frac{T^4}{20} + \frac{a_{6,s}}{T} - a_{7,s} , \qquad (62)$$

and for the Vibrational Model as

$$\Omega_s(T) = 1 + n_s + \ln(1 - e^{-\theta_{v,s}/T}) - (1 + n_s)\ln T + h_s^0/R_s T - s_s^0/R_s . \qquad (63)$$

The last two terms of the above relations are identical, because the constants $a_{6,s}$ and $a_{7,s}$ read

$$a_{6,s} = h_s^0/R_s , \qquad a_{7,s} = s_s^0/R_s , \qquad (64)$$

where h_s^0 and s_s^0 are the species enthalpy and entropy at a reference temperature of absolute zero.

3. CHEMISTRY MODELS

As stated in Section I, a main requirement of the solver is the capability to handle arbitrary mixtures. The incorporation of additional models to the Black Box is a relatively painless process, provided that a few key reference values (i.e. heats of formation) can be supplied for the mixture components. The Black Box currently has available 12 different chemistry models. These include 6 air models (ranging from a simple 5-species to a relatively complex 17-species), 3 combustion models and an argon plasma model. In order to provide the flow solver with the capability to revert to a perfect gas solver, a perfect gas model is also included, with the specific gas being selected at input from a set comprising air, Ar, CO_2, CO, N_2, O_2, H_2 and steam. Debugging and testing of the code was accomplished using an ideally dissociating oxygen model

$$O_2 \rightleftarrows 2O , \qquad (65)$$

where the constants for the dissociation of oxygen were obtained from Vincenti and Kruger[Reference 14]. In the following, the latter model will be referred to as Oxygen Model.

a. AIR MODELS

The first air model is composed of five species, N_2, O_2, NO, N and O, where three independent reactions are used

$$N_2 \leftrightarrows 2N \ , \tag{66}$$

$$O_2 \leftrightarrows 2O \ , \tag{67}$$

$$NO \leftrightarrows N + O \ . \tag{68}$$

Atomic nitrogen and oxygen are the two elemental species and N_2, O_2, NO are the non–elemental species. Two mass constraints are used to preserve the total mass of atomic oxygen and nitrogen. This model will be referred to as 5–Species Air Model. Unless otherwise noted, the air models will be referred to by the number of species present.

The second model adds two more species, NO^+ and e^-, to the model listed above, for a total of seven. The additional independent reaction

$$NO \leftrightarrows NO^+ + e^- \ , \tag{69}$$

is needed to describe the ionization of NO. Conservation of the total number of electrons is provided as an additional mass constraint and NO^+ will act as a non–elemental species.

The third model utilizes nine species, adding N^+ and O^+ to the seven above. Two more independent reactions are needed, describing the ionization of atomic oxygen and nitrogen

$$N \leftrightarrows N^+ + e^- \ , \tag{70}$$

$$O \leftrightarrows O^+ + e^- \ , \tag{71}$$

and bringing the total number of reactions to six. No additional mass constraints are necessary, due to the fact that the two additional species are non–elemental species.

Two more independent reactions are needed for the fourth model

$$N_2 \leftrightarrows N_2^+ + e^- \ , \tag{72}$$

$$O_2 \leftrightarrows O_2^+ + e^- \ , \tag{73}$$

which comprises eleven species, with the addition of N_2^+ and O_2^+ to the previous nine. Again, there are no new mass constraints, because the additional species are not elements.

The fifth model is obtained by adding the base element argon to the previous model, for a total of thirteen species. The two additional species considered are Ar and Ar^+. The ionization of argon is described by the additional reaction

$$Ar \leftrightarrows Ar^+ + e^- \; , \tag{74}$$

and Ar^+ acts as a nonelemental species. An additional mass constraint for the preservation of argon is also required.

The sixth and most complex air model employs seventeen species, the thirteen above plus C, C^+, CO and CO_2. Three more independent reactions are needed

$$2CO_2 \leftrightarrows 2CO + O_2 \; , \tag{75}$$

$$2CO \leftrightarrows 2C + O_2 \; , \tag{76}$$

$$C \leftrightarrows C^+ + e^- \; , \tag{77}$$

along with the previous nine. The inclusion of carbon requires the addition of another mass constraint conserving this element, and the additional nonelemental species are C^+, CO and CO_2. The 17-Species Air Model employs consistent equilibrium constants only, since no curvefits for the last three equations have been found.

b. COMBUSTION MODELS

Combustion mixtures provide good examples of the difficulties associated with the use of curvefits for the determination of equilibrium compositions, since there are nearly infinite possibilities for the mixture ratio. Utilizing curvefits would require a matching number of tabulations. The only viable alternatives are either the method presented in this study or finite-rate chemistry investigations with all their inherent complexities.

The first combustion model is the simple two-reaction hydrogen combustion in air presented in Rogers and Chinitz [Reference 20], and will be referred to as the Hydrogen-Air Combustion Model. A total of five species are utilized, where the nonelemental species are H_2 and O_2. The two independent reactions are

$$H_2 + O_2 \leftrightarrows 2OH \; , \tag{78}$$

$$2OH + O_2 \leftrightarrows 2H_2O \; , \tag{79}$$

where nitrogen is considered to be inert, and three mass constraints provide for the conservation of nitrogen, oxygen and hydrogen. N_2, OH, and H_2O were selected as the elemental species, where the latter two were chosen in order to show how arbitrary the differentiation between elemental and nonelemental species can be.

The second combustion model corresponds to the combustion of hydrogen in oxygen and will be referred to as Hydrogen-Oxygen Combustion Model. The six species O_2, H_2, OH, H_2O, O and H comprise the mixture and the four required reactions are

$$O_2 \leftrightarrows 2O \ , \tag{80}$$

$$H_2 \leftrightarrows 2H \ , \tag{81}$$

$$OH \leftrightarrows O + H \ , \tag{82}$$

$$H_2O \leftrightarrows 2H + O \ , \tag{83}$$

Here, two mass constraints are used for the preservation of oxygen and hydrogen, and the elemental species are O and H.

The last model is taken from Meintjes and Morgan [Reference 4], and is composed of the above six species plus CO_2, CO and N_2. One additional independent reaction is required

$$CO_2 \leftrightarrows CO + O \ . \tag{84}$$

Conservation of hydrogen, oxygen, carbon and nitrogen is ensured through the use of four mass constraints, where the elemental species are H, O, CO and the inert N_2. This model will be referred to as the Hydrocarbon Combustion Model.

c. ARGON PLASMA MODEL

The Argon Model provides a simple example of high energy plasmas. It employs three species Ar^+, Ar and e^-, and one reaction is required

$$Ar \leftrightarrows Ar^+ + e^- \ , \tag{85}$$

describing the ionization of argon. Two mass constraints are employed for the conservation of electrons and argon, and Ar^+ will act as the nonelemental species. Constants for the equilibrium constant are obtained from Glass and Takano [Reference 21].

Implementation of all the above models in the Black Box is accomplished through the use of a chemical model database. For each of the species listed above, this database contains all the various chemical and thermodynamic properties necessary for the solution of the governing equations. Moreover, the stoichiometric coefficients and curvefit constants for various reactions are given in terms of all the species available in the database. The chemistry model of interest is then constructed from this database by specifying which species are present, which reactions to use, etc. The presence of the database makes the implementation of additional models a very simple process.

4. TRANSPORT PROPERTIES

After the equilibrium composition has been obtained by means of the techniques discussed in Section I, the mixture transport properties can be easily evaluated by following two sequential steps. The first is the determination of the properties for the individual species, whereas the second involves the application of a mixing rule to obtain the global values.

a. SPECIES VISCOSITY

Two models for species viscosity are implemented in the Black Box. The first model for species viscosity is a straightforward extension of Sutherland's Law to multicomponent mixtures and is referred to as the Sutherland Model. The species viscosity is given by the relation

$$\mu_i = T^{3/2}\frac{F_{\mu,i}}{T + G_{\mu,i}}\ , \tag{86}$$

where the constant $F_{\mu,i}$ and $G_{\mu,i}$ are empirically determined.

The second model is based on the curvefit tabulations by Gupta et al. [Reference 17], which are valid for air chemistry up to eleven species and 30,000 K. The equation for species viscosity will read

$$\mu_i = e^{C_{\mu,i}}\ T^{\left[A_{\mu,i}\ln T + B_{\mu,i}\right]}\ , \tag{87}$$

where $A_{\mu,i}$, $B_{\mu,i}$ and $C_{\mu,i}$ are the curvefit coefficients. This model will be referred to as Gupta Model. While more accurate at higher temperatures than Sutherland's Law, the Gupta Model does not fair well below 1000 K. Therefore for temperatures below this limit, the Sutherland Model will be used.

b. SPECIES THERMAL CONDUCTIVITY

Similarly to what has been seen for viscosity, two models are employed for the species thermal conductivity. The Sutherland Model reads

$$\mathcal{K}_i = T^{3/2}\frac{F_{\mathcal{K},i}}{T + G_{\mathcal{K},i}}\ , \tag{88}$$

where the constants $F_{\mathcal{K},i}$ and $G_{\mathcal{K},i}$ are empirically determined. The Gupta Model is given by

$$\mathcal{K}_i = e^{E_{\mathcal{K},i}}\ T^{\left[A_{\mathcal{K},i}(\ln T)^3 + B_{\mathcal{K},i}(\ln T)^2 + C_{\mathcal{K},i}\ln T + D_{\mathcal{K},i}\right]}\ , \tag{89}$$

where $A_{\mathcal{K},i}$, $B_{\mathcal{K},i}$, $C_{\mathcal{K},i}$, $D_{\mathcal{K},i}$ and $E_{\mathcal{K},i}$ are the curvefit coefficients. Again, the Sutherland Model is used for temperatures below 1000 K.

c. MIXTURE RULES

Once the species values for the transport properties have been found, then an appropriate mixing rule is applied to give the total mixture property. Two mixture rules are implemented and can be used with either the Sutherland Model or Gupta Model for the transport properties. The first mixing rule is the "standard" Wilke's Rule as follows

$$\mathcal{P} = \sum_{i=1}^{N} W_i \mathcal{P}_i \,, \tag{90}$$

where the weighting function is given by

$$W_i = \frac{X_i}{\sum_{j=1}^{N} X_j \, \phi_{i,j}} \,, \tag{91}$$

with the coefficient $\phi_{i,j}$ given by the following expression

$$\phi_{i,j} = \frac{1}{\sqrt{8}} \left(1 + \frac{\mathcal{M}_i}{\mathcal{M}_j} \right)^{-1/2} \left[1 + \sqrt{\frac{\mu_i}{\mu_j}} \left(\frac{\mathcal{M}_j}{\mathcal{M}_i} \right)^{1/4} \right]^2 . \tag{92}$$

In the above, $\mathcal{P}$ denotes transport property and stands for either viscosity or thermal conductivity. Also, the species concentration $X_i = \varrho_i / \mathcal{M}_i$ has been introduced. This mixing rule will be referred to as Wilke's Rule.

Gupta et al. [Reference 17], propose an improved, but more complicated mixing rule based on the collision cross-sections. The mixture rule will have the same form as in Equation (90) but the weighting function is now given by

$$W_i = \frac{\sqrt{2}}{2} X_i \, \overline{\Omega}_{ii} \sum_{j=1}^{N} \frac{\sqrt{1 + \mathcal{M}_i / \mathcal{M}_j}}{X_j \, \overline{\Omega}_{ij}} \,, \tag{93}$$

where

$$\overline{\Omega}_{ij} = e^{D_{\overline{\Omega}_{ij}}} \, T^{\left[A_{\overline{\Omega}_{ij}} (\ln T)^2 + B_{\overline{\Omega}_{ij}} \ln T + C_{\overline{\Omega}_{ij}} \ln T \right]} . \tag{94}$$

Here, the collision cross-sections $\overline{\Omega}_{ij}$ have been introduced and $A_{\Omega_{ij}}$, $B_{\Omega_{ij}}$, $C_{\Omega_{ij}}$ and $D_{\Omega_{ij}}$ are the curvefit coefficients. This will be referred to as Gupta's Rule.

SECTION IV

NUMERICAL FORMULATION: BLACK BOX

In the following, details of the numerical algorithms used to determine the equilibrium composition are given. In addition, the methods developed in Section II to obtain the thermodynamic properties of a gas mixture in local chemical equilibrium are further illustrated. The possibility of multiple solutions to the chemical equilibrium problem and the correction strategies employed to prevent non-physical results are also discussed. Finally, methods used to enhance the robustness and efficiency of the "Black Box" are detailed.

1. "BLACK BOX" SOLVER

The first step in the numerical solution of the systems of nonlinear governing equations developed in Section II involves the linearization of the equations using the Newton-Raphson technique. The linear system will have the form

$$Ax = b \ , \tag{95}$$

where A is the $(H + 1) \times (H + 1)$ Jacobian matrix. For the Mass Constraint Technique H equals N, and for the Degree of Advancement Technique H will be equal to $N - NE$. The second step comprises the direct inversion of the linear system by means of a LU decomposition, where partial pivoting is employed. Relative and absolute reduction of the residual vector is checked and iterations are performed using double-byte arithmetic until either has reached a prescribed tolerance. For use with the flow solver, the matrix of computational cells are converted to a vector, so that the Black Box solves one system of equations per cell in the flow field, and vectorizes easily over the number of computational cells.

a. MASS CONSTRAINT TECHNIQUE

The specific components of the linearized system of equations, Equation (95), for the Mass Constraint Technique, written for constant density and internal energy, will have the following form

$$A = \begin{bmatrix} \frac{\partial w_1}{\partial \varrho_1} & \cdots & \frac{\partial w_1}{\partial \varrho_N} & \frac{\partial w_1}{\partial T} \\ \vdots & \ddots & \vdots & \vdots \\ \frac{\partial w_{N-NE}}{\partial \varrho_1} & \cdots & \frac{\partial w_{N-NE}}{\partial \varrho_N} & \frac{\partial w_{N-NE}}{\partial T} \\ \frac{\partial w_{N-NE+1}}{\partial \varrho_1} & \cdots & \frac{\partial w_{N-NE+1}}{\partial \varrho_N} & \frac{\partial w_{N-NE+1}}{\partial T} \\ \vdots & \ddots & \vdots & \vdots \\ \frac{\partial w_N}{\partial \varrho_1} & \cdots & \frac{\partial w_N}{\partial \varrho_N} & \frac{\partial w_N}{\partial T} \\ \frac{\partial d}{\partial \varrho_1} & \cdots & \frac{\partial d}{\partial \varrho_N} & \frac{\partial d}{\partial T} \end{bmatrix} \tag{96}$$

$$x^T = \left[\Delta\varrho_1, \ldots, \Delta\varrho_N, \Delta T\right] , \tag{97}$$

$$b^T = -\left[w_1, \ldots, w_{N-NE}, w_{N-NE+1}, \ldots, w_N, d\right] . \tag{98}$$

In the above, w denotes the laws of mass action and the mass constraints, and d denotes the energy equation. These have been already defined by Equations (30–32). In addition, the partial derivatives of the laws of mass action will read

$$\frac{\partial w_i}{\partial \varrho_j} = \frac{\mathcal{M}_i}{\mathcal{M}_j} \sum_{r=1}^{NR} (\nu''_{i,r} - \nu'_{i,r}) k_{b,r} \left[K_{c,r} \prod_{m=1}^{N} \left(\frac{\varrho_m}{\mathcal{M}_m}\right)^{\bar{\nu}'_{m,r}} \nu'_{j,r} - \prod_{m=1}^{N} \left(\frac{\varrho_m}{\mathcal{M}_m}\right)^{\bar{\nu}''_{m,r}} \nu''_{j,r} \right] , \tag{99}$$

$$\frac{\partial w_i}{\partial T} = \mathcal{M}_i \sum_{r=1}^{NR} (\nu''_{i,r} - \nu'_{i,r}) k_{b,r} \left[\frac{dK_{c,r}}{dT} \prod_{m=1}^{N} \left(\frac{\varrho_m}{\mathcal{M}_m}\right)^{\nu'_{m,r}} \right] , \qquad i = 1, \ldots, N - NE , \tag{100}$$

where in Equation (99)

$$\bar{\nu}'_{m,r}\ (\bar{\nu}''_{m,r}) = \begin{cases} \nu'_{m,r}\ (\nu''_{m,r}) & \text{if } m \neq j , \\ \nu'_{m,r} - 1\ (\nu''_{m,r} - 1) & \text{if } m = j \text{ and } \nu'_{m,r}\ (\nu''_{m,r}) \neq 0 , \\ 0 & \text{if } \nu'_{m,r}\ (\nu''_{m,r}) = 0 . \end{cases}$$

The partial derivatives of the mass constraints are

$$\frac{\partial w_{N-NE+i}}{\partial \varrho_j} = \frac{a_{i,j}}{\varrho \mathcal{M}_j} , \tag{101}$$

$$\frac{\partial w_{N-NE+i}}{\partial T} = 0 , \qquad i = 1, \ldots, NE . \tag{102}$$

Finally, the partial derivatives of the equation of state are given by

$$\frac{\partial d}{\partial \varrho_j} = e_j = \int_{T_{ref}}^{T} c_{v_j}(\tau)d\tau + h_{f_i} \ , \tag{103}$$

$$\frac{\partial d}{\partial T} = \varrho \tilde{c_v} \ . \tag{104}$$

b. DEGREE OF ADVANCEMENT TECHNIQUE

The specific components of the linearized system of equations, Equation (95), for the Degree of Advancement Technique, written for constant density and internal energy, will have the following form

$$A = \begin{bmatrix} \frac{\partial w_1}{\partial \xi_1} & \cdots & \frac{\partial w_1}{\partial \xi_{N-NE}} & \frac{\partial w_1}{\partial T} \\ \vdots & \ddots & \vdots & \vdots \\ \frac{\partial w_{N-NE}}{\partial \xi_1} & \cdots & \frac{\partial w_{N-NE}}{\partial \xi_{N-NE}} & \frac{\partial w_{N-NE}}{\partial T} \\ \frac{\partial d}{\partial \xi_1} & \cdots & \frac{\partial d}{\partial \xi_{N-NE}} & \frac{\partial d}{\partial T} \end{bmatrix} \tag{105}$$

$$x^T = \left[\Delta\xi_1, \ldots, \Delta\xi_{N-NE}, \Delta T\right] \ , \tag{106}$$

$$b^T = -\left[w_1, \ldots, w_{N-NE}, d\right] \ . \tag{107}$$

The advantage of the Degree of Advancement Technique should be readily apparent in the above. The system has been reduced from N + 1 to N – NE + 1 equations. However, while the Jacobian is smaller component-wise, it has been rendered computationally more complex. Using the differential form of the transformation relation, Equation (37), the partial derivatives with respect to the degrees of advancement can be written in terms of the previous entries as follows

$$\frac{\partial w_i}{\partial \xi_j} = \varrho \sum_{m=1}^{N} \mathcal{M}_m(\nu''_{m,r} - \nu'_{m,r})\frac{\partial w_i}{\partial \varrho_m} \ , \tag{108}$$

$$\frac{\partial d}{\partial \xi_j} = \varrho \sum_{m=1}^{N} \mathcal{M}_m(\nu''_{m,r} - \nu'_{m,r})\frac{\partial d}{\partial \varrho_m} \ , \tag{109}$$

where the partials with respect to temperature remain the same and the mass constraint equations have been eliminated.

2. ALTERNATE THERMODYNAMIC SYSTEMS

The preceding subsection dealt with the general situation of the complete thermodynamic system being defined by density and internal energy, CTS = f(ϱ, e). As was discussed in Section II, situations arise where the complete thermodynamic system is known as a function of pressure and density, CTS = f(p, ϱ), or as a function of pressure and temperature, CTS = f(p, T). In the following discussion on these alternate thermodynamic systems, only the Mass Constraint Technique will be considered.

For the situation where CTS = f(p, ϱ), the linearized system for the Mass Constraint Technique, given by Equations (96–98), remains the same, with the exception that closure is now provided by the thermal equation of state

$$d(\varrho_j, T) = \sum_{j=1}^{N} \varrho_j R_j T - (p)_0 = 0 \ , \tag{110}$$

where $(p)_0$ is the initial pressure. The partial derivatives of the equation of state, previously given by Equations (103) and (104), are now written as

$$\frac{\partial d}{\partial \varrho_j} = R_j T \ , \tag{111}$$

$$\frac{\partial d}{\partial T} = \varrho \tilde{R} \ . \tag{112}$$

The situation where pressure and temperature are known, CTS = f(p, T), requires more modification. As stated previously, the dependent variables are now species densities and total density, and the thermal equation of state has replaced the caloric equation of state in the governing equations. Although total density is nothing more than the sum of the species densities and would indicate that one equation could be dropped from the system, reducing the size of the problem is not practical. In fact, the state relationship is required to define the thermodynamic state and while it could be substituted into the rate equations, this would increase the complexity of the Jacobians, making them more expensive to compute. The linearized system for constant pressure and temperature will be

$$A = \begin{bmatrix} \frac{\partial w_1}{\partial \varrho_1} & \cdots & \frac{\partial w_1}{\partial \varrho_N} & \frac{\partial w_1}{\partial \varrho} \\ \vdots & \ddots & \vdots & \vdots \\ \frac{\partial w_{N-NE}}{\partial \varrho_1} & \cdots & \frac{\partial w_{N-NE}}{\partial \varrho_N} & \frac{\partial w_{N-NE}}{\partial \varrho} \\ \frac{\partial w_{N-NE+1}}{\partial \varrho_1} & \cdots & \frac{\partial w_{N-NE+1}}{\partial \varrho_N} & \frac{\partial w_{N-NE+1}}{\partial \varrho} \\ \vdots & \ddots & \vdots & \vdots \\ \frac{\partial w_N}{\partial \varrho_1} & \cdots & \frac{\partial w_N}{\partial \varrho_N} & \frac{\partial w_N}{\partial \varrho} \\ \frac{\partial d}{\partial \varrho_1} & \cdots & \frac{\partial d}{\partial \varrho_N} & \frac{\partial d}{\partial \varrho} \end{bmatrix} , \tag{113}$$

$$x^T = [\, \Delta\varrho_1, \ldots, \Delta\varrho_N, \Delta\varrho \,] , \tag{114}$$

and the residual vector remains the same. The partial derivatives of the laws of mass action with respect to the species densities remain the same and are given by Equation (99), whereas the partial derivatives of the laws of mass action with respect to total density are zero. The partial derivatives of the mass constraints are given as

$$\frac{\partial w_{N-NE+i}}{\partial \varrho_j} = \frac{a_{i,j}}{\varrho \mathcal{M}_j} , \tag{115}$$

$$\frac{\partial w_{N-NE+i}}{\partial \varrho} = -\frac{1}{\varrho} \sum_{j=1}^{N} \frac{a_{i,j}}{\mathcal{M}_j} Y_j , \qquad i = 1, \ldots, NE . \tag{116}$$

Recognizing that pressure and temperature are constant, the thermal equation of state can be written in the form

$$d(\varrho_j, \varrho) = \sum_{j=1}^{N} \varrho_j R_j (T)_0 - (p)_0 = 0 , \tag{117}$$

where the terms denoted by $(\;)_0$ represent initial conditions. The partial derivatives of the thermal equation of state will then be

$$\frac{\partial d}{\partial \varrho_j} = R_j T_0 , \tag{118}$$

$$\frac{\partial d}{\partial \varrho} = 0 . \tag{119}$$

3. THERMODYNAMIC PROPERTIES

Once the composition of a mixture of thermally perfect gases has been evaluated, the thermodynamic properties of the mixture can be determined. These are primarily functions of the temperature and density derivatives of the species densities. As was discussed in Section II, the determination of these derivatives is a straightforward process involving the solution of two linear systems of algebraic equations, provided that temperature and density derivatives of the governing equations are readily available. This is indeed the case when the Newton–Raphson algorithm is utilized.

Taking the Mass Constraint Technique as an example, it should be readily apparent that the first N rows and columns of the converged Jacobian matrix corresponds to the matrix A required to determine the partial derivatives. Also, the last column of the Jacobian matrix is the RHS, given by C in Equation (47), for the temperature derivative computation. The RHS for the density derivatives, given by B in Equation (46), is also easily derived and will be

$$\frac{\partial w_i}{\partial \varrho} = 0 \ , \qquad i = 1,\ldots,N - NE, \tag{120}$$

and

$$\frac{\partial w_{N-NE+i}}{\partial \varrho} = -\frac{1}{\varrho}\sum_{j=1}^{N}\frac{a_{i,j}}{\mathcal{M}_j}Y_j \ , \qquad i = 1,\ldots,NE\,. \tag{121}$$

Similar considerations can be applied to the Degree of Advancement Technique, where the matrix A is now given by the first N – NE rows and columns of the Jacobian matrix at convergence. The RHS terms will be the same as those for the Mass Constraint Technique. Therefore, at convergence, the temperature and density derivatives are easily evaluated. At this point, the reason behind the choice of density and temperature as the two fundamental state variables to describe the properties of a mixture in local chemical equilibrium becomes apparent. If one were to choose density and internal energy, for example, evaluation of the partial derivatives with respect to *e* would be computationally more expensive than the method presented above, due to the fact that the laws of mass action are not explicitly defined in terms of internal energy.

4. MULTIPLE SOLUTIONS

The possibility of multiple solutions is an interesting yet troublesome problem that affects chemical equilibrium calculations. The nonlinear nature of the governing equations potentially allows several different mathematical solutions for the same set of equations.

An example of this occurrence can be given for the 5-Species Air Model using the Vibrational Model and Curvefit K_c. The initial guess for the temperature is 5000 K and the initial guesses for the mass fractions are the exact values, where density $\varrho = 8.676 \times 10^{-2} \mathrm{kg/m^3}$ and internal energy $e = 6.271 \times 10^6 \mathrm{kJ/kg}$ have been specified. Table 1 gives the temperature and composition for two solutions obtained for the problem defined above. Although both mathematically satisfy the laws of mass action, mass constraints and energy equation, the first solution is physically not possible since mass fractions cannot have negative values. Physically, there can be only one solution with nonnegative mass fractions, since the specification of two state variables describes a unique thermodynamic state. The above example illustrates the possibility of negative densities, but it is also possible to obtain solutions with negative temperatures.

In light of the problem mentioned above, three techniques were developed to guide convergence to the one physical solution. The first two methods employ a scaling factor to reduce the magnitude of the species densities updates, $\Delta\varrho_i = \varrho_i^{n+1} - \varrho_i^n$, where the superscript ^{n} represents the iteration level. The first method will be called Catastrophic Limiter and it intervenes only when a species density is going to become negative from the iteration update. The second method limits the magnitude of the relative change in species densities at every iteration, and is called Relative Limiter. If the same scaling factor is used on all the species densities updates, then it can be shown that the mass constraints will not be violated. This is important when using these methods with the Degree of Advancement Technique, which does not explicitly enforce the mass constraints. The scaling factor σ will have the form

$$\sigma = \max\left\{ \sigma_{\min} \, , \left[\min_i \left[1, \frac{\beta \, \varrho_i^n}{\left| \Delta\varrho_i^{\text{old}} \right|} \right] , \quad \varrho_i > 0 \, , \quad i = 1,\ldots,N \right] \right\} , \tag{122}$$

where β is the maximum allowed relative change in species densities

$$\beta \geq \left| \frac{\Delta\varrho_i^{\text{new}}}{\varrho_i^n} \right| , \qquad i = 1,\ldots,N \, . \tag{123}$$

The only difference between the two methods is that Relative Limiter applies the correction at each iteration, while Catastrophic Limiter applies the correction only when a species density would become negative as a result of the update. In order to prevent the convergence process from slowing down dramatically, the scaling factor is limited to a minimum value, $\sigma_{\min}$. The new value for the species densities updates will then be given by

$$\Delta\varrho_i^{\text{new}} = \sigma \, \Delta\varrho_i^{\text{old}} \, , \qquad i = 1,\ldots,N \, . \tag{124}$$

Neither of the above methods can prevent negative species densities from occurring in the transient when extenuating circumstances occur (i.e. $\varrho_i^n = 0$ and $\Delta\varrho_i < 0$). However, the negative species densities are omitted from the scaling factor evaluation, see Equation (122), since enforcing a scaling factor on the negative species densities would prevent those densities from becoming positive again.

While the use of a common scaling factor ensures satisfaction of the mass constraints, the linearized equation of state would not be satisfied by the modified species densities updates, unless the temperature update is also suitably modified. This can be accomplished by resolving the last row of the governing system for the modified temperature update, using the modified species densities updates.

The third correction method is based on the absolute Newton's method described by Meintjes and Morgan [Reference 4], and will be called Absolute Newton Limiter. Negative species are avoided by taking the new values of the species densities, to be the absolute value of the sum of the old values and their updates, $\varrho_i^{n+1} = | \varrho_i^n + \Delta\varrho_i |$. This method does not use a common scaling factor and hence violation of the mass constraints is possible during the iterative process. Due to this violation, the Absolute Newton Limiter is unsuitable for use with the Degree of Advancement Technique, as will be shown in the results.

Another occurrence associated with the Newton–Raphson method is the over–shooting of the temperature, which can lead to negative temperatures. This is especially possible for ill–posed problems involving low temperature compositions where the initial guess for temperature is given as a large value. When written in terms of temperature instead of species density, the Relative Limiter and Absolute Newton Limiter can be used to prevent these over–shootings.

5. ROBUSTNESS AND EFFICIENCY

Several techniques were employed to enhance the robustness and efficiency of the Black Box. These techniques include improving the initial estimates of the dependent variables, reducing the size of the vector of computational cells solved by the Black Box, and freezing the chemistry.

a. INITIAL GUESS

One of the key factors in the robustness and efficiency of a numerical scheme employing the Newton–Raphson method is the availability of "good" initial guesses. Two methods are employed in the Black Box to provide these "good" initial guesses for the species densities and temperature. The first one consists of assigning the values obtained at the previous time step to the new values. Thus given new values for density and total energy per unit volume from the flow solver, the initial guesses for the species densities and temperature will be

$$\varrho_i^{n+1} = (Y_i)^n \varrho^{n+1} , \qquad T^{n+1} = T^n , \tag{125}$$

where the superscript ^{n} again denotes the time step.

The second method uses the mass fraction derivatives to provide an improved initial guess. The updated values will be given by

$$\varrho_i^{n+1} = \varrho^{n+1}\left[Y_i^n + \left(\frac{\partial Y_i}{\partial \varrho}\right)_e^n \Delta\varrho + \left(\frac{\partial Y_i}{\partial e}\right)_\varrho^n \Delta e\right], \qquad i = 1,\ldots,N, \tag{126}$$

$$T^{n+1} = T^n + \left(\frac{\partial T}{\partial \varrho}\right)_e^n \Delta\varrho + \left(\frac{\partial T}{\partial e}\right)_\varrho^n \Delta e\,, \tag{127}$$

where the partial derivatives are

$$\left(\frac{\partial T}{\partial e}\right)_\varrho = \frac{1}{c_v}\,, \tag{128}$$

$$\left(\frac{\partial T}{\partial \varrho}\right)_e = -\frac{1}{c_v}\sum_{j=1}^{N} e_j\left(\frac{\partial Y_j}{\partial \varrho}\right)_T\,, \tag{129}$$

$$\left(\frac{\partial Y_i}{\partial e}\right)_\varrho = \left(\frac{\partial Y_i}{\partial T}\right)_\varrho\left(\frac{\partial T}{\partial e}\right)_\varrho = \frac{1}{c_v}\left(\frac{\partial Y_i}{\partial T}\right)_\varrho\,, \tag{130}$$

$$\left(\frac{\partial Y_i}{\partial \varrho}\right)_e = \left(\frac{\partial Y_i}{\partial \varrho}\right)_T + \left(\frac{\partial Y_i}{\partial T}\right)_\varrho\left(\frac{\partial T}{\partial \varrho}\right)_e = \left(\frac{\partial Y_i}{\partial \varrho}\right)_T - \left(\frac{\partial Y_i}{\partial T}\right)_\varrho \frac{1}{c_v}\sum_{j=1}^{N} e_j\left(\frac{\partial Y_j}{\partial \varrho}\right)_T\,, \tag{131}$$

and $\Delta\varrho = \varrho^{n+1} - \varrho^n$ and $\Delta e = e^{n+1} - e^n$ are provided by the flow solver. The partial derivatives of the species mass fractions with respect to density and temperature are obtained from the approach already described.

b. VECTOR REDUCTION

A very effective method used to increase the efficiency of the Black Box is vector reduction, whereby the vector of computational cells is reduced in size as cells converge. Considering three-dimensional flow simulations, initially all the computational cells are stored in an active vector with a vector length equal to the product of the three dimensions of the computational matrix under consideration. The residuals for each of the governing systems is checked at each iteration for convergence. As a cell converges it is removed from the active vector and the vector length is correspondingly reduced. Thus the expense associated with the computation of the Jacobians for converged cells is not incurred and iterations are performed on the unconverged cells only. The efficiency of vector reduction does not come without cost. In order to implement the vector reduction, a memory intensive data structure is used to keep track of the cells in the vector and their corresponding positions in the computational matrix. However, it will be seen in the results section that the benefits definitely outweigh the costs.

c. FREEZING THE CHEMISTRY

As should be apparent, use of the Black Box to provide the composition and thermodynamic properties of a gas mixture for use in a flow solver requires some computational expense. This expense can be reduced by freezing the chemistry for a desired number of iterations of the flow solver, where the chemical composition would be evaluated at every k^{th} iteration instead of at every iteration of the flow solver. At the iterations where the chemistry is frozen, the mass fractions are considered to be constants. Thus the governing system of equations in the Black Box would reduce to an equation of state only and the unknowns would reduce to just temperature or total density, depending on the known state variables. Iterations still need to be performed for the general case, $CTS = f(\varrho, e)$, since the caloric equation of state is a nonlinear function of temperature and cannot be solved directly. However, solutions for the cases $CTS = f(p, \varrho)$ and $CTS = f(p, T)$ are easily obtained, where the thermal equation of state can be solved directly. In the first case, temperature is readily given as

$$T = \frac{p}{\varrho \tilde{R}} , \tag{132}$$

and for the second case, density is easily obtained by

$$\varrho = \frac{p}{T \tilde{R}} , \tag{133}$$

where the right-hand sides of both equations are known constants. In practice, the number of iterations at frozen chemistry will be small at the beginning of the flow computation, when the thermodynamic state and hence chemical composition is changing rapidly. Towards convergence, this number can be significantly increased, and the overall computational time reduced.

	Negative	Exact
Temp. (K)	3932.45	4000.00
N_2 Mass Fraction	0.803368	0.740236
O_2 Mass Fraction	0.079529	0.042519
NO Mass Fraction	−0.076377	0.055901
N Mass Fraction	−0.000622	0.000761
O Mass Fraction	0.194102	0.160582

Table 1 Example of multiple solution.

SECTION V

BLACK BOX RESULTS

Numerical results were obtained for each of the chemistry models detailed in Section III using different densities over varying ranges of temperature. Unless otherwise stated, all calculations were performed using the Vibrational Model and Consistent K_c.

1. AIR MODELS

In the following, equilibrium compositions for air were computed at densities $\varrho = 1.293$, $1.293\ 10^{-2}$ and $1.293\ 10^{-4}$ kg/m^3, where the first value corresponds to standard conditions. The compositions computed using 5-Species Air Model, plotted as mole percentage versus temperature, are shown in Figure 1, Figure 2 and Figure 3 for the three respective densities. Of importance is the result that as density decreases, so does the temperature at which the mixture has totally dissociated into monatomic components. For the density $\varrho = 1.293$ kg/m^3, the mixture still contains diatomic species up to 16,000 K, as seen in Figure 1. The equilibrium composition for density $\varrho = 1.293\ 10^{-2}$ kg/m^3, as seen in Figure 2, becomes almost completely monatomic at around 14,000 K. Also, the mole percentage of NO peaks at around 3,000 K, which is consistent with the findings of other researchers [Reference 23]. In Figure 3, where the composition for density $\varrho = 1.293\ 10^{-4}$ kg/m^3 is plotted, it can be seen that the temperature at which the mixture is virtually dissociated has dropped to around 9,000 K.

The variation of temperature versus internal energy, computed using 5-Species Air Model, is shown in Figure 4 for the three density values given. The effect of chemical reactions are readily apparent in this figure. For an ideal gas, temperature would be a linear function of internal energy and independent of density.

The variation of isentropic index versus temperature is given in Figure 5 for the same three densities and same air model. At low temperatures, the index starts at its diatomic limit of 7/5. It then follows a series of peaks and valleys until it finally reaches its monatomic limit of 5/3. Comparing each density curve with its corresponding composition plot given in Figure 1 through Figure 3, it can be seen that the first valley correlates well with the point of massive O_2 dissociation. The subsequent peak correlates with a peak in O production. The second valley correlates with the point of massive N_2 dissociation. It can be inferred from Figure 5 that it may be hazardous to assume a constant "gamma" in the derivation of flux-split algorithms. The variation of speed of sound versus temperature is shown in Figure 6. Again, deviation from ideal behavior is noticeable, as this plot would reduce to a single parabolic shape for an ideal gas.

Equilibrium compositions for density $\varrho = 1.293 \ 10^{-2} \ \mathrm{kg/m^3}$ are shown in Figure 7 through Figure 10 for the 7, 9, 11 and 13-Species Air Model respectively. The 7-Species Air Model solution given in Figure 7 is nearly identical to Figure 2 except for the two additional species NO^+ and e^-. The mole percent for these two species is identical due to preservation of electrical charge. However, it should be noted that the physical behavior of the 7-Species mixture is inaccurate, since at the high end of the temperature range the mixture should be entirely monatomic. This is because the 7-Species Air Model has no mechanism for the production of atomic ions, specifically N^+ and O^+. A more noticeable change, other than the addition of more species, occurs in the more complex models which incorporate reactions describing the production of atomic ions. At the higher temperatures, the mixture is composed entirely of monatomic species, as can be seen in Figure 8 through Figure 10 . Furthermore, these mixtures are becoming increasingly more ionized.

Plots of mole percentage versus temperature for the 17-Species Air Model and the three densities given previously are depicted in Figure 11 , Figure 12 and Figure 13. Again the dependence of the level of dissociation on density is readily apparent. These plots are in excellent agreement with similar results obtained by Hilsenrath, Klein and Wooley [Reference 24], where the equilibrium computations were performed using 27 species.

The variation of temperature versus internal energy is given in Figure 14 for the three densities and 17-Species Air Model. The curves are nearly identical to those computed using 5-Species Air Model, shown in Figure 4, up to an internal energy e = 40 MJ/kg. At this value for internal energy the curves for the 5-Species Air Model reach their limiting linear functional form, since the composition is fairly constant past that point. However, for the 17-Species Air Model, this limit is not reached until around 200 MJ/kg. The reason for this difference is that the more complex air model incorporates charged species, where internal energy is used in the ionization reactions.

Plots of the isentropic index versus temperature for the same three values of density and 17-Species Air Model are given in Figure 15. As in the results for 5-Species Air Model, the isentropic index starts at its diatomic limit and follows a series of peaks and valleys until it reaches its monatomic limit. Again, when compared to the corresponding plots of composition given by Figure 11 through Figure 13, the first two valleys and first peak correlate in a similar manner as the results for the 5-Species Air Model. Additionally, the second peak correlates with the peak in N production and the subsequent valley correlates nicely with the beginning of massive ionization. The variation of speed of sound versus temperature for the 17-Species Air Model is shown in Figure 16.

Comparisons of the air models are made in Figure 17 and Figure 18 for density $\varrho = 1.293\ 10^{-2}\ \mathrm{kg/m^3}$. The variation of temperature versus internal energy for all the air models is given in Figure 17. Here the effects of ionization incorporated in the more complex models, 9, 11, 13 and 17-Species Air Model, are readily apparent. The variation of isentropic index versus temperature is shown in Figure 18. The inaccuracy of the 7-Species Air Model is very apparent in this plot, where at high temperatures the isentropic index tends towards the diatomic limit and then drops off. Moreover, it should be pointed out that for the simpler air models the diatomic limit is reached at a much lower temperature than for the more complex models.

It is important to point out that the results from all the chemistry models are the same up to a temperature corresponding to the onset of ionization, which for the density $\varrho = 1.293\ 10^{-2}\ \mathrm{kg/m^3}$ results shown is about 8,000 K. At higher temperatures, where ionization effects are important, the 9, 11, 13 and 17-Species Air Models are in perfect agreement. Thus for high-speed, high-temperature air flow simulations, there should be no loss in accuracy through the use of the simpler 9-Species Air Model instead of the computationally more expensive 17-Species Air Model. Moreover, if the maximum temperature of the flow field is less than the temperature at which ionization occurs, then further computational savings can be realized through the use of the simple 5-Species Air Model without any appreciable loss in accuracy.

2. COMBUSTION MODELS

The equilibrium composition obtained for Hydrogen-Air Combustion Model is given in Figure 19 for a density $\varrho = 1.324\ 10^{-3}\ \mathrm{kg/m^3}$. The equivalence ratio $\Phi = 0.29841$ corresponds to a lean mixture. The accuracy of this model is questionable, since at the higher temperatures oxygen should be dissociated.

The variation of temperature versus internal energy for Hydrogen-Air Combustion Model is shown in Figure 20 for densities of $\varrho = 1.324\ 10^{-1}$, $1.324\ 10^{-3}$ and $1.324\ 10^{-5}\ \mathrm{kg/m^3}$. The variation of speed of sound versus temperature is given in Figure 21 for the same three densities. It can be seen that the thermodynamic properties of the mixture are not strongly affected by density for this combustion model. This is probably due to the high concentration of inert nitrogen in the mixture.

Equilibrium compositions computed for Hydrogen-Oxygen Combustion Model are shown in Figure 22 and Figure 23 for densities $\varrho = 2.8306$ and $2.8306\ 10^{-2}\ \mathrm{kg/m^3}$, and a mixture ratio of 6:1. This is the same composition used in the space shuttle main engine (SSME) nozzle studies of Wang and Chen [Reference 13]. At low temperatures, water and excess diatomic hydrogen are the prevalent species, while at higher temperatures, where the dissociation reactions are predominant, atomic hydrogen and oxygen are noticeable. This figure illustrates the dependence on temperature as to whether the mixture is fully or partially combusted.

The variation of temperature versus internal energy for the Hydrogen–Oxygen Combustion Model is shown in Figure 24 for the two densities given above. A much stronger dependence on density is registered for this model as opposed to the previous model. The variation of isentropic index versus temperature is given in Figure 25 for the same two densities and same combustion model. When compared to the composition plots of Figure 22 and Figure 23, the minimas of the isentropic index curves correlate with the points where oxygen is beginning to massively dissociate. The composition of both mixtures are fairly constant up to a temperature around 3,000 K. This is reflected in the plot of speed of sound versus temperature, given in Figure 26, where the curves for the two densities begin to deviate at this temperature.

The equilibrium composition obtained using Hydrocarbon Combustion Model for density $\varrho = 3.295\ 10^{-2}\ \mathrm{kg/m^3}$ is shown in Figure 27, where the equivalence ratio $\Phi = 1.2$ corresponds to a fuel–rich mixture. This is the same composition studied by Meintjes and Morgan [Reference 4]. Again, the dependence of the combustion process from the temperature is readily apparent.

The variation of temperature with internal energy for the Hydrocarbon Combustion Model is shown in Figure 28, where three curves are plotted for densities $\varrho = 3.295$, $3.295\ 10^{-2}$ and $3.295\ 10^{-4}\ \mathrm{kg/m^3}$. Similar to the comparisons made earlier, the valley in the density $\varrho = 3.295\ 10^{-2}\ \mathrm{kg/m^3}$ curve, in the plot of isentropic index versus temperature shown in Figure 29, is seen to correlate well to the point of massive dissociation of O_2 seen in Figure 27. The variation of speed of sound is given in Figure 30 for the same three densities.

3. PLASMA MODEL

Equilibrium compositions obtained from the Argon Plasma Model are plotted in Figure 31 for the densities $\varrho = 1.303\ 10^{-5}$, $1.303\ 10^{-3}$ and $1.303\ 10^{-1}\ \mathrm{kg/m^3}$, proceeding from left to right. Plots of the variation of temperature versus internal energy, isentropic index versus temperature and speed of sound versus temperature are given in Figure 32, Figure 33 and Figure 34 respectively, for the same three values of density. A strong dependence on density is registered in all the plots.

4. TRANSPORT PROPERTIES

Comparisons of the transport property evaluation methods were made using the 11–Species Air Model under a constant pressure of one atmosphere. Either of the two models used to compute the species transport property, Sutherland Model or Gupta Model, can be combined with either of the mixture rules, Wilke Rule or Gupta Rule, to give the value for the mixture. The variation of the mixture viscosity versus temperature is given in Figure 35 for each of four permutations possible, while the variation of mixture thermal conductivity is given in Figure 36. In both plots the values have been normalized using the appropriate Sutherland's Law for air as a homogeneous mixture. There is relatively little difference between the models at low temperatures. However, at the higher temperatures, the Gupta–Gupta technique, which incorporates collision cross sections, could prove to be more accurate.

5. ROBUSTNESS

The problem of multiple solutions to the equilibrium equations and the limiters developed to correct this problem were discussed in Section IV. Five different strategies were developed, incorporating the limiters in various combinations in order to improve the robustness of the Black Box. These correction strategies were tested using Ideal Dissociating Oxygen Model as well as the 5 and 11–Species Air Models. Initial guesses for species densities and temperature for each cell were selected with a certain arbitrariness and all calculations were performed driving the residual to machine zero, using double byte arithmetic.

In the following, Strategy 1 will refer to the baseline solution, where no limiters were used. Strategy 2 uses the Catastrophic Limiter for density correction and the Relative Limiter for temperature correction. The Relative Limiter was used for both density and temperature correction in Strategy 3. Strategy 4 uses Absolute Newton Limiter for both density and temperature correction. Strategy 5 is similar, except temperature correction is performed using Relative Limiter. Preliminary numerical experiments were performed on the value of β used in Equation (122) and the value $\beta = 1/3$ was found to be the optimal choice.

a. OXYGEN DISSOCIATION RESULTS

The Ideal Dissociating Oxygen Model was utilized to evaluate the equilibrium composition at three different thermodynamic states, where each is characterized by a density $\varrho = 3.0\ 10^{-4}\ \mathrm{kg/m^3}$. Case 1 corresponds to heavy dissociation and internal energy $e = 8.14398\ \mathrm{MJ/kg}$. The equilibrium temperature and degree of dissociation are $T = 2775.15\ \mathrm{K}$ and $\alpha = 0.386874$, respectively. Case 2 corresponds to light dissociation and internal energy $e = 3.0758\ \mathrm{MJ/kg}$, where the equilibrium temperature and degree of dissociation are $T = 2377.85\ \mathrm{K}$ and $\alpha = 0.079069$, respectively. Case 3 corresponds to almost total dissociation and internal energy $e = 17.0\ \mathrm{MJ/kg}$. The equilibrium temperature and degree of dissociation are $T = 3392.0\ \mathrm{K}$ and $\alpha = 0.928500$, respectively.

The results of the robustness study for the Ideal Dissociating Oxygen Model are presented in Table 2 and Table 3 for the Mass Constraint Technique and Degree of Advancement Technique, respectively. For each category, the percentage of results that are correct, blowup, wrong and exceed the maximum number of iterations (50) are given, and are denoted in the table by %C, %B, %W and %M, respectively. A total of 10,100 computations were performed for each case, strategy and technique. The initial guesses for temperature and degree of dissociation were varied in the range $100\ K \leq T \leq 10{,}000\ K$ and $0 \leq \alpha \leq 1$ in equal increments of 100 *K* for the temperature and 0.01 for the degree of dissociation. It should be apparent that Case 2 is the most difficult case of the three since it has the lowest percentage of solutions that are correct when no corrections are made. Strategy 2 is completely successful at guiding convergence to the correct solution. Strategies 4 and 5 work perfectly with the Mass Constraint Technique, but their performance with the Degree of Advancement is worse than no correction at all. This was expected, since the Degree of Advancement does not enforce the mass constraints directly. The result is solutions where density is not conserved. Strategy 3 is not quite as successful as Strategy 2. The limit on the relative change per iteration slows convergence down, especially for particularly poor initial estimates for species densities. Hence, Strategy 3 shows an increase in computations where the maximum number of iterations have been exceeded, as is seen in the table. Also shown in Table 2 is the average number of iterations for the computations converging to the correct solution, which rarely exceeds 12. As was expected Strategy 3 appears to retard convergence. Strategies 2 and 5 seem to be the most efficient methods.

b. AIR DISSOCIATION AND IONIZATION RESULTS

In a similar fashion, robustness studies were performed using the 5 and 11–Species Air Models. Three cases were used, characterized by a density $\varrho = 1.293\ 10^{-2}\ \mathrm{kg/m^3}$. Case 1 corresponds to massive oxygen dissociation and internal energy $e = 6.94\ \mathrm{MJ/kg}$, where the equilibrium temperature is 4000 K. Case 2 corresponds to a halfway complete nitrogen dissociation and internal energy $e = 26.65\ \mathrm{MJ/kg}$, where the equilibrium temperature is 7000 K. Complete dissociation of nitrogen, disappearance of NO and appearance of some charged species characterize Case 3, where internal energy $e = 36.621\ \mathrm{MJ/kg}$, and the equilibrium temperature is 9000 K.

Initial guesses for temperature were varied in equal increments of 300 K over the range $300\ K \leq T \leq 30{,}000\ K$. Five sets of initial compositions were used: the first three are the equilibrium compositions corresponding to the three cases above; and the final two compositions correspond to totally undissociated and dissociated nitrogen and oxygen states, respectively. These initial compositions are given in two sets denoted Set 1 and Set 2, comprising the first three compositions and all five compositions, respectively. Set 1 has a total of 300 computations, while Set 2 encompasses all 500 computations. In light of the Ideal Dissociating Oxygen results, computations were performed using only Strategies 2 and 5 along with the baseline Strategy 1.

Results for 5-Species Air Model are shown in Table 4 and Table 5 for the Mass Constraint Technique and Degree of Advancement Technique, respectively. Notably apparent is the lack of robustness when no correction strategies are implemented, especially for Case 1. Strategy 2 provides a significant improvement over the baseline, particularly when used with the Degree of Advancement Technique. Strategy 5 is completely successful when used in conjunction with the Mass Constraint Technique. However, as was already seen in the oxygen dissociation results, it is ill-suited for use with the Degree of Advancement Technique.

Results obtained using 11-Species Air Model are given in Table 6 and Table 7 for the Mass Constraint Technique and Degree of Advancement Technique, respectively, and follow the same trend as the previous results for the 5-Species Air Model. However, the overall percentage of correct results has dropped slightly. This is due to the inclusion of charged species. It should be pointed out that the computations presented in these robustness studies were performed with poor initial estimates in order to test the robustness of the Black Box. These extreme situations should rarely occur when the Black Box is utilized in a flow solver, where good estimates are usually available. Again, the average number of iterations rarely exceeds 16.

6. EFFICIENCY

Comparative timing runs were made on a Cray XMP for the Mass Constraint Technique and Degree of Advancement Technique, using the Ideal Dissociating Oxygen Model, and 5, 11 and 17-Species Air Models. The Degree of Advancement Technique outperformed the Mass Constraint Technique: the CPU times per iteration per computational cell were 0.0355, 0.141, 0.98 and 2.72 msec, respectively for the Degree of Advancement Technique, and were 0.0533, 0.215, 1.20 and 3.25 msec, respectively for the Mass Constraint Technique. Thus, the increase in the complexity of the Jacobians is less time consuming than the computational savings afforded by the reduced set of equations.

Numerical experiments were performed in order to test the efficiency of the vector reduction implementation. The 5-Species Air Model was employed for the computation of the equilibrium state corresponding to complete dissociation of oxygen, with density $\varrho = 1.293 \ 10^{-2}$ kg/m^3 and internal energy $e = 6.614$ MJ/kg. The equilibrium temperature is 3996.0 K. The initial problem was composed of 1000 cells in which the composition is given by the equilibrium solution, and only the initial estimates for temperature are perturbed. Two cases were studied. The first case corresponds to a uniform unconverged field, where all the unconverged cells start with the same initial conditions and hence will have the same convergence rate. The second case utilizes a variable unconverged field, in which the unconverged cells start at different initial values for temperature, with convergence varying from 1 to 20 iterations. For each case, five computations were performed for fields in which the percentage of initially converged cells are 0, 33, 50, 67, 90 and 99 percent. All computations were performed on a Cray XMP, and the cpu times were recorded.

The results showing the vector reduction performance appear in Figure 37, where the percent reduction in computational time is given versus the percentage of initially converged cells. The case of the uniform unconverged field represents the baseline for all the calculations. The initial overhead of the vector reduction implementation, given for the computation for which there are no converged cells, was found to increase the cpu time by about 6 percent. For the variable unconverged field, an initial savings of 30 percent can be realized. The break even point for the uniform unconverged case occurs when about 9 percent of the field is initially converged. For higher percentages of initially converged cells, vector reduction produces substantial savings in cpu time. This is especially true for the case of a variable unconverged field, which is a more realistic model. When used in conjunction with a flow solver, in which a relatively high percentage of the computational cells are initially converged or nearly converged, a significant decrease in the computational expense of the Black Box should be realized. This last statement will be verified in the results for the flow solver.

Numerical studies were also made of the effects of freezing the Jacobian matrix utilized for the Newton–Raphson iterations, with mixed results. Different strategies were employed, changing the residual value at which freezing was initiated and the number of frozen iterations. The results showed that for computations starting with a good initial guess for the composition and temperature, a freezing strategy could be useful. A more detailed discussion is given in Cinnella and Cox [Reference 25].

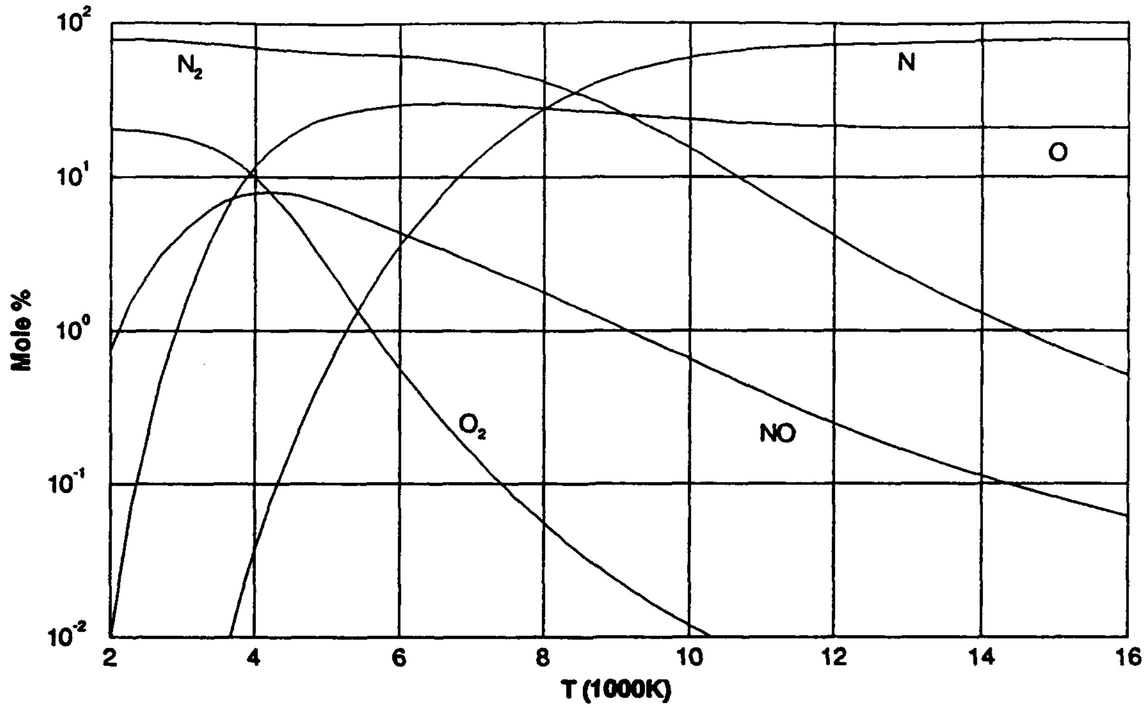

Figure 1 Mole fractions versus temperature. 5–Species Air Model, Vibrational Model, $\varrho = 1.293\ \mathrm{kg/m^3}$.

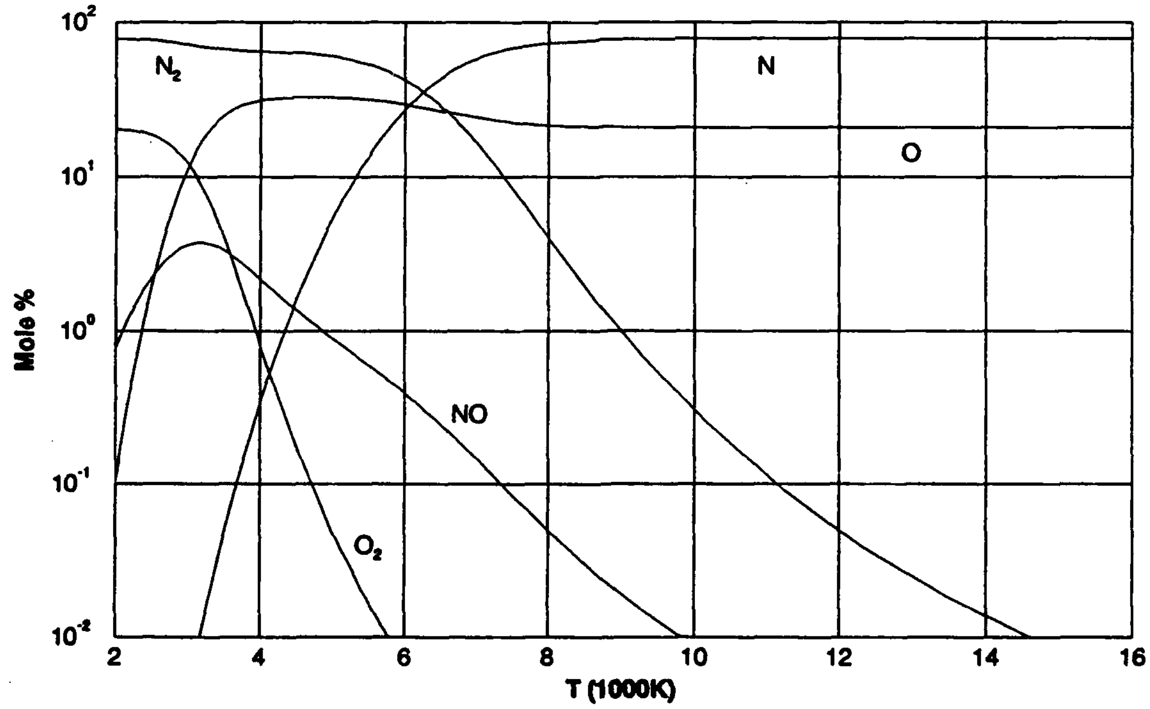

Figure 2 Mole fractions versus temperature. 5–Species Air Model, Vibrational Model, $\varrho = 1.293\ 10^{-2}\ \mathrm{kg/m^3}$.

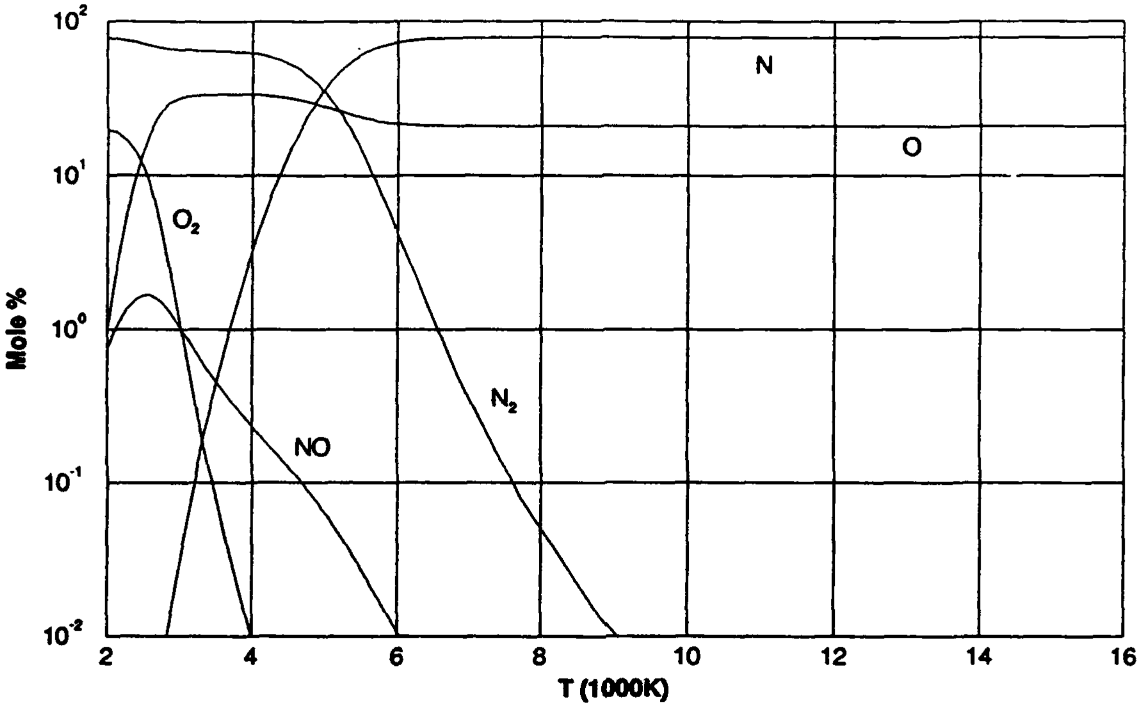

Figure 3 Mole fractions versus temperature. 5-Species Air Model, Vibrational Model, $\varrho = 1.293\ 10^{-4}$ kg/m^3.

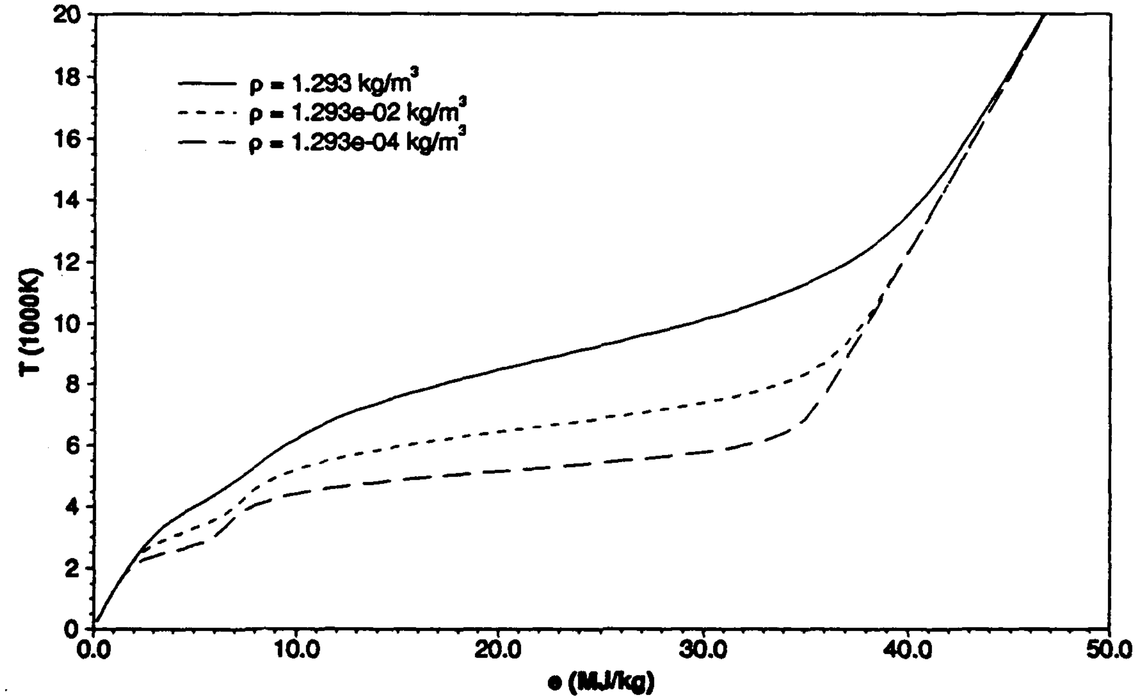

Figure 4 Temperature versus internal energy. 5-Species Air Model, Vibrational Model.

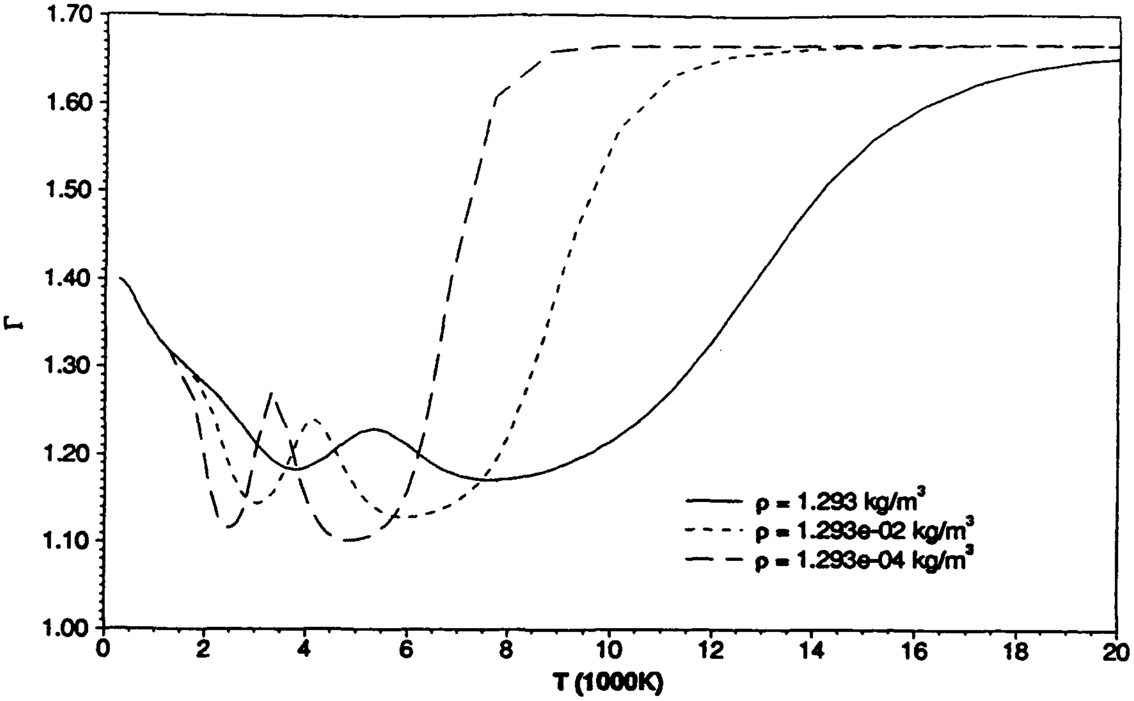

Figure 5 Isentropic index versus temperature. 5-Species Air Model, Vibrational Model.

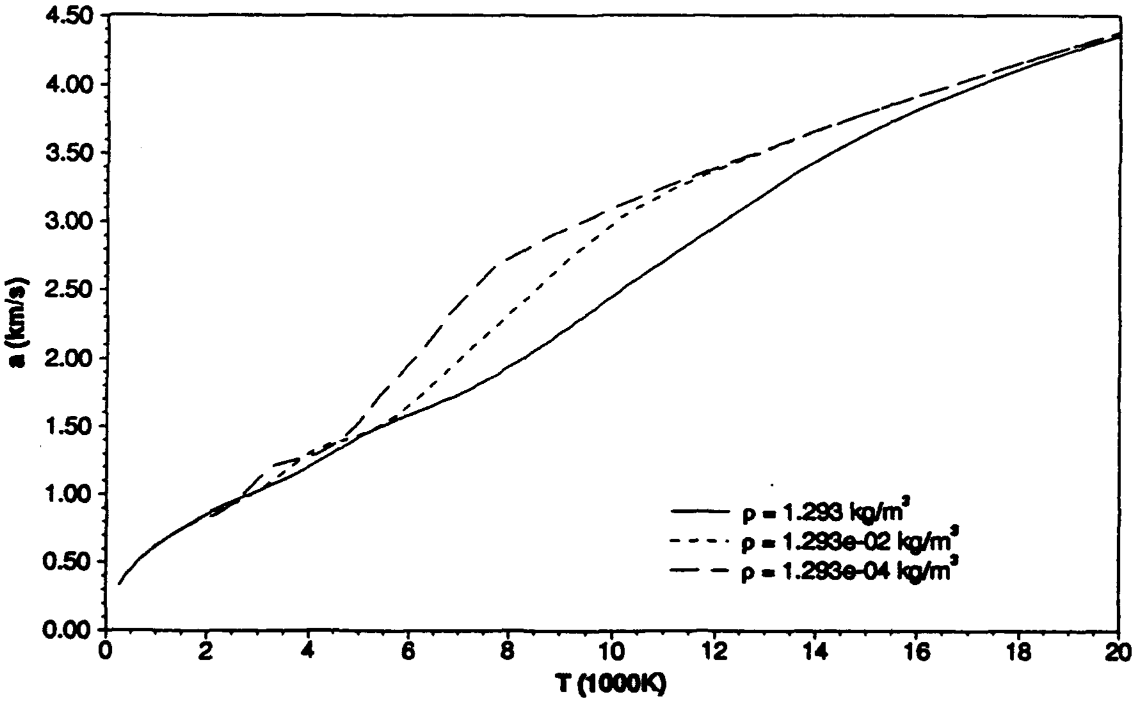

Figure 6 Speed of sound versus temperature. 5-Species Air Model, Vibrational Model.

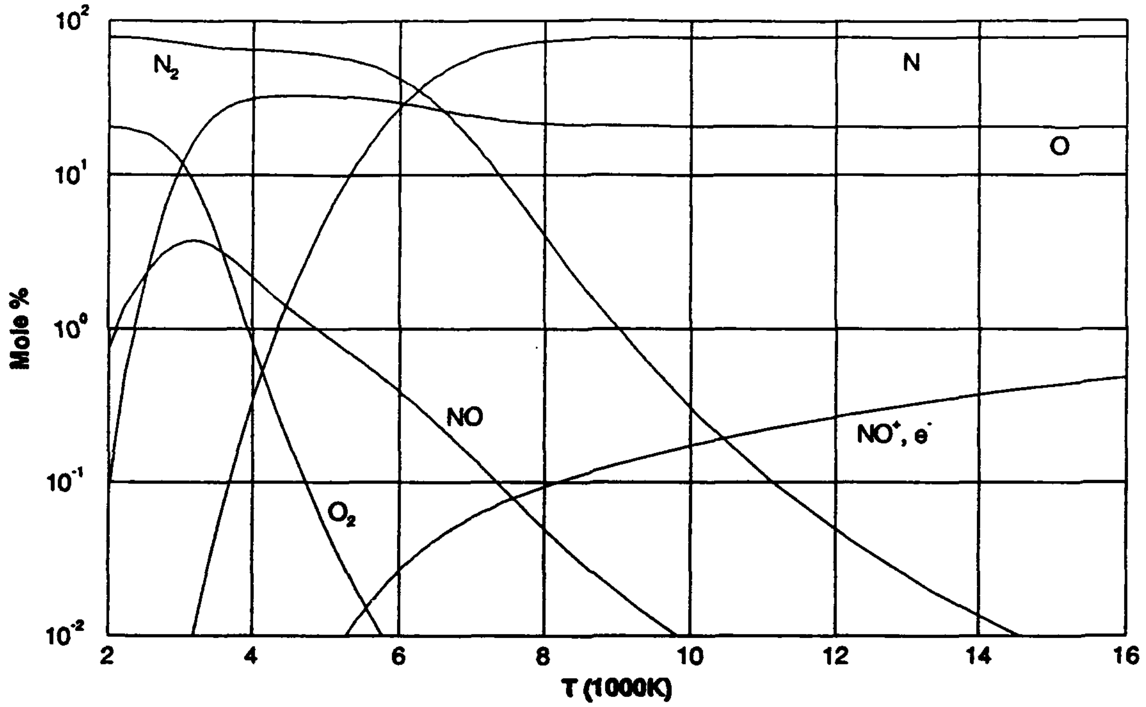

Figure 7 Mole fractions versus temperature. 7-Species Air Model, Vibrational Model, $\varrho = 1.293\ 10^{-2}$ kg/m^3.

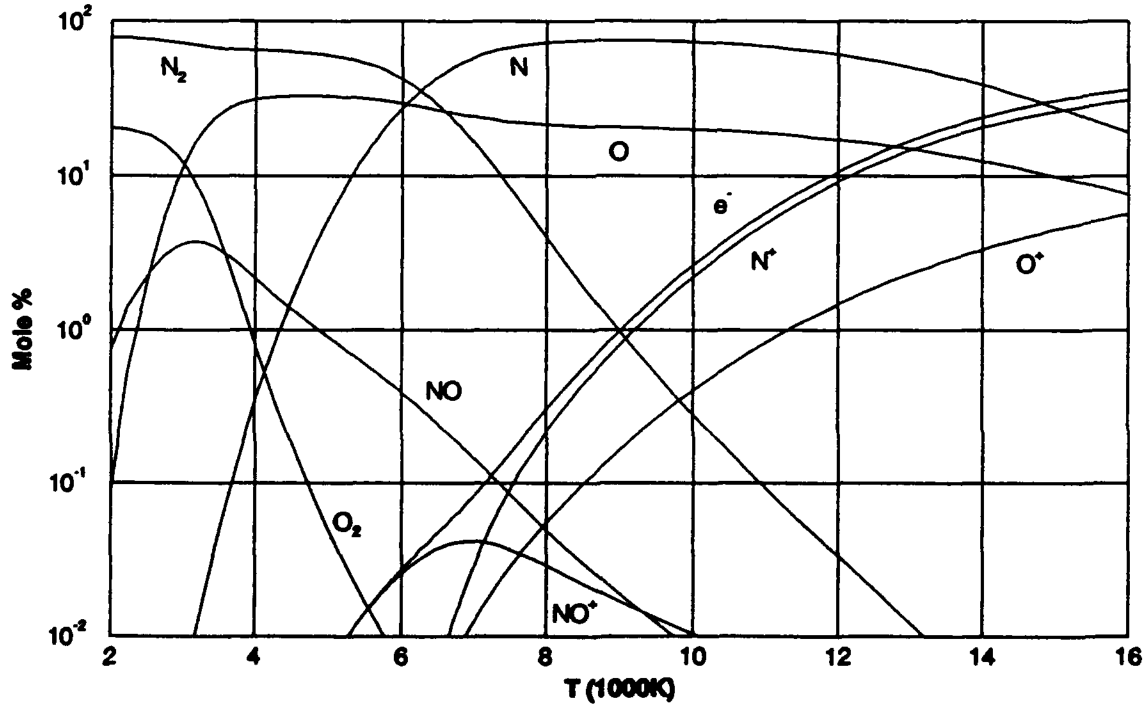

Figure 8 Mole fractions versus temperature. 9-Species Air Model, Vibrational Model, $\varrho = 1.293\ 10^{-2}$ kg/m^3.

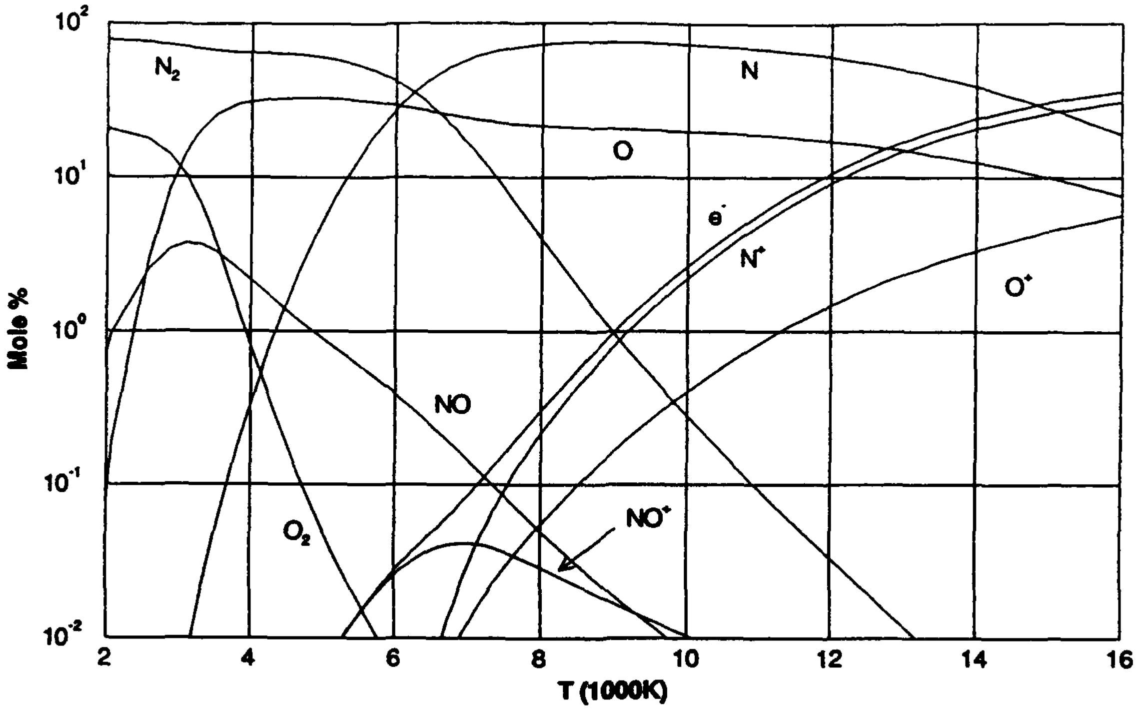

Figure 9 Mole fractions versus temperature. 11–Species Air Model, Vibrational Model, $\varrho = 1.293\ 10^{-2}\ \mathrm{kg/m^3}$.

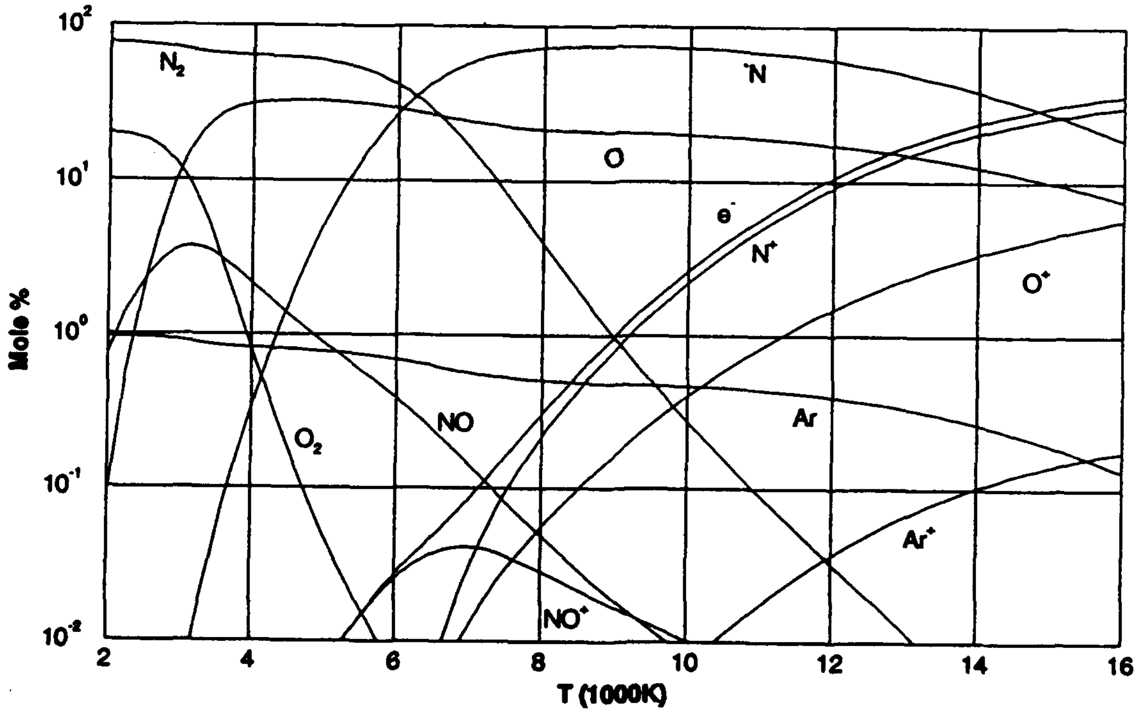

Figure 10 Mole fractions versus temperature. 13–Species Air Model, Vibrational Model, $\varrho = 1.293\ 10^{-2}\ \mathrm{kg/m^3}$.

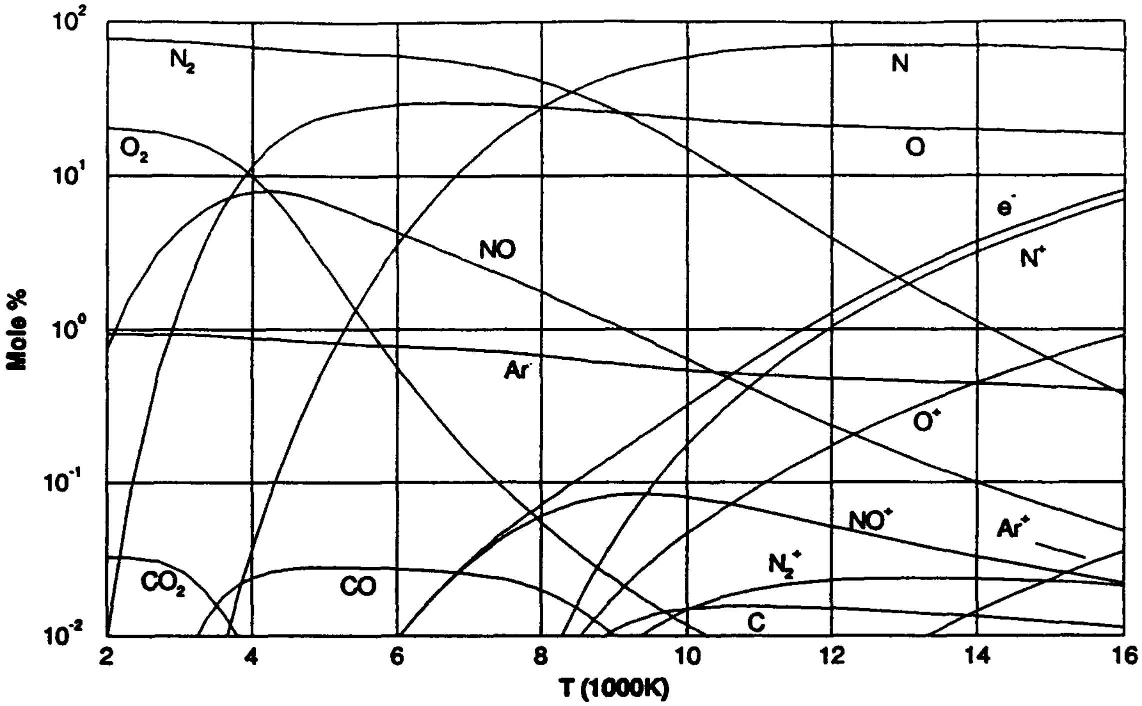

Figure 11 Mole fractions versus temperature. 17–Species Air Model, Vibrational Model, $\varrho = 1.293$ kg/m^3.

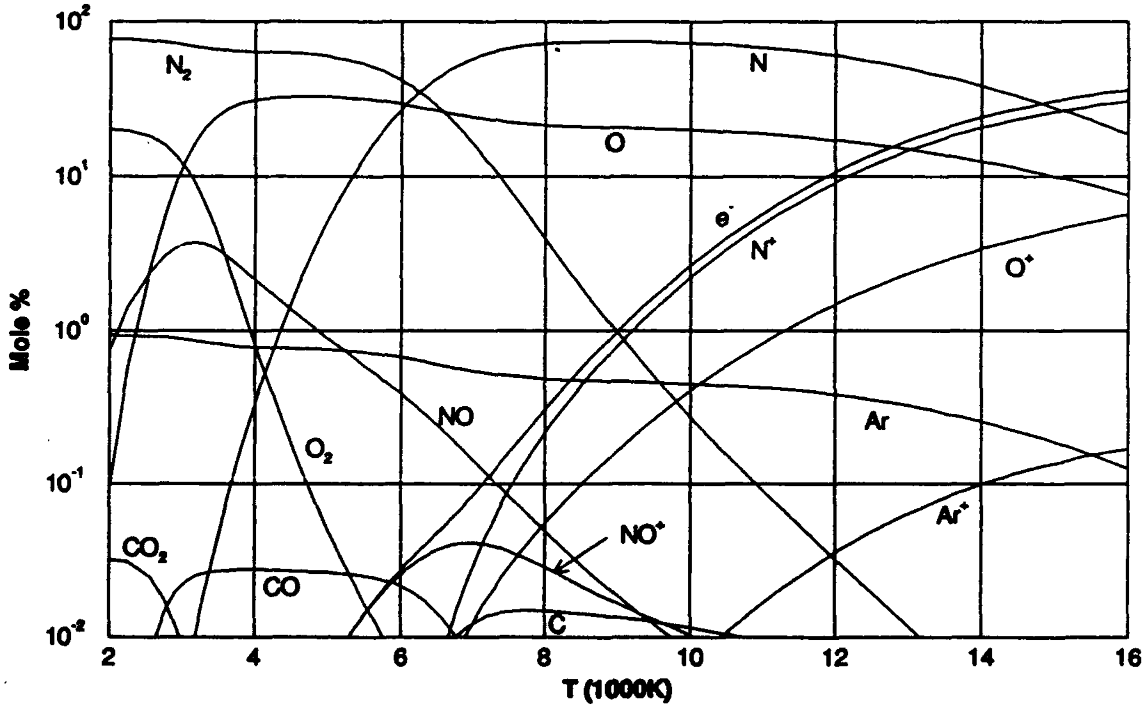

Figure 12 Mole fractions versus temperature. 17–Species Air Model, Vibrational Model, $\varrho = 1.293\ 10^{-2}$ kg/m^3.

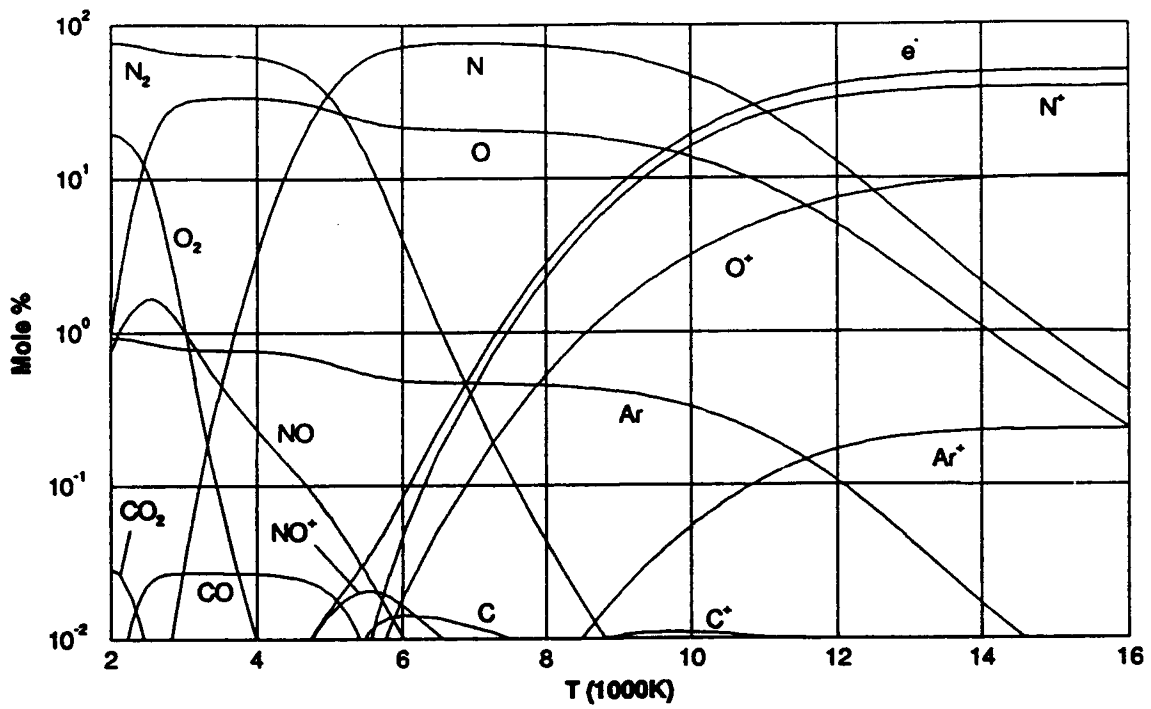

Figure 13 Mole fractions versus temperature. 17-Species Air Model, Vibrational Model, $\varrho = 1.293\ 10^{-4}\ \mathrm{kg/m^3}$.

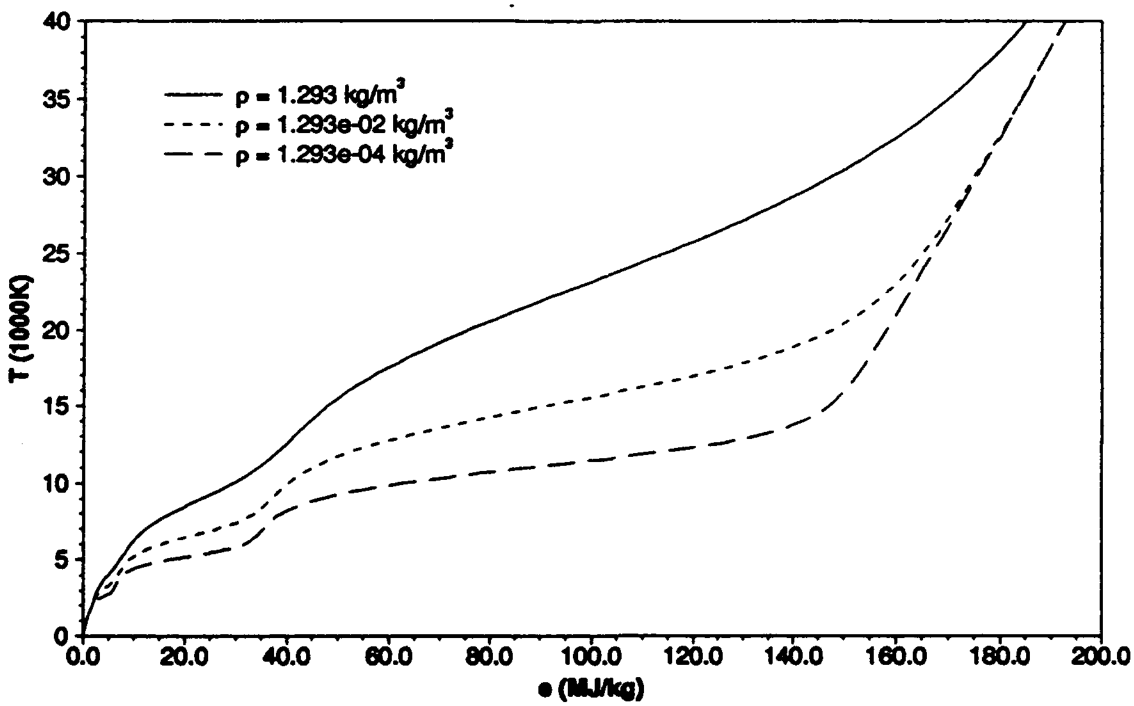

Figure 14 Temperature versus internal energy. 17-Species Air Model, Vibrational Model.

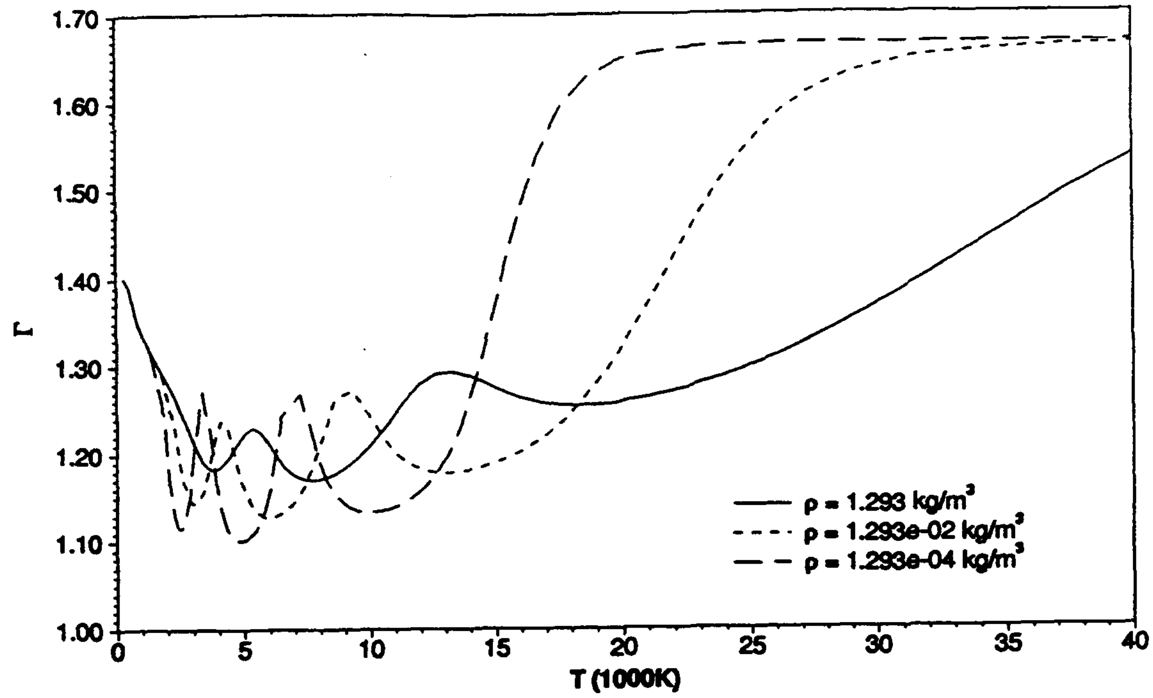

Figure 15 Isentropic index versus temperature. 17–Species Air Model, Vibrational Model.

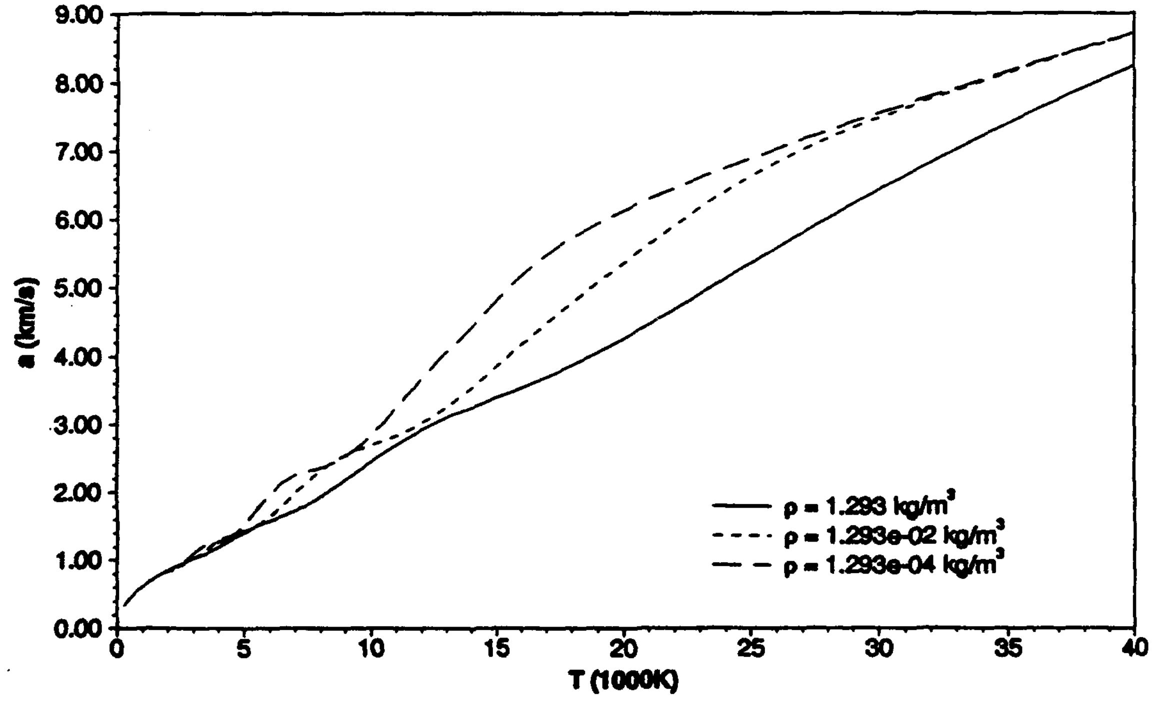

Figure 16 Speed of sound versus temperature. 17–Species Air Model, Vibrational Model.

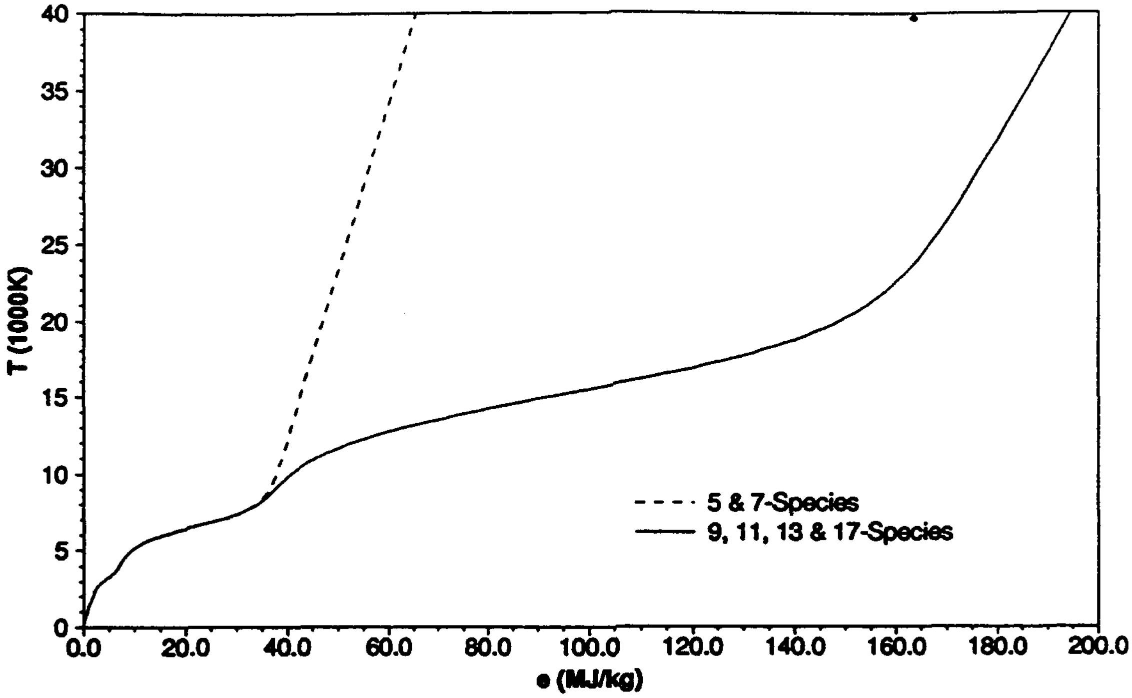

Figure 17 Temperature versus internal energy. All air models, Vibrational Model, $\varrho = 1.293\ 10^{-2}$ kg/m^3.

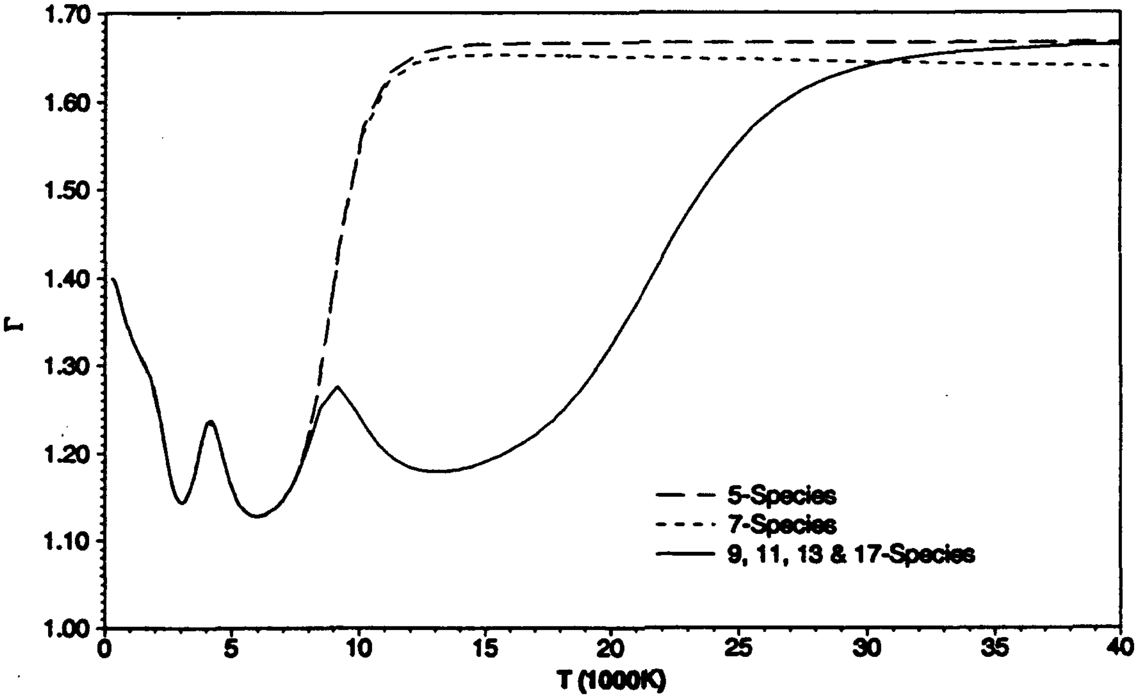

Figure 18 Isentropic index versus temperature. All air models, Vibrational Model, $\varrho = 1.293\ 10^{-2}$ kg/m^3.

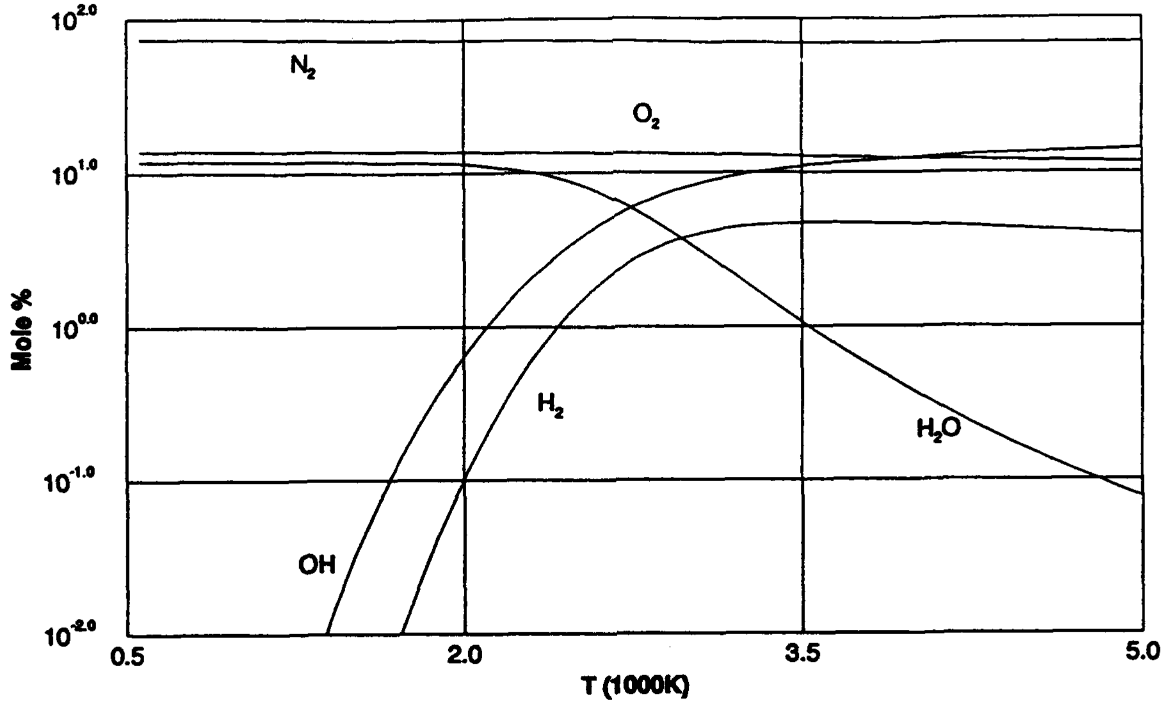

Figure 19 Mole fractions versus temperature. Hydrogen-Air Combustion Model, Vibrational Model, $\varrho = 1.324\ 10^{-3}\ \mathrm{kg/m^3}$.

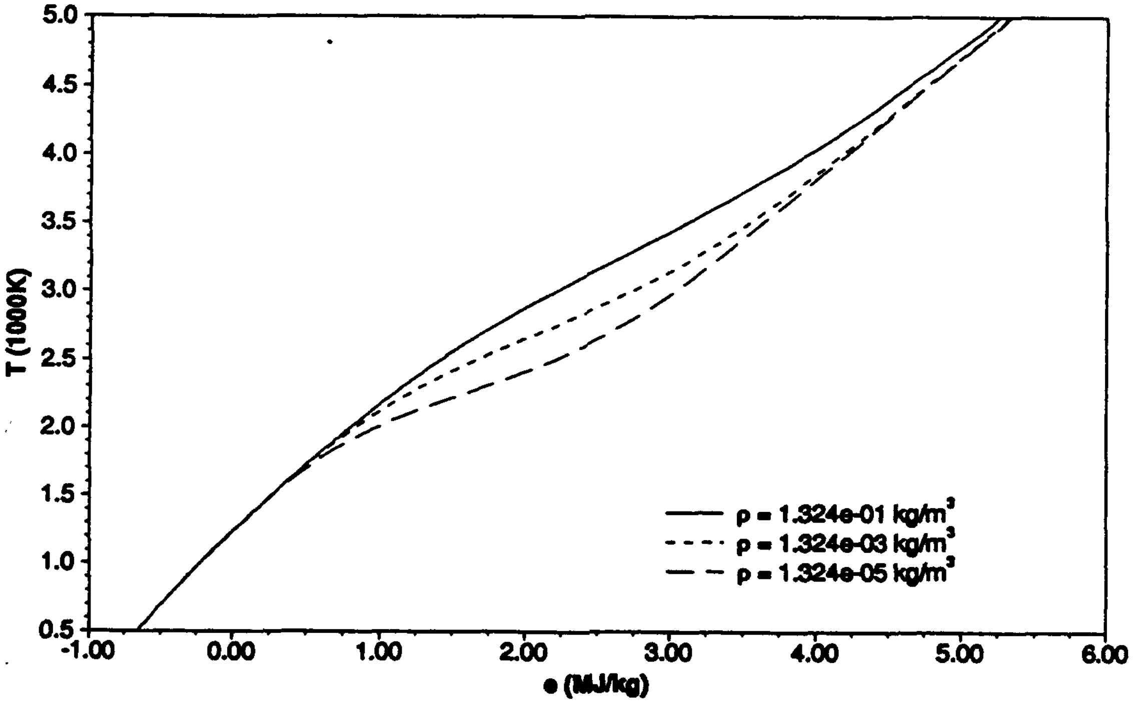

Figure 20 Temperature versus internal energy. Hydrogen-Air Combustion Model, Vibrational Model.

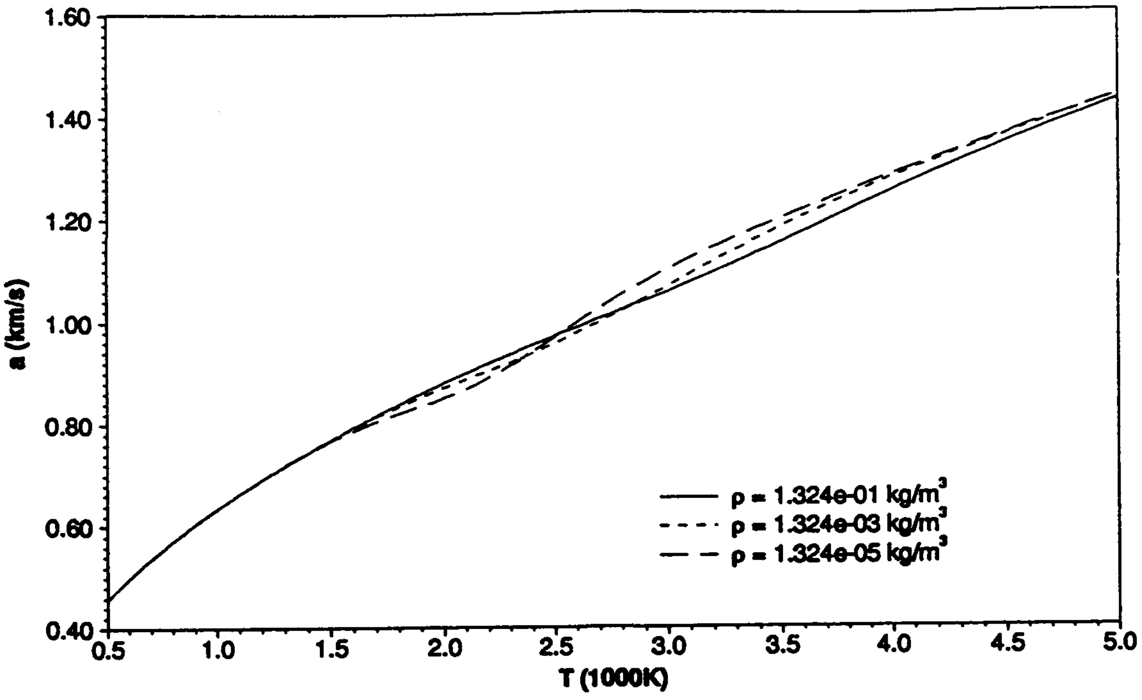

Figure 21 Speed of sound versus temperature. Hydrogen–Air Combustion Model, Vibrational Model.

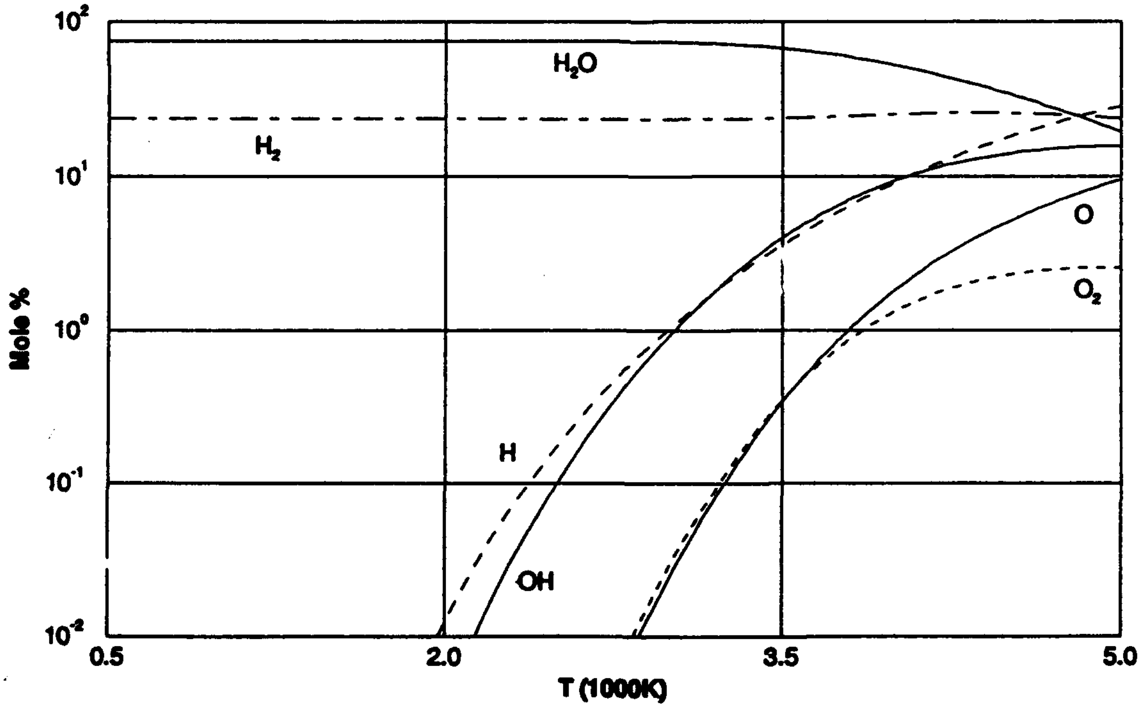

Figure 22 Mole fractions versus temperature. Hydrogen–Oxygen Combustion Model, Vibrational Model, $\rho = 2.8306$ kg/m^3.

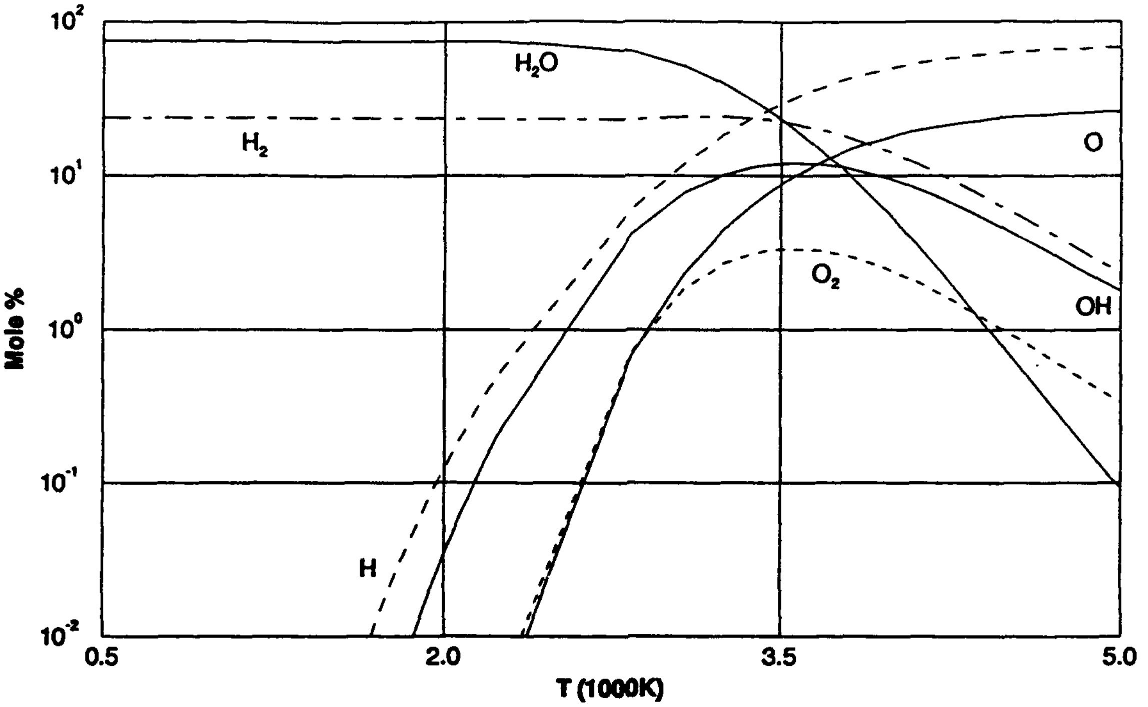

Figure 23 Mole fractions versus temperature. Hydrogen–Oxygen Combustion Model, Vibrational Model, $\varrho = 2.8306\ 10^{-2}\ kg/m^3$.

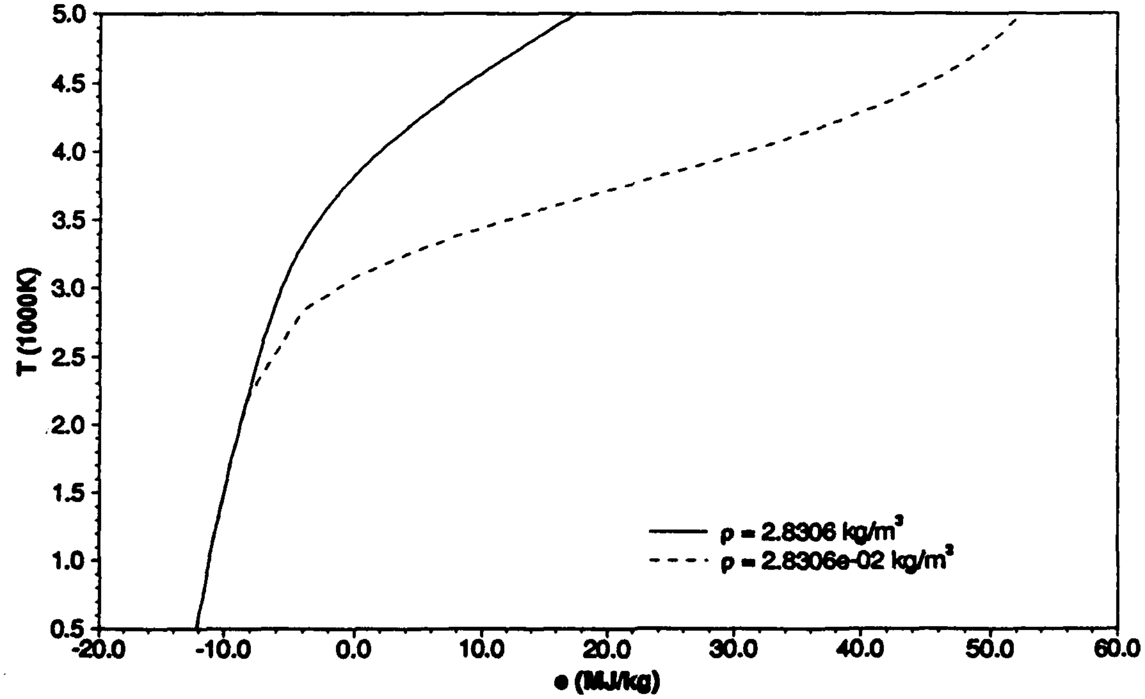

Figure 24 Temperature versus internal energy. Hydrogen–Oxygen Combustion Model, Vibrational Model.

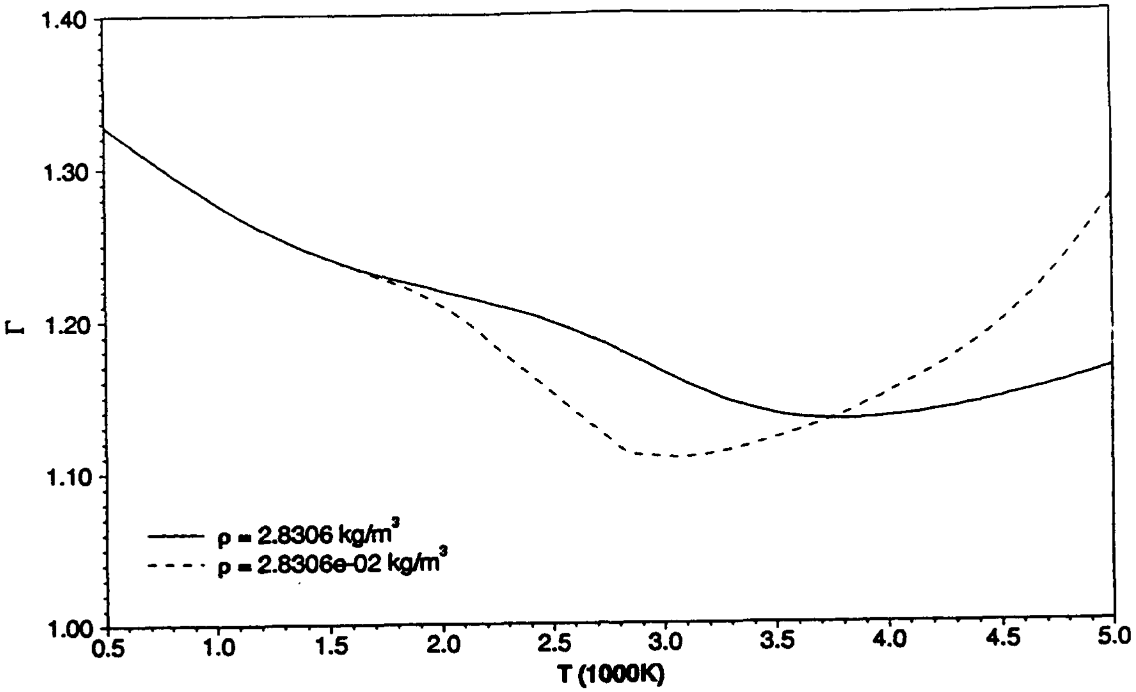

Figure 25 Isentropic index versus temperature. Hydrogen–Oxygen Combustion Model.

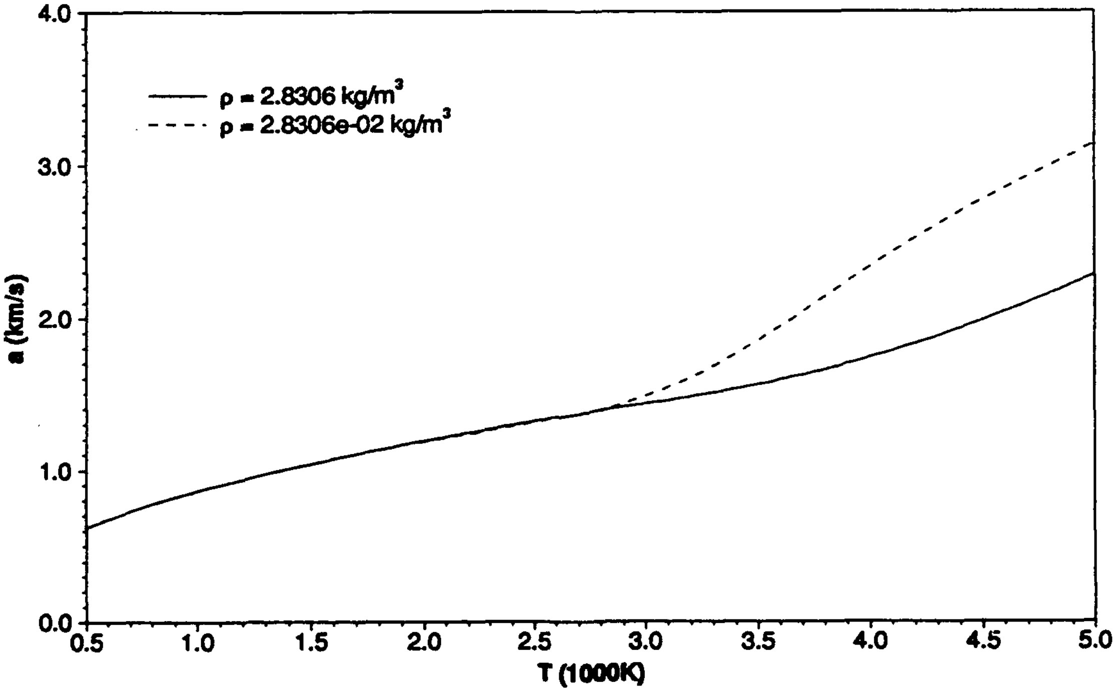

Figure 26 Speed of sound versus temperature. Hydrogen–Oxygen Combustion Model.

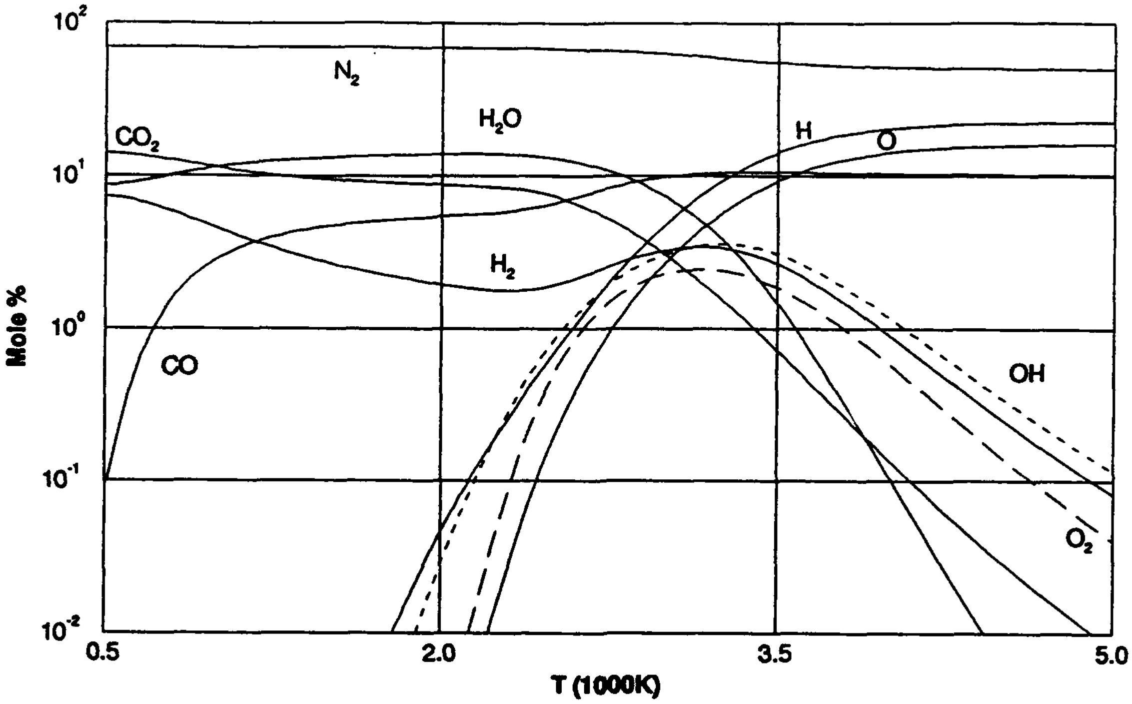

Figure 27 Mole fractions versus temperature. Hydrocarbon Combustion Model, $\varrho = 3.295\ 10^{-2}$ kg/m^3.

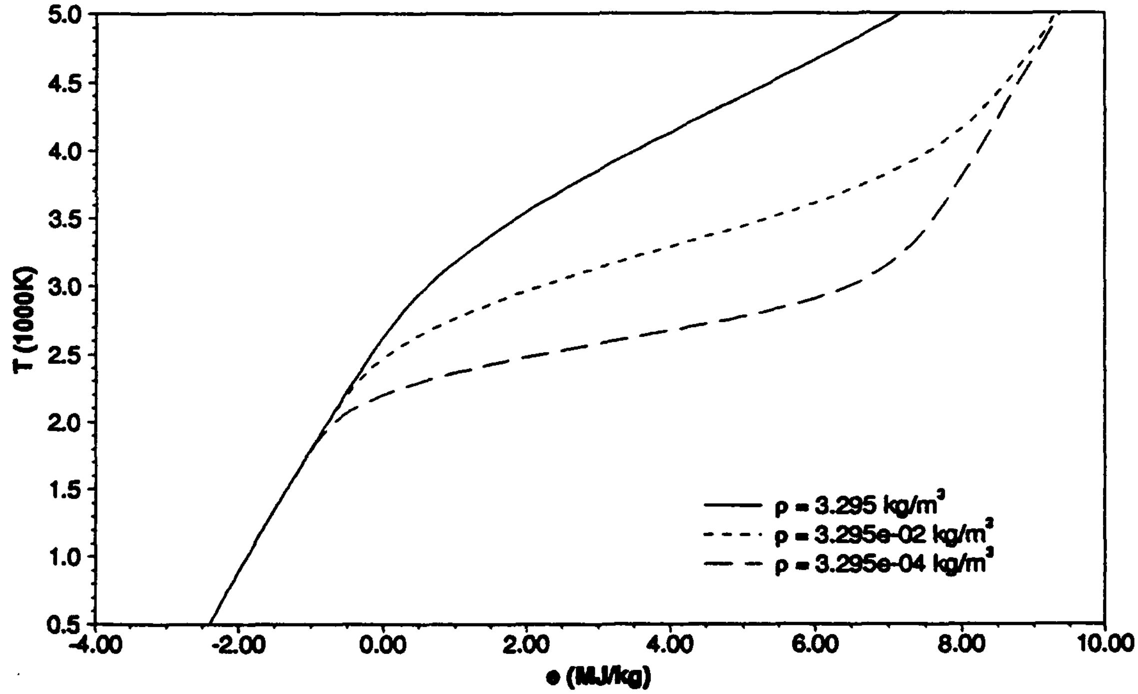

Figure 28 Temperature versus internal energy. Hydrocarbon Combustion Model.

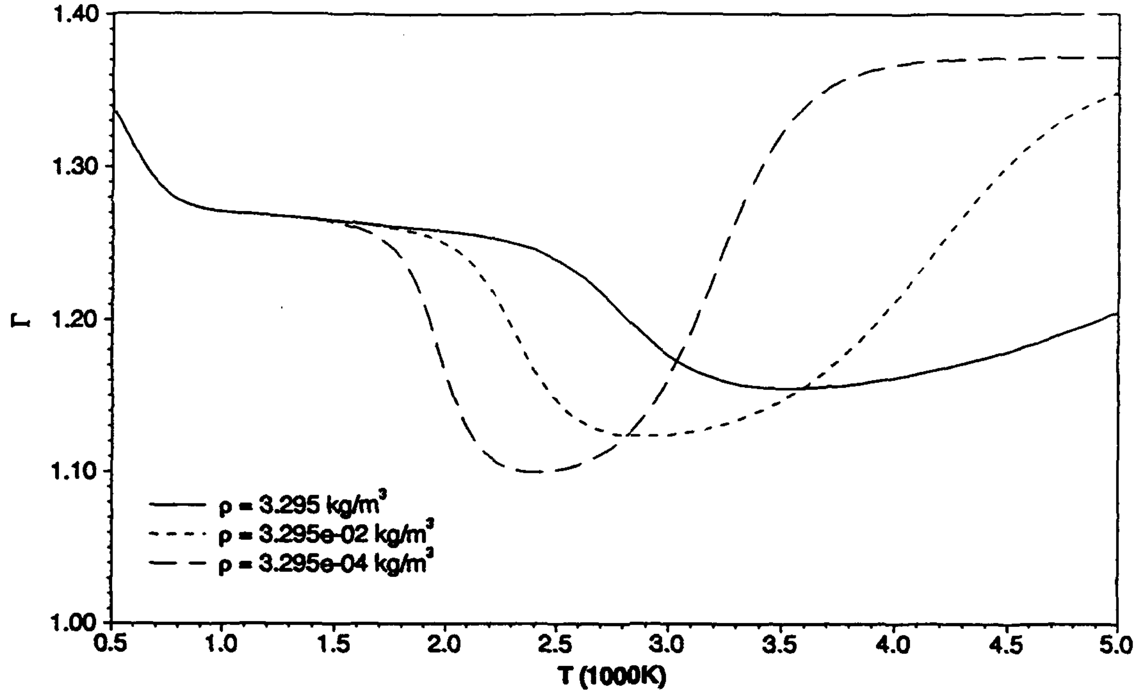

Figure 29 Isentropic index versus temperature. Hydrocarbon Combustion Model.

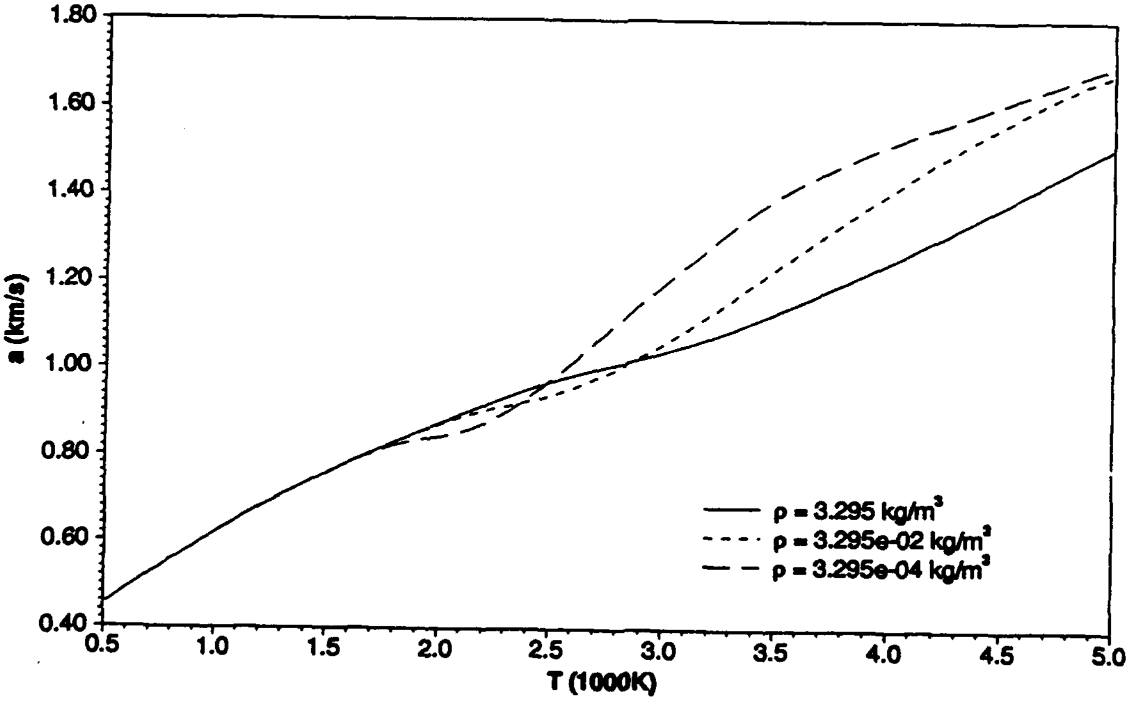

Figure 30 Speed of sound versus temperature. Hydrocarbon Combustion Model.

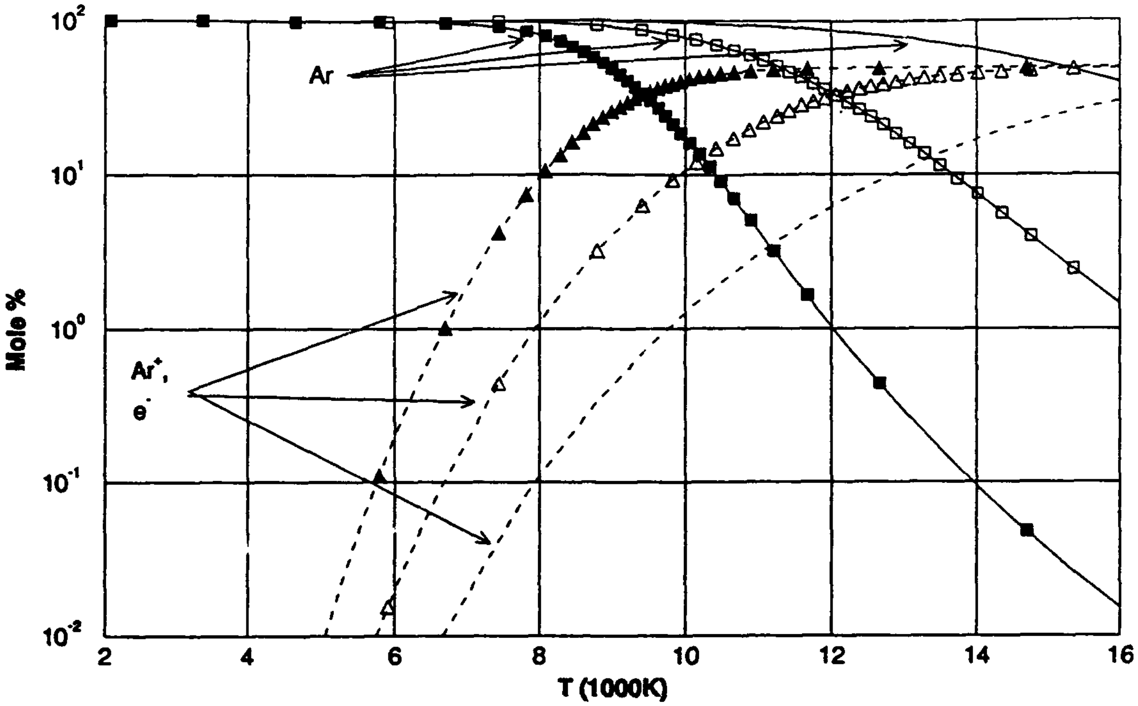

Figure 31 Mole fractions versus temperature. Argon Plasma Model.

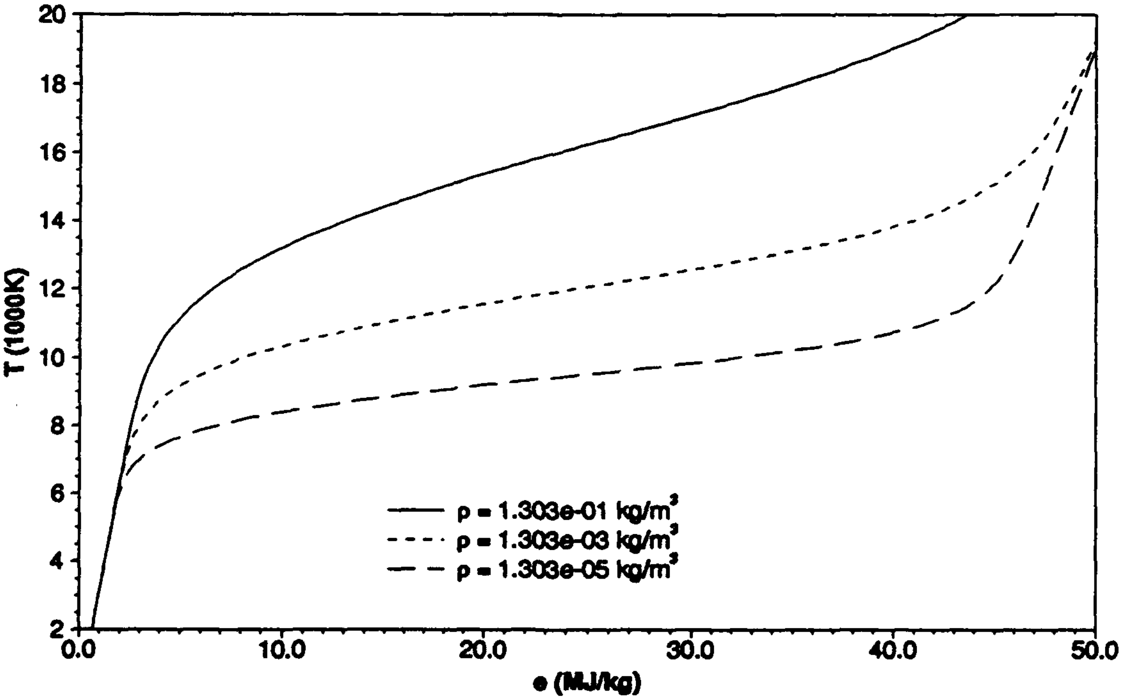

Figure 32 Temperature versus internal energy. Argon Plasma Model.

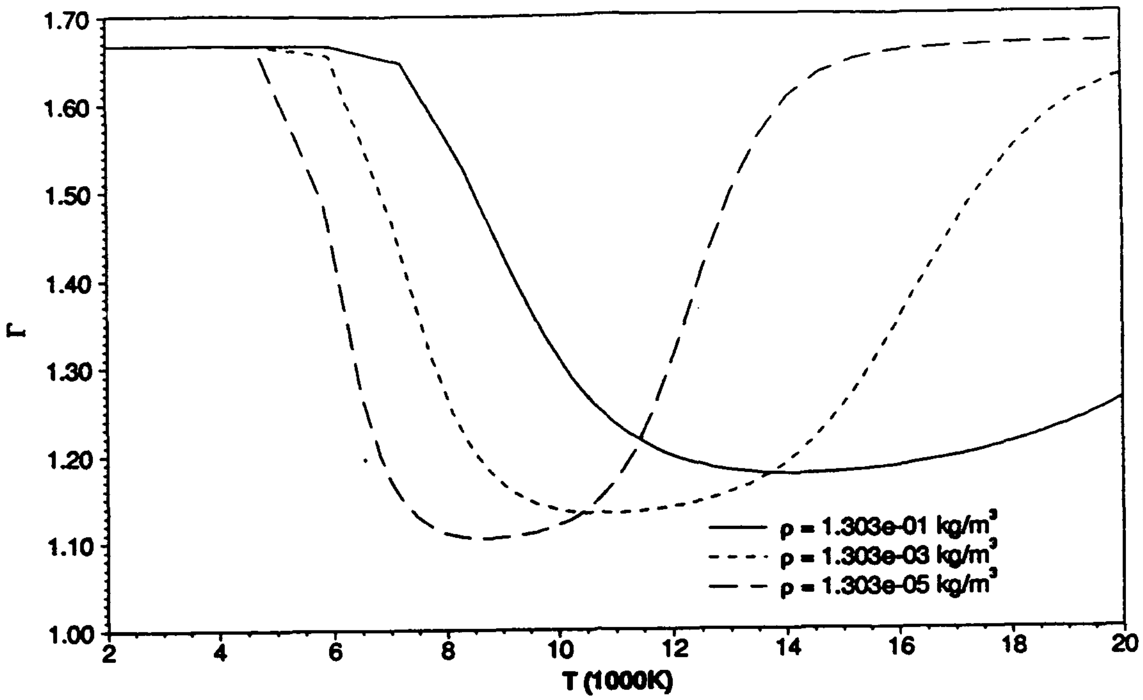

Figure 33 Isentropic index versus temperature. Argon Plasma Model.

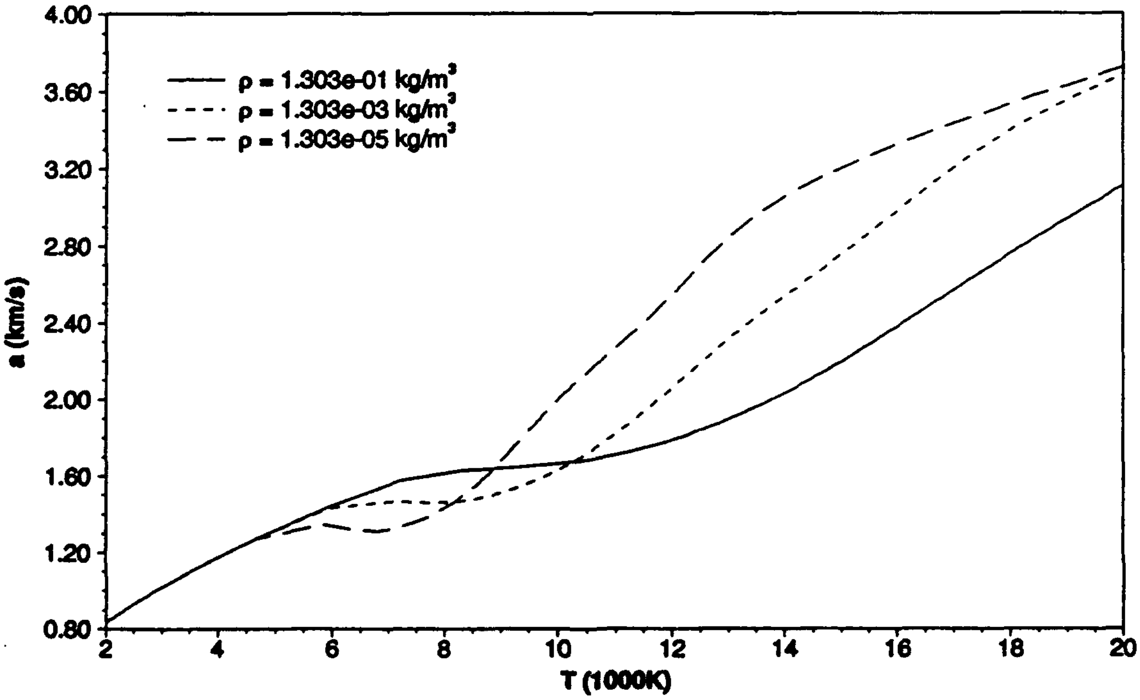

Figure 34 Speed of sound versus temperature. Argon Plasma Model.

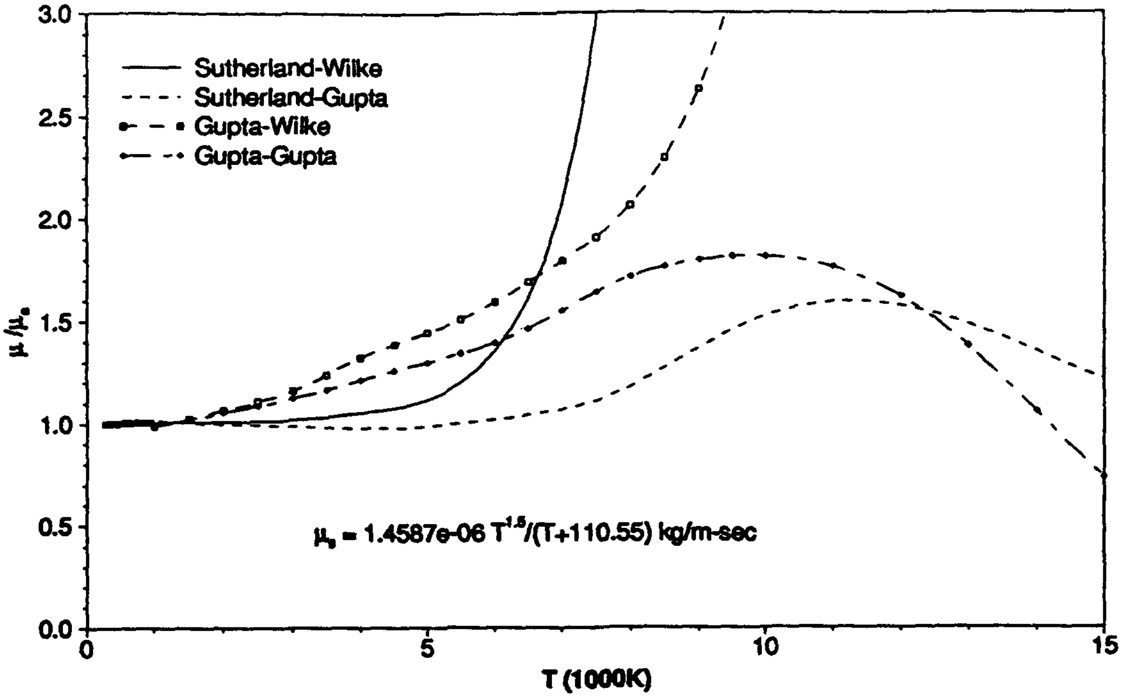

Figure 35 Comparison of mixture viscosity evaluation methods. 11–Species Air Model, p = 1 atm.

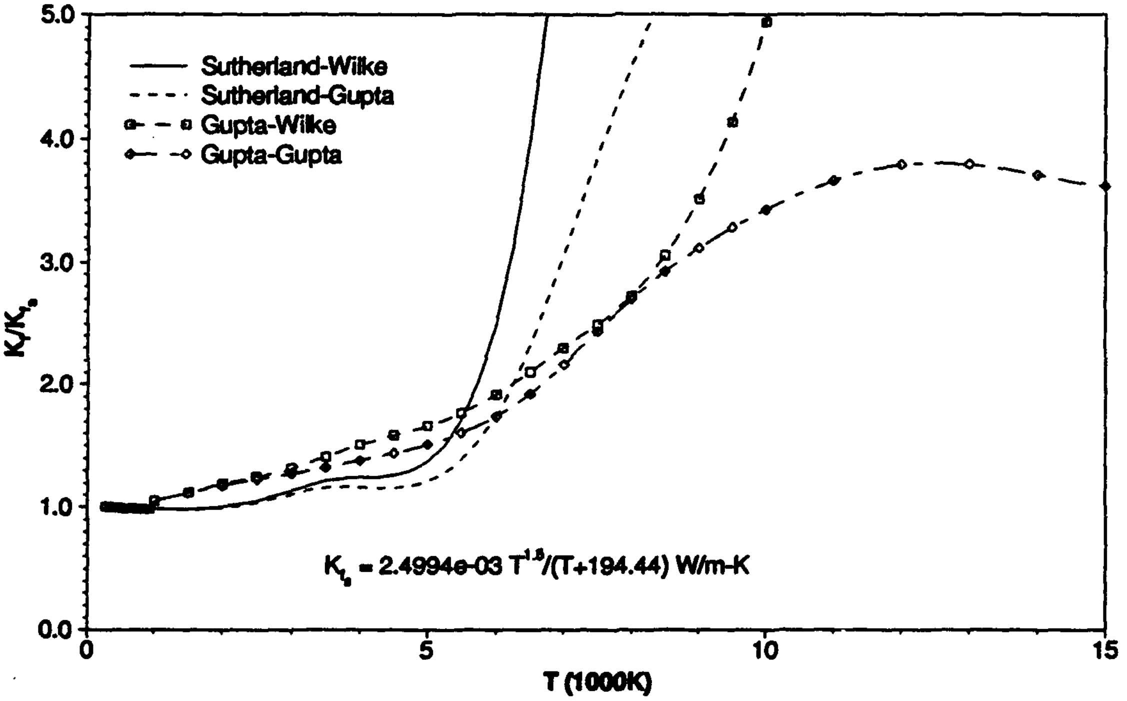

Figure 36 Comparison of mixture thermal conductivity evaluation methods. 11–Species Air Model, p = 1 atm.

		Method 1	Method 2	Method 3	Method 4	Method 5
Case 1	% C	95.98	100.00	97.15	100.00	100.00
	% B	0.07	0.00	0.00	0.00	0.00
	% W	2.94	0.00	0.00	0.00	0.00
	% M	1.01	0.00	2.85	0.00	0.00
	Avg. It.	12.43	10.91	16.56	12.38	10.91
Case 2	% C	78.29	100.00	96.87	100.00	100.00
	% B	0.38	0.00	0.00	0.00	0.00
	% W	16.57	0.00	0.00	0.00	0.00
	% M	4.76	0.00	3.13	0.00	0.00
	Avg. It.	12.05	10.34	15.08	11.72	12.66
Case 3	% C	100.00	100.00	100.00	100.00	100.00
	% B	0.00	0.00	0.00	0.00	0.00
	% W	0.00	0.00	0.00	0.00	0.00
	% M	0.00	0.00	0.00	0.00	0.00
	Avg. It.	12.88	10.50	16.89	12.88	10.50

Table 2. Robustness study, Ideal Dissociating Oxygen Model, Mass Constraint Technique

		Method 1	Method 2	Method 3	Method 4	Method 5
Case 1	% C	95.98	100.00	98.57	100.00	100.00
	% B	0.07	0.00	0.00	0.00	0.00
	% W	2.94	0.00	0.00	0.00	0.00
	% M	1.01	0.00	1.43	0.00	0.00
	Avg. It.	12.43	10.91	15.06	12.38	10.91
Case 2	% C	78.29	100.00	98.57	58.80	55.28
	% B	0.38	0.00	0.00	0.00	0.00
	% W	16.57	0.00	0.00	41.20	44.72
	% M	4.76	0.00	1.43	0.00	0.00
	Avg. It.	12.00	10.30	15.31	8.44	9.48
Case 3	% C	100.00	100.00	100.00	99.83	99.83
	% B	0.00	0.00	0.00	0.00	0.00
	% W	0.00	0.00	0.00	0.17	0.17
	% M	0.00	0.00	0.00	0.00	0.00
	Avg. It.	12.85	10.47	13.49	12.85	10.47

Table 3. Robustness study, Ideal Dissociating Oxygen Model, Degree of Advancement Technique

		Method 1		Method 2		Method 5	
		Set 1	Set 2	Set 1	Set 2	Set 1	Set 2
Case 1	%C	3.33	6.00	98.67	84.00	100.00	100.00
	%B	45.67	47.60	0.00	0.00	0.00	0.00
	%W	51.00	46.40	0.00	0.20	0.00	0.00
	%M	0.00	0.00	1.33	15.80	0.00	0.00
	Avg. It.	9.80	11.50	13.13	13.84	15.01	15.34
Case 2	%C	86.33	71.20	98.00	90.80	100.00	100.00
	%B	0.00	10.40	0.00	0.00	0.00	0.00
	%W	13.67	18.40	0.33	3.40	0.00	0.00
	%M	0.00	0.00	1.67	5.80	0.00	0.00
	Avg. It.	17.24	17.28	15.53	16.09	14.24	14.69
Case 3	%C	73.67	62.00	81.00	65.20	100.00	100.00
	%B	0.33	1.60	0.00	0.00	0.00	0.00
	%W	26.00	36.40	1.33	1.20	0.00	0.00
	%M	0.00	0.00	17.67	33.60	0.00	0.00
	Avg. It.	15.93	15.72	13.65	13.42	15.60	15.88

Table 4. Robustness study, 5-Species Air Model, Mass Constraint Technique

		Method 1		Method 2		Method 5	
		Set 1	Set 2	Set 1	Set 2	Set 1	Set 2
Case 1	%C	3.33	6.00	99.00	84.20	28.67	34.80
	%B	45.67	47.60	0.00	0.00	0.00	0.00
	%W	51.00	46.40	0.00	10.80	71.33	65.20
	%M	0.00	0.00	1.00	5.00	0.00	0.00
	Avg. It.	9.60	11.17	12.84	13.64	13.08	14.11
Case 2	%C	86.33	71.20	100.00	91.40	57.67	55.20
	%B	0.00	10.40	0.00	0.00	0.00	0.00
	%W	13.67	18.40	0.00	6.80	42.33	44.80
	%M	0.00	0.00	0.00	1.80	0.00	0.00
	Avg. It.	16.73	16.78	15.75	16.09	12.01	12.28
Case 3	%C	73.67	62.00	98.33	90.00	49.00	48.40
	%B	0.33	1.60	0.00	0.00	0.00	0.00
	%W	26.00	36.40	0.00	1.20	51.00	51.60
	%M	0.00	0.00	1.67	8.80	0.00	0.00
	Avg. It.	15.35	15.12	14.72	14.60	10.88	10.95

Table 5. Robustness study, 5-Species Air Model, Degree of Advancement Technique

		Method 1		Method 2		Method 5	
		Set 1	Set 2	Set 1	Set 2	Set 1	Set 2
Case 1	%C	3.00	3.80	69.67	54.40	97.67	98.40
	%B	43.67	47.00	0.00	0.00	0.00	0.00
	%W	46.00	41.00	0.33	0.80	0.00	0.00
	%M	7.33	8.20	30.00	44.80	2.33	1.60
	Avg. It.	9.89	14.00	15.31	17.75	18.65	20.01
Case 2	%C	22.00	23.40	36.33	28.20	99.33	99.40
	%B	19.00	35.60	0.00	0.00	0.00	0.00
	%W	43.67	31.00	0.00	0.00	0.00	0.00
	%M	15.33	10.00	63.67	71.80	0.67	0.40
	Avg. It.	15.14	16.14	12.72	15.34	15.44	17.06
Case 3	%C	42.67	27.60	25.67	16.20	100.00	100.00
	%B	27.67	41.00	0.00	0.00	0.00	0.00
	%W	20.33	25.20	0.00	0.40	0.00	0.00
	%M	9.33	6.20	74.33	83.40	0.00	0.00
	Avg. It.	14.90	15.79	15.79	16.43	16.39	17.95

Table 6. Robustness study, 11-Species Air Model, Mass Constraint Technique

		Method 1		Method 2		Method 5	
		Set 1	Set 2	Set 1	Set 2	Set 1	Set 2
Case 1	%C	3.00	3.60	67.00	66.40	26.67	30.00
	%B	44.00	49.40	0.00	0.00	51.00	45.40
	%W	51.00	44.40	7.00	5.00	22.33	24.60
	%M	2.00	2.60	26.00	28.60	0.00	0.00
	Avg. It.	10.00	13.44	17.09	20.10	14.24	18.25
Case 2	%C	22.00	23.40	53.33	37.20	16.33	10.40
	%B	22.00	37.40	0.00	0.00	29.00	25.60
	%W	54.00	38.00	0.00	0.60	54.67	64.00
	%M	2.00	1.20	46.67	62.20	0.00	0.00
	Avg. It.	14.79	15.85	14.59	16.64	10.10	10.56
Case 3	%C	43.00	27.80	29.00	20.00	10.00	10.20
	%B	29.33	41.00	0.00	0.00	26.00	23.40
	%W	26.67	30.40	0.00	0.00	64.00	66.40
	%M	1.00	0.80	71.00	80.00	0.00	0.00
	Avg. It.	13.90	14.38	11.09	13.95	9.60	11.88

Table 7. Robustness study, 11-Species Air Model, Degree of Advancement Technique

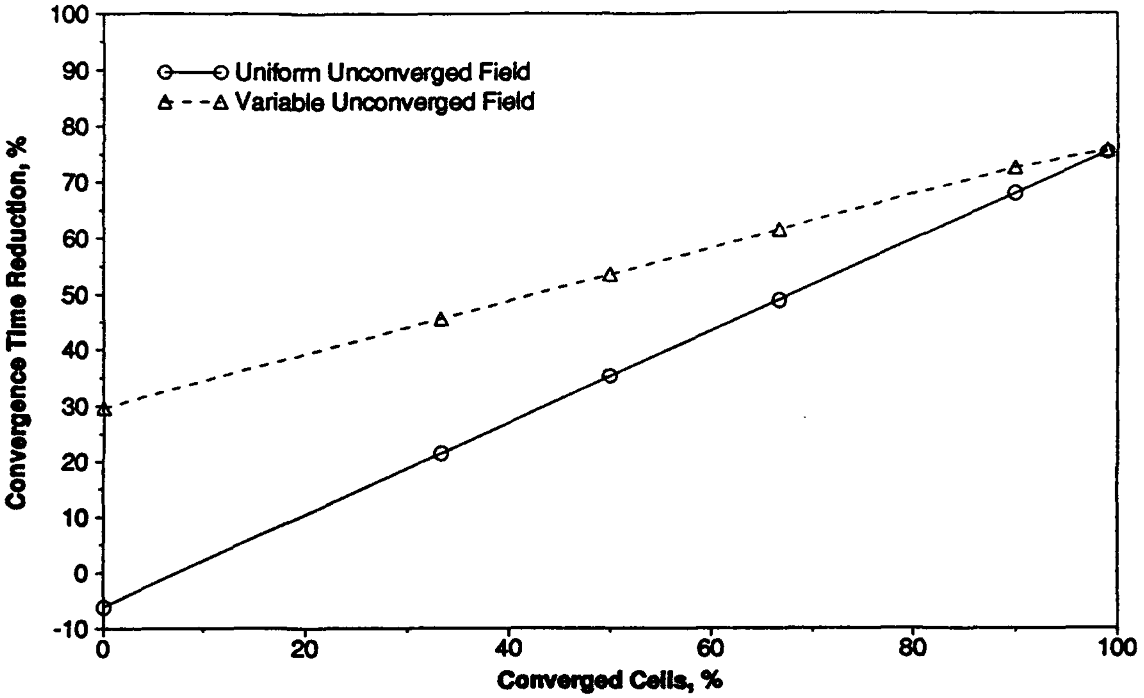

Figure 37 Vector reduction performance.

SECTION VI

MATHEMATICAL FORMULATION: FLOW SOLVER

The governing equations for three-dimensional, compressible, viscous fluid flow (neglecting body forces) for a generalized, time dependent, curvilinear coordinate system have been presented by several authors [References 26, 27, 28]. In the following, the density of the fluid will be denoted by ϱ, pressure p, total specific energy e_o , thermal conductivity $\mathcal{K}$, viscosity μ and the Cartesian velocity components will be u, v, w for the x, y, z coordinate directions, respectively. The governing equations, written in strong conservation law form, read

$$\frac{\partial Q}{\partial \tau} + \frac{\partial F}{\partial \xi} + \frac{\partial G}{\partial \eta} + \frac{\partial H}{\partial \zeta} = \frac{\partial F_v}{\partial \xi} + \frac{\partial G_v}{\partial \eta} + \frac{\partial H_v}{\partial \zeta} \quad , \tag{134}$$

where the dependent variable vector is

$$Q = J \begin{bmatrix} \varrho \\ \varrho u \\ \varrho v \\ \varrho w \\ \varrho e_o \end{bmatrix} , \tag{135}$$

the inviscid flux vectors are

$$F = J \begin{bmatrix} \varrho U \\ \varrho u U + \xi_x p \\ \varrho v U + \xi_y p \\ \varrho w U + \xi_z p \\ \varrho e_o U + p(\xi_x u + \xi_y v + \xi_z w) \end{bmatrix} , \tag{136}$$

$$G = J \begin{bmatrix} \varrho V \\ \varrho u V + \eta_x p \\ \varrho v V + \eta_y p \\ \varrho w V + \eta_z p \\ \varrho e_o V + p(\eta_x u + \eta_y v + \eta_z w) \end{bmatrix} , \tag{137}$$

$$H = J\begin{bmatrix} \varrho W \\ \varrho uW + \zeta_x p \\ \varrho vW + \zeta_y p \\ \varrho wW + \zeta_z p \\ \varrho e_o W + p(\zeta_x u + \zeta_y v + \zeta_z w) \end{bmatrix}, \tag{138}$$

the viscous flux vectors are

$$F_v = J\begin{bmatrix} 0 \\ T_{\xi 1} \\ T_{\xi 2} \\ T_{\xi 3} \\ \mathcal{Q}_\xi + uT_{\xi 1} + vT_{\xi 2} + wT_{\xi 3} \end{bmatrix}, \tag{139}$$

$$G_v = J\begin{bmatrix} 0 \\ T_{\eta 1} \\ T_{\eta 2} \\ T_{\eta 3} \\ \mathcal{Q}_\eta + uT_{\eta 1} + vT_{\eta 2} + wT_{\eta 3} \end{bmatrix}, \tag{140}$$

$$H_v = J\begin{bmatrix} 0 \\ T_{\zeta 1} \\ T_{\zeta 2} \\ T_{\zeta 3} \\ \mathcal{Q}_\zeta + uT_{\zeta 1} + vT_{\zeta 2} + wT_{\zeta 3} \end{bmatrix}, \tag{141}$$

and the Jacobian of the coordinate transformation is

$$J = \det\left|\frac{\partial(x, y, z)}{\partial(\xi, \eta, \zeta)}\right| . \tag{142}$$

In the above, the curvilinear coordinates have been defined as

$$\xi = \xi\ (x, y, z, t\ ) ,$$

$$\eta = \eta\ (x, y, z, t\ ) ,$$

$$\zeta = \zeta\ (x, y, z, t\ ) ,$$

$$\tau = t \ , \tag{143}$$

and the contravariant velocities normal to constant ξ , η and ς surfaces are defined to be

$$U = \xi_\tau + u\xi_x + v\xi_y + w\xi_z \ , \tag{144}$$

$$V = \eta_\tau + u\eta_x + v\eta_y + w\eta_z \ , \tag{145}$$

$$W = \zeta_\tau + u\zeta_x + v\zeta_y + w\zeta_z \ . \tag{146}$$

The heat flux and shear stress terms of the viscous flux vectors, given in Equations (139)-(141), are

$$\begin{aligned}
\mathcal{Q}_\xi &= q_x\xi_x + q_y\xi_y + q_z\xi_z \ , & T_{\xi 1} &= \tau_{xx}\xi_x + \tau_{xy}\xi_y + \tau_{xz}\xi_z \ , \\
\mathcal{Q}_\eta &= q_x\eta_x + q_y\eta_y + q_z\eta_z \ , & T_{\xi 2} &= \tau_{xy}\xi_x + \tau_{yy}\xi_y + \tau_{yz}\xi_z \ , \\
\mathcal{Q}_\zeta &= q_x\zeta_x + q_y\zeta_y + q_z\zeta_z \ , & T_{\xi 3} &= \tau_{xz}\xi_x + \tau_{yz}\xi_y + \tau_{zz}\xi_z \ , \\
T_{\eta 1} &= \tau_{xx}\eta_x + \tau_{xy}\eta_y + \tau_{xz}\eta_z \ , & T_{\zeta 1} &= \tau_{xx}\zeta_x + \tau_{xy}\zeta_y + \tau_{xz}\zeta_z \ , \\
T_{\eta 2} &= \tau_{xy}\eta_x + \tau_{yy}\eta_y + \tau_{yz}\eta_z \ , & T_{\zeta 2} &= \tau_{xy}\zeta_x + \tau_{yy}\zeta_y + \tau_{yz}\zeta_z \ , \\
T_{\eta 3} &= \tau_{xz}\eta_x + \tau_{yz}\eta_y + \tau_{zz}\eta_z \ , & T_{\zeta 3} &= \tau_{xz}\zeta_x + \tau_{yz}\zeta_y + \tau_{zz}\zeta_z \ ,
\end{aligned} \tag{147}$$

where

$$\begin{aligned}
\tau_{xx} = \frac{2}{3}\mu\ [\ 2\ (\ \xi_x\frac{\partial u}{\partial \xi} + \eta_x\frac{\partial u}{\partial \eta} + \zeta_x\frac{\partial u}{\partial \zeta}\ ) - (\ \xi_y\frac{\partial v}{\partial \xi} + \eta_y\frac{\partial v}{\partial \eta} + \zeta_y\frac{\partial v}{\partial \zeta}\ ) \\
- (\ \xi_z\frac{\partial w}{\partial \xi} + \eta_z\frac{\partial w}{\partial \eta} + \zeta_z\frac{\partial w}{\partial \zeta}\ )\ ] \ ,
\end{aligned}$$

$$\begin{aligned}
\tau_{yy} = \frac{2}{3}\mu\ [\ 2\ (\ \xi_y\frac{\partial v}{\partial \xi} + \eta_y\frac{\partial v}{\partial \eta} + \zeta_y\frac{\partial v}{\partial \zeta}\ ) - (\ \xi_x\frac{\partial u}{\partial \xi} + \eta_x\frac{\partial u}{\partial \eta} + \zeta_x\frac{\partial u}{\partial \zeta}\ ) \\
- (\ \xi_z\frac{\partial w}{\partial \xi} + \eta_z\frac{\partial w}{\partial \eta} + \zeta_z\frac{\partial w}{\partial \zeta}\ )\ ] \ ,
\end{aligned}$$

$$\begin{aligned}
\tau_{zz} = \frac{2}{3}\mu\ [\ 2\ (\ \xi_z\frac{\partial w}{\partial \xi} + \eta_z\frac{\partial w}{\partial \eta} + \zeta_z\frac{\partial w}{\partial \zeta}\ ) - (\ \xi_x\frac{\partial u}{\partial \xi} + \eta_x\frac{\partial u}{\partial \eta} + \zeta_x\frac{\partial u}{\partial \zeta}\ ) \\
- (\ \xi_y\frac{\partial v}{\partial \xi} + \eta_y\frac{\partial v}{\partial \eta} + \zeta_y\frac{\partial v}{\partial \zeta}\ )\ ] \ ,
\end{aligned}$$

$$\tau_{xy} = \mu \left[\left(\xi_y \frac{\partial u}{\partial \xi} + \eta_y \frac{\partial u}{\partial \eta} + \zeta_y \frac{\partial u}{\partial \zeta} \right) + \left(\xi_x \frac{\partial v}{\partial \xi} + \eta_x \frac{\partial v}{\partial \eta} + \zeta_x \frac{\partial v}{\partial \zeta} \right) \right] ,$$

$$\tau_{xz} = \mu \left[\left(\xi_z \frac{\partial u}{\partial \xi} + \eta_z \frac{\partial u}{\partial \eta} + \zeta_z \frac{\partial u}{\partial \zeta} \right) + \left(\xi_x \frac{\partial w}{\partial \xi} + \eta_x \frac{\partial w}{\partial \eta} + \zeta_x \frac{\partial w}{\partial \zeta} \right) \right] ,$$

$$\tau_{yz} = \mu \left[\left(\xi_z \frac{\partial v}{\partial \xi} + \eta_z \frac{\partial v}{\partial \eta} + \zeta_z \frac{\partial v}{\partial \zeta} \right) + \left(\xi_y \frac{\partial w}{\partial \xi} + \eta_y \frac{\partial w}{\partial \eta} + \zeta_y \frac{\partial w}{\partial \zeta} \right) \right] ,$$

$$q_x = \mathcal{K} \left(\xi_x \frac{\partial T}{\partial \xi} + \eta_x \frac{\partial T}{\partial \eta} + \zeta_x \frac{\partial T}{\partial \zeta} \right) ,$$

$$q_y = \mathcal{K} \left(\xi_y \frac{\partial T}{\partial \xi} + \eta_y \frac{\partial T}{\partial \eta} + \zeta_y \frac{\partial T}{\partial \zeta} \right) ,$$

$$q_z = \mathcal{K} \left(\xi_z \frac{\partial T}{\partial \xi} + \eta_z \frac{\partial T}{\partial \eta} + \zeta_z \frac{\partial T}{\partial \zeta} \right) . \tag{148}$$

In the above, the additional assumption that the flowfield is considered to be a homogeneous mixture has been made, hence diffusion effects are neglected. The modeling of diffusion would require writing additional partial differential equations describing the conservation of mass for each of the elemental species comprising the mixture [Reference 12].

The continuity equation is represented by the first row in Equations (134) - (141), whereas rows two through four correspond to the momentum equations and the last row is the energy equation. The entire set of equations is commonly referred to as the Navier–Stokes equations, although incorrectly so, since this name originally defined only the momentum equations. However, the author will adhere to the accepted practice. The system of equations is closed by the “Black Box”, which provides pressure, temperature, viscosity and thermal conductivity as functions of density and internal energy.

1. NONDIMENSIONALIZATION

The dimensional quantities in the above equations are scaled using the following relations

$$\bar{x} = \frac{x}{L} , \quad \bar{y} = \frac{y}{L} , \quad \bar{z} = \frac{z}{L} , \quad \bar{u} = \frac{u}{a_r} , \quad \bar{v} = \frac{v}{a_r} , \quad \bar{w} = \frac{w}{a_r} ,$$

$$\bar{p} = \frac{p}{\varrho_r a_r^2} , \quad \bar{\varrho} = \frac{\varrho}{\varrho_r} , \quad \bar{\tau} = \frac{a_r \tau}{L} , \quad \bar{e}_o = \frac{e_o}{a_r^2} ,$$

$$\bar{\mu} = \frac{\mu}{\mu_r} , \quad \bar{\mathcal{K}} = \frac{\mathcal{K}}{\mathcal{K}_r} , \quad \bar{T} = \frac{T}{T_r} , \tag{149}$$

where the bar denotes the nondimensional quantities, and L, ϱ_r, T_r, and α_r are the reference length, density, temperature and speed of sound, respectively. The reference viscosity μ_r and thermal conductivity $\mathcal{K}_r$ used in the previous relations are

$$\mu_r = \varrho_r a_r L \ ,$$

$$\mathcal{K}_r = \mu_r R_r \ , \tag{150}$$

where the reference gas constant has been introduced, and is defined by the relation

$$a_r^2 = R_r T_r \ , \tag{151}$$

Normally, viscosity and thermal conductivity are scaled by introducing the Reynolds and Prandtl numbers, where perfect gas relations are used to define the latter [References 26, 27, 28]]. This is not practical for real gas flows. After dropping the bar over the scaled variables, the resulting set of nondimensional Navier–Stokes equations will appear identical to Equations (134) – (141).

2. THIN–LAYER APPROXIMATION

Solution of the complete Navier–Stokes equations is both computationally expensive and memory intensive. This is due to the complexity of the viscous terms and the large number of computational volumes that would be required to resolve the mixed second derivatives in those terms. Boundary–layer simplifications, while reducing the complexity of the Navier–Stokes equations, are not applicable to flows where there is a strong interaction between the inviscid and boundary–layer regions [Reference 28].

The concept of the thin–layer approximation, where the viscous terms comprising derivatives in directions parallel to the body are neglected, not only provides a reduction in the complexity of the equations but allows for the determination of mildly separated and reverse flow regions [Reference 29]. The neglected terms are small in comparison with the other viscous terms containing derivatives normal to the body surface, and this makes the procedure justifiable. Moreover, adequate resolution of these terms is difficult to achieve unless grids which are densely packed in a direction parallel to the body surface are employed, and this is beyond the current capability of practical viscous calculations.

Neglecting derivatives in the ξ–direction, as an example, the thin–layer Navier–Stokes (TLNS) equations will read

$$\frac{\partial Q}{\partial \tau} + \frac{\partial F}{\partial \xi} + \frac{\partial G}{\partial \eta} + \frac{\partial H}{\partial \zeta} = \frac{\partial G_v}{\partial \eta} + \frac{\partial H_v}{\partial \zeta} \ , \tag{152}$$

where the dependent variable and inviscid flux vectors remain the same, as given by Equations (135) – (138). However, the viscous flux vectors G_v and H_v are simplified. They can be written in the general form

$$S_v = J\begin{bmatrix} 0 \\ T_{k1} \\ T_{k2} \\ T_{k3} \\ \mathcal{Q}_k + uT_{k1} + vT_{k2} + wT_{k3} \end{bmatrix} , \tag{153}$$

where S_v denotes the viscous flux vector in the direction k. The viscous shear stress and heat flux terms are now given by

$$\begin{aligned} T_{k1} &= \tau_{xx}k_x + \tau_{xy}k_y + \tau_{xz}k_z , \\ T_{k2} &= \tau_{xy}k_x + \tau_{yy}k_y + \tau_{yz}k_z , \\ T_{k3} &= \tau_{xz}k_x + \tau_{yz}k_y + \tau_{zz}k_z , \\ \mathcal{Q}_k &= q_xk_x + q_yk_y + q_zk_z , \end{aligned} \tag{154}$$

where

$$\begin{aligned} \tau_{xx} &= \frac{2}{3}\mu \left[2\, k_x\frac{\partial u}{\partial k} - k_y\frac{\partial v}{\partial k} - k_z\frac{\partial w}{\partial k} \right] , \\ \tau_{yy} &= \frac{2}{3}\mu \left[2\, k_y\frac{\partial v}{\partial k} - k_x\frac{\partial u}{\partial k} - k_z\frac{\partial w}{\partial k} \right] , \\ \tau_{zz} &= \frac{2}{3}\mu \left[2\, k_z\frac{\partial w}{\partial k} - k_x\frac{\partial u}{\partial k} - k_y\frac{\partial v}{\partial k} \right] , \end{aligned}$$

$$\begin{aligned} \tau_{xy} &= \mu \left[k_y\frac{\partial u}{\partial k} + k_x\frac{\partial v}{\partial k} \right] , \\ \tau_{xz} &= \mu \left[k_z\frac{\partial u}{\partial k} + k_x\frac{\partial w}{\partial k} \right] , \\ \tau_{yz} &= \mu \left[k_z\frac{\partial v}{\partial k} + k_y\frac{\partial w}{\partial k} \right] , \end{aligned}$$

$$q_x = \mathcal{K}\, k_x\frac{\partial T}{\partial k} ,$$

$$q_y = \mathcal{K}\, k_y\frac{\partial T}{\partial k} ,$$

and

$$q_z = \mathcal{K}\, k_z\frac{\partial T}{\partial k} . \tag{155}$$

In the following, all the viscous solutions will be obtained by numerical solutions of the TLNS equations.

SECTION VII

NUMERICAL FORMULATION: FLOW SOLVER

1. FINITE-VOLUME DISCRETIZATION

The governing fluid dynamic equations, which were presented in Section VI, can be reduced to a set of solvable algebraic equations using the finite-volume technique, where the computational domain is discretized by small, but finite, control volumes or computational cells.

Integrating Equation (152) over the unit computational cell ($\Delta\xi=\Delta\eta=\Delta\varsigma=1$) and noting that the dependent variables become cell-averaged values, the following discretized form of the governing equations is obtained

$$\frac{\partial Q}{\partial \tau} + \delta_i(F) + \delta_j(G - G_v) + \delta_k(H - H_v) = 0 \ , \qquad (156)$$

where the central difference operator

$$\delta_l(\ ) = (\ )_{l+\frac{1}{2}} - (\ )_{l-\frac{1}{2}} \ , \qquad (157)$$

has been introduced, and indices i, j, k correspond to the directions ξ, η, ς, respectively.

2. IMPLICIT ALGORITHM

Considering for a moment only the inviscid fluxes of Equation (156), a fully implicit formulation can be written as

$$\Delta Q^n = Q^{n+1} - Q^n = -\Delta\tau \sum \delta_l \, S^{n+1} \ , \qquad (158)$$

where ^{n} represents the time level and $\Delta\tau = \tau^{n+1} - \tau^n$ is the time step. In the above, the summation is over all three flux vectors, where S corresponds to F, G and H, and l corresponds to i, j and k, respectively.

The inviscid fluxes are nonlinear functions of Q and can be linearized in the manner used by Beam and Warming [Reference 30], and Briley and McDonald [Reference 31], as follows

$$S^{n+1} = S^n + \bar{S}(Q^n)\, \Delta Q^n \ , \qquad (159)$$

where

$$\bar{S}(Q^n) = \frac{\partial S(Q^n)}{\partial Q} \ . \qquad (160)$$

Applying this linearization to Equation (158), the Euler-Implicit difference formulation is obtained

$$(I + \Delta\tau \sum \delta_l \, \overline{S} \cdot)\Delta Q^n = - \Delta\tau \sum \delta_l \, S^n \, , \tag{161}$$

which is first-order accurate in time. The dot indicates that ΔQ^n is included in the operation of δ_l.

Similar considerations can be applied to the viscous flux vectors, resulting in the following fully-implicit algorithm for the TLNS equations

$$\begin{aligned} &\left\{ I + \Delta\tau \left[\delta_i A \cdot + \delta_j (B - B_v) \cdot + \delta_k (C - C_v) \cdot \right] \right\} \Delta Q^n \\ &\quad = - \Delta\tau \left[\delta_i (F)^n + \delta_j (G - G_v)^n + \delta_k (H - H_v)^n \right] , \end{aligned} \tag{162}$$

where the Jacobians of the inviscid and viscous fluxes are

$$\begin{gathered} A = \frac{\partial F}{\partial Q} \, , \\ B = \frac{\partial G}{\partial Q} \, , \qquad C = \frac{\partial H}{\partial Q} \, , \\ B_v = \frac{\partial G_v}{\partial Q} \, , \qquad C_v = \frac{\partial H_v}{\partial Q} \, . \end{gathered} \tag{163}$$

3. FLUX-SPLIT ALGORITHMS

The governing equations given in Equation (134) are hyperbolic in nature and consequently information is propagated only in certain characteristic directions. Numerical techniques, whereby the fluxes are discretized in a manner to allow information to propagate in the "correct" direction, are known as upwind methods. The two most popular categories of upwind methods are flux-vector splitting and flux-difference splitting. Both of these techniques involve the discretization of the inviscid flux vector in one space dimension, and extensions to three dimensions are accomplished by considering three separate one-dimensional problems.

The flux-vector split scheme that is used in this study is of the Steger-Warming type. Originally developed for perfect gases [Reference 32], it has been extended to flows in chemical equilibrium by Vinokur and Montagné [Reference 33]. The basic premise behind the scheme is that flux vectors are split and discretized in directions corresponding to the sign of the propagating wave speeds.

The flux-difference split scheme that is employed is a newly derived approximate Riemann solver for arbitrary gas mixtures. It is based on the perfect gas version developed by Roe [Reference 34]. Essentially, this scheme involves the solution of local Riemann problems at each cell face, where a discontinuity, created by differences between the left and right states, is assumed to exist. In contrast to the flux-vector split scheme, the inviscid flux vector is not split but reconstructed from the left and right states.

The inviscid flux Jacobians are analytically derived from the Steger–Warming split fluxes in a manner similar to the work of Belk [Reference 35], with the exception that the present formulation is based on flows in chemical equilibrium. Both Steger–Warming and Roe fluxes can be used to determine the right hand side of the discretized governing equations, where for hypersonic flows the former is more robust and the latter is more accurate [Reference 36].

a. EIGENVALUES AND EIGENVECTORS

Using the generic formulation, where S is F, G or H when k is ξ, η, ς, the inviscid flux vectors can be written as

$$S = J|\nabla k| \begin{bmatrix} \varrho\tilde{\beta}_k \\ \varrho u\tilde{\beta}_k + p\tilde{k}_x \\ \varrho v\tilde{\beta}_k + p\tilde{k}_y \\ \varrho w\tilde{\beta}_k + p\tilde{k}_z \\ \varrho h_o\tilde{\beta}_k - p\tilde{k}_t \end{bmatrix} , \tag{164}$$

where $\tilde{k}_x$, $\tilde{k}_y$, $\tilde{k}_z$, and $\tilde{k}_t$ are the normalized metrics and are given by

$$\tilde{k}_i = \frac{k_i}{|\nabla k|} ,$$

$$|\nabla k| = \sqrt{k_x^2 + k_y^2 + k_z^2} .$$

In the above, $\tilde{\beta}_k$ is the relative contravariant velocity with respect to direction k, and is defined to be the sum of the absolute contravariant velocity $\tilde{\theta}_k$ and the velocity due to the time rate of change of the curvilinear coordinate $\tilde{k}_t$, as follows

$$\tilde{\beta}_k = \tilde{\theta}_k + \tilde{k}_t , \qquad \tilde{\theta}_k = u\tilde{k}_x + v\tilde{k}_y + w\tilde{k}_z . \tag{165}$$

The Jacobian matrices of the inviscid flux vectors, as well as the eigenvalues and eigenvectors, have been determined in the manner of the perfect gas formulations developed by Whitfield and Janus [Reference 37], with extensions to chemical equilibrium made in this work. The details of this determination are given in Appendix B. In summary, the eigenvalues are

$$\lambda_k^1 = \lambda_k^2 = \lambda_k^3 = J|\nabla k|\tilde{\beta}_k \,,$$

$$\lambda_k^4 = J|\nabla k|(\,\tilde{\beta}_k + a\,) \,, \tag{166}$$

$$\lambda_k^5 = J|\nabla k|(\,\tilde{\beta}_k - a\,) \,,$$

and the right and left eigenvectors are given by Equations (B.19) and (B.20), respectively. In the relations for the eigenvectors, real gas effects are accounted for in the term

$$\psi = a^2 - h(\bar{\gamma} - 1) \,, \tag{167}$$

where $\bar{\gamma}$ was defined in Equation (29). It is interesting to point out that for a perfect gas, $\bar{\gamma} = \gamma$, ψ is identically zero, and the eigenvectors will identically reduce to their perfect gas counterpart.

b. STEGER-WARMING FLUX-VECTOR SPLIT

The Steger-Warming flux-vector split scheme for a perfect gas utilizes the homogeneity property to split the fluxes as follows

$$S^{\pm} = \sum_{i=1}^{3} S_i^{\pm} = \sum_{i=1}^{3} \overline{S}_i^{\pm} Q \,, \tag{168}$$

where $\overline{S}_i^{\pm}$ corresponds to the positive and negative contributions of the three distinct eigenvalues to the Jacobian matrix $\overline{S}$. Liou, Van Leer and Shuen [Reference 5] have shown that the flux vector for a real gas no longer possesses the homogeneous property and in fact is composed of homogeneous and nonhomogeneous contributions

$$S = S_h + S' \,. \tag{169}$$

They proposed the following pseudo splitting for the flux vector

$$S^{\pm} = S_h^{\pm} + \frac{1}{2}S' \,, \tag{170}$$

where the homogeneous contributions are split according to the "standard" Steger-Warming type scheme and central differences are used for the nonhomogeneous contributions. Alternatively, Vinokur and Montagné [Reference 33] have shown that the split flux scheme derived using the homogeneity property is just one solution of an entire family of one-parameter flux-vector splittings. The scheme they proposed is based on "gamma" being defined as the isentropic index. The final result is a generalized formulation of the Steger-Warming flux-vector splitting for an arbitrary gas. The latter method is utilized in this study due to the simplicity of the formulation.

The split fluxes, for the generalized Steger-Warming flux-vector split formulation developed by Vinokur and Montagné [Reference 33], are given by

$$K_1^{\pm} = \frac{\Gamma - 1}{\Gamma}\begin{bmatrix} \varrho \\ \varrho u \\ \varrho v \\ \varrho w \\ \varrho\left(h_o - \frac{a^2}{\Gamma - 1}\right) \end{bmatrix} \lambda_k^{1(\pm)} ,$$

$$K_4^{\pm} = \frac{1}{2\Gamma}\begin{bmatrix} \varrho \\ \varrho(u + ak_x) \\ \varrho(v + ak_y) \\ \varrho(w + ak_z) \\ \varrho(h_o + a\tilde{\theta}_k) \end{bmatrix} \lambda_k^{4(\pm)} , \qquad K_5^{\pm} = \frac{1}{2\Gamma}\begin{bmatrix} \varrho \\ \varrho(u - ak_x) \\ \varrho(v - ak_y) \\ \varrho(w - ak_z) \\ \varrho(h_o - a\tilde{\theta}_k) \end{bmatrix} \lambda_k^{5(\pm)} , \tag{171}$$

where

$$\lambda_k^{1(\pm)} = J|\nabla k|\frac{\tilde{\beta}_k \pm |\tilde{\beta}_k|}{2} ,$$

$$\lambda_k^{4(\pm)} = J|\nabla k|\frac{(\tilde{\beta}_k + a) \pm |\tilde{\beta}_k + a|}{2} ,$$

$$\lambda_k^{5(\pm)} = J|\nabla k|\frac{(\tilde{\beta}_k - a) \pm |\tilde{\beta}_k - a|}{2} . \tag{172}$$

In the above, Γ is the isentropic index defined by Equation (28). Similarly to what has been seen for the eigenvectors, the above formulas will reduce to the perfect gas formulation, when $\Gamma \equiv \gamma$.

As was discussed previously, the inviscid flux Jacobians are constructed from the analytical differentiation of the split flux vectors in the manner used by Belk [Reference 35]. The details of the differentiation as well as the resulting components of the Jacobian matrices are given in Appendix C. The components of the Jacobians contain derivatives of the isentropic index, which is a nonlinear function of density and temperature. In the present study, these derivatives are neglected.

Discretization of the inviscid flux Jacobians at cell face $l + 1/2$ is implemented as follows

$$\left[\frac{\partial S}{\partial Q}\,\Delta Q\right]_{l+\frac{1}{2}} = \left[\bar{S}\,\Delta Q\right]_{l+\frac{1}{2}} = \bar{S}^{+}_{l+\frac{1}{2}}\,\Delta Q_l + \bar{S}^{-}_{l+\frac{1}{2}}\,\Delta Q_{l+1} . \tag{173}$$

As with the split fluxes, the Jacobians of the split fluxes can be shown to reduce to their perfect gas formulation.

c. APPROXIMATE RIEMANN SOLVER

The flux–difference–split algorithm used is based on the scheme developed for perfect gases by Roe [Reference 38]. It involves the solution of local Riemann problems at each cell interface, where a left state $(\cdot)_l$ and a right state $(\cdot)_r$ are defined by extrapolation of the cell–centered values to the left and right, respectively.

Development of an approximate Riemann solver hinges on the determination of appropriate averages for the eigenvalues $\hat{\lambda}_i$, right eigenvectors $\hat{r}_i$ and wave strengths $\hat{\sigma}_i$ such that the following jump conditions are satisfied

$$\llbracket Q \rrbracket = \sum_{i=1}^{5} \hat{\sigma}_i \, \hat{r}_i \, , \qquad \llbracket S \rrbracket = \sum_{i=1}^{5} \hat{\sigma}_i \, \hat{\lambda}_i \, \hat{r}_i \, , \tag{174}$$

where the cell interface states need not be close and thus $\llbracket Q \rrbracket$ is arbitrary. In the above, the jump operator is defined as the difference or jump in values between the right and left states, $\llbracket(\cdot)\rrbracket = (\cdot)_r - (\cdot)_l$. The averaged eigenvalues will read

$$\begin{aligned}
\hat{\lambda}_1 &= \hat{\lambda}_2 = \hat{\lambda}_3 = J|\nabla k|\hat{\beta}_k \, , \\
\hat{\lambda}_4 &= J|\nabla k|(\, \hat{\beta}_k + \hat{a} \,) \, , \\
\hat{\lambda}_5 &= J|\nabla k|(\, \hat{\beta}_k - \hat{a} \,) \, ,
\end{aligned} \tag{175}$$

where the directional subscript k has been dropped for clarity. The averaged eigenvectors will read

$$\hat{r}_1 = \begin{bmatrix} \hat{\alpha}\tilde{k}_x \\ \hat{\alpha}\hat{u}\tilde{k}_x \\ \hat{\alpha}\hat{v}\tilde{k}_x + \hat{\varrho}\tilde{k}_z \\ \hat{\alpha}\hat{w}\tilde{k}_x - \hat{\varrho}\tilde{k}_y \\ \hat{\alpha}\tilde{k}_x\left(\hat{h}_o - \hat{a}^2/(\hat{\gamma} - 1)\right) + \hat{\varrho}(\hat{v}\tilde{k}_z - \hat{w}\tilde{k}_y) \end{bmatrix},$$

$$\hat{r}_2 = \begin{bmatrix} \hat{\alpha}\tilde{k}_y \\ \hat{\alpha}\hat{u}\tilde{k}_y - \hat{\varrho}\tilde{k}_z \\ \hat{\alpha}\hat{v}\tilde{k}_y \\ \hat{\alpha}\hat{w}\tilde{k}_y + \hat{\varrho}\tilde{k}_x \\ \hat{\alpha}\tilde{k}_y\left(\hat{h}_o - \hat{a}^2/(\hat{\gamma} - 1)\right) + \hat{\varrho}(\hat{w}\tilde{k}_x - \hat{u}\tilde{k}_z) \end{bmatrix},$$

$$\hat{r}_3 = \begin{bmatrix} \hat{\alpha}\tilde{k}_z \\ \hat{\alpha}\hat{u}\tilde{k}_z + \hat{\varrho}\tilde{k}_y \\ \hat{\alpha}\hat{v}\tilde{k}_z - \hat{\varrho}\tilde{k}_x \\ \hat{\alpha}\hat{w}\tilde{k}_z \\ \hat{\alpha}\tilde{k}_z\left(\hat{h}_o - \hat{a}^2/(\hat{\gamma} - 1)\right) + \hat{\varrho}(\hat{u}\tilde{k}_y - \hat{v}\tilde{k}_x) \end{bmatrix} ,$$

$$\hat{r}_{4,5} = \hat{\alpha}\begin{bmatrix} 1 \\ \hat{u} \pm \hat{a}\tilde{k}_x \\ \hat{v} \pm \hat{a}\tilde{k}_x \\ \hat{w} \pm \hat{a}\tilde{k}_z \\ \hat{h}_o \pm \hat{a}\hat{\theta}_k \end{bmatrix} , \tag{176}$$

and the wave strengths read

$$\hat{\sigma}_1 = \frac{\tilde{k}_x}{\hat{\alpha}}\left(\llbracket \varrho \rrbracket - \frac{\llbracket p \rrbracket}{\hat{a}^2} \right) + \tilde{k}_z\llbracket v \rrbracket - \tilde{k}_y\llbracket w \rrbracket ,$$

$$\hat{\sigma}_2 = \frac{\tilde{k}_y}{\hat{\alpha}}\left(\llbracket \varrho \rrbracket - \frac{\llbracket p \rrbracket}{\hat{a}^2} \right) - \tilde{k}_z\llbracket u \rrbracket + \tilde{k}_x\llbracket w \rrbracket ,$$

$$\hat{\sigma}_3 = \frac{\tilde{k}_z}{\hat{\alpha}}\left(\llbracket \varrho \rrbracket - \frac{\llbracket p \rrbracket}{\hat{a}^2} \right) + \tilde{k}_y\llbracket u \rrbracket - \tilde{k}_z\llbracket v \rrbracket ,$$

$$\hat{\sigma}_{4,5} = \frac{1}{\sqrt{2}}\left(\frac{\llbracket p \rrbracket}{\hat{\varrho}\hat{a}} \pm \llbracket \tilde{\theta}_k \rrbracket \right) . \tag{177}$$

In the above, the hat ^ denotes averaged terms. Determination of these algebraic averages is the key step in the development of an approximate Riemann solver. Abgrall [Reference 6] pointed out that there are multiple solutions to the system given in Equation (174) and hence the averages are not unique, as is apparent by the variety of values published in the literature [References 5–9]. The approach taken in this work is similar to that of Abgrall, however the averages developed here are for an arbitrary chemical composition. The primary difference between the present method and others is in the determination of the pressure derivative averages, where relatively complex formulas are used by Vinokur [Reference 7] and Glaister [Reference 8]. Grossman and Walters [Reference 9] use an approximate algorithm which is valid for near isentropic flows.

The present formulation utilizes averages of the ratio of enthalpy and internal energy derivatives $\bar{\gamma}$ and isentropic index Γ, which can be used to construct averages for the pressure derivatives.

In the following, the standard Roe average, denoted by $\mathfrak{R}$, will be given as follows

$$\mathfrak{R}(\cdot) = \frac{\left[\sqrt{\varrho_l}(\cdot)_l + \sqrt{\varrho_r}(\cdot)_r\right]}{\sqrt{\varrho_l} + \sqrt{\varrho_r}} , \tag{178}$$

and $\hat{\varrho}$ is given by the standard geometric average, $\hat{\varrho} = \sqrt{\varrho_l \varrho_r}$. The averages are obtained through the solution of Equation (174). The full derivation of the Roe averaged variables for the approximate Riemann solver is given in Appendix D. The averages for all Cartesian and contravariant velocity vectors are found to be the standard Roe averages; i.e. $\hat{u} = \mathfrak{R}(u)$ and $\hat{\theta}_k = \mathfrak{R}(\theta_k)$. Total enthalpy is given in the same manner, $\hat{h}_o = \mathfrak{R}(h_o)$. The speed of sound $\hat{a}$ will read

$$\hat{a}^2 = \hat{\Gamma}\hat{R}\hat{T} + (\hat{\gamma} - 1)\left[\hat{h}_o - \frac{\hat{q}^2}{2} - \sum_{i=1}^{N} \hat{Y}_i \hat{e}_i - \hat{R}\hat{T}\right] , \tag{179}$$

where

$$\begin{aligned} \hat{q}^2 &= \hat{u}^2 + \hat{v}^2 + \hat{w}^2 , \\ \hat{\Gamma} &= \hat{\gamma} + \frac{\hat{\varrho}}{\hat{R}\hat{T}} \sum_{i=1}^{N} \left(\overline{\frac{\partial Y_i}{\partial \varrho}}\right) [R_i \hat{T} - (\hat{\gamma} - 1)\hat{e}_i] , \\ \hat{\gamma} &= 1 + \frac{\hat{R} + \hat{T} \sum_{i=1}^{N} R_i \left(\overline{\frac{\partial Y_i}{\partial T}}\right)}{\sum_{i=1}^{N} \hat{Y}_i \bar{c}_{v_i} + \sum_{i=1}^{N} \hat{e}_i \left(\overline{\frac{\partial Y_i}{\partial \varrho}}\right)} . \end{aligned} \tag{180}$$

In the preceding relations, the mixture gas constant $\hat{R}$, temperature $\hat{T}$, species internal energy $\hat{e}_i$, and species mass fractions $\hat{Y}_i$, are all defined using the standard Roe average as follows

$$\hat{R} = \mathfrak{R}(R) , \quad \hat{T} = \mathfrak{R}(T) , \quad \hat{e}_i = \mathfrak{R}(e_i) , \quad \hat{Y}_i = \mathfrak{R}(Y_i) , \tag{181}$$

and the barred terms, specifically the species specific heats at constant volume and mass fraction derivatives, are taken as integral averages. The simplest method of evaluating these integral averages is to use the trapezoidal rule, which results in the following arithmetic averages

$$\bar{c}_{v_i} = \frac{1}{2}\left[c_{v_i}(T_l) + c_{v_i}(T_r)\right] ,$$

$$\left(\overline{\frac{\partial Y_i}{\partial \varrho}}\right) = \frac{1}{2}\left[\left(\frac{\partial Y_i}{\partial \varrho}\right)_l + \left(\frac{\partial Y_i}{\partial \varrho}\right)_r\right] ,$$

$$\left(\overline{\frac{\partial Y_i}{\partial T}}\right) = \frac{1}{2}\left[\left(\frac{\partial Y_i}{\partial T}\right)_l + \left(\frac{\partial Y_i}{\partial T}\right)_r\right] . \qquad (182)$$

Again, the Roe averages given above can be shown to reduce to their perfect gas formulations.

Implementation of the approximate Riemann solver follows the methodology of Whitfield, Janus and Simpson [Reference 39], where the first-order flux at cell face $l + 1/2$ is computed from the following

$$S_{l+\frac{1}{2}} = \frac{1}{2}(S_l + S_r) - \frac{1}{2}\sum_{i=1}^{5} \hat{\sigma}_i|\hat{\lambda}_i|\hat{r}_i , \qquad (183)$$

where

$$S_l = S(Q_l) , \qquad S_r = S(Q_{l+1}) . \qquad (184)$$

Higher-order spatial accuracy is achieved using the flux interpolation approach, where higher-order terms, involving the averaged eigenvalues, right eigenvectors and wave strengths, given in Equations (175) - (177), are added to the first-order flux given above [Reference 39].

4. MODIFIED TWO-PASS

The discretized equations, Equation (156), are advanced in time using the modified two-pass factorization developed by Whitfield [Reference 43], which is a basic modification of the standard two-pass scheme. Assuming that the viscous flux Jacobians can be split into positive and negative contributions, Equation (162) can be written as

$$(I + \Delta\tau\delta_l M^+ \cdot + \Delta\tau\delta_l M^- \cdot)\Delta Q^n = -\Delta\tau R^n \qquad (185)$$

where

$$\delta_l M^+ = \delta_i A^+ + \delta_j(B^+ - B_v^+) + \delta_k(C^+ - C_v^+) , \qquad (186)$$

$$\delta_l M^- = \delta_i A^- + \delta_j(B^- - B_v^-) + \delta_k(C^- - C_v^-) , \qquad (187)$$

and $\Delta\tau R^n$ represents the entire RHS of Equation (162). After expanding and manipulating Equation (185), the result can be written in the following factored form

$$(I - D_l^{-1}M_{l-1}^{+})(I + D_l^{-1}M_{l+1}^{-})\Delta Q^n = - D_l^{-1}R_l^n \ , \tag{188}$$

where

$$D_l = \frac{I}{\Delta\tau} + M_l^{+} + M_l^{-} \ . \tag{189}$$

The above equation can be solved in the following two steps

$$\begin{aligned} (D_l - M_{l-1}^{+})\Delta Q^{*} &= - R_l^n \ , \\ (D_l + M_{l+1}^{-})\Delta Q^{n} &= D_l \, \Delta Q^{*} \ . \end{aligned} \tag{190}$$

using an efficient LU decomposition.

5. VISCOUS FLUXES

Computation of the viscous fluxes follows the methodology of Chen [Reference 28], with the Black Box providing the necessary transport and thermodynamic properties in place of the perfect gas relations. However, Chen [Reference 28] and others treat the viscous terms explicitly, since implicit treatment using a characteristic-based splitting is not possible. In the following, the method used to split the viscous fluxes, in a manner that allows implicit treatment of these terms and preserves the efficiency of the existing LU algorithm, will be discussed. Also, a brief discussion will be given as to the modeling of turbulent flows.

a. VISCOUS FLUX DISCRETIZATION

The generic viscous flux vector given in Equation (153) can be rewritten as

$$S_v = J|\Delta k|^2 \begin{bmatrix} 0 \\ \mu\dfrac{\partial u}{\partial k} + \dfrac{\mu}{3}\tilde{k}_x V^{*} \\ \mu\dfrac{\partial v}{\partial k} + \dfrac{\mu}{3}\tilde{k}_y V^{*} \\ \mu\dfrac{\partial w}{\partial k} + \dfrac{\mu}{3}\tilde{k}_z V^{*} \\ \mathcal{K}\dfrac{\partial T}{\partial k} + \mu\dfrac{\partial(q^2/2)}{\partial k} + \dfrac{\mu}{3}\tilde{\theta}_k V^{*} \end{bmatrix} , \tag{191}$$

where

$$\begin{aligned} q^2 &= u^2 + v^2 + w^2 \ , \\ V^{*} &= \tilde{k}_x\frac{\partial u}{\partial k} + \tilde{k}_y\frac{\partial v}{\partial k} + \tilde{k}_z\frac{\partial w}{\partial k} \ . \end{aligned} \tag{192}$$

A symbolic representation of the terms comprising the viscous flux at face $l + 1/2$ can be given as follows

$$[S_v(Q)]_{l+\frac{1}{2}} = (\bigcirc)_{l+\frac{1}{2}} \left[\frac{\partial(*)}{\partial k}\right]_{l+\frac{1}{2}} . \tag{193}$$

In the above, the flux is divided into derivative terms ($*$) and all others ($\bigcirc$), where the latter comprises transport properties, μ and $\mathcal{K}$, and metric terms $\tilde{k}_{x_i}$. The derivatives are discretized using central differences as follows

$$\left[\frac{\partial(*)}{\partial k}\right]_{l+\frac{1}{2}} = (*)_{l+1} - (*)_l . \tag{194}$$

All other terms are evaluated as averages

$$(\bigcirc)_{l+\frac{1}{2}} = \frac{(\bigcirc)_l + (\bigcirc)_{l+1}}{2} , \tag{195}$$

with the exception of the metric terms, which are discretized in the following manner

$$|\Delta k|(\tilde{k}_{x_i})_{l+\frac{1}{2}} = \frac{(J|\Delta k|\tilde{k}_{x_i})_{l+\frac{1}{2}}}{\frac{1}{2}(J_l + J_{l+1})} , \tag{196}$$

where J is the Jacobian of the coordinate transformation.

b. VISCOUS JACOBIANS

As was stated previously, the viscous fluxes can be linearized in a similar fashion as the inviscid fluxes

$$S_v^{n+1} = S_v^n + \bar{S}_v(Q^n)\, \Delta Q^n , \tag{197}$$

where the viscous Jacobians are given as

$$\bar{S}_v(Q^n) = \frac{\partial S_v(Q^n)}{\partial Q} . \tag{198}$$

Dropping the temporal superscript and recalling the notation used in the previous subsection, the viscous flux correction at cell face $l + 1/2$ can be written in the following manner

$$\left[\frac{\partial S_v(Q)}{\partial Q}\right]_{l+\frac{1}{2}} \Delta Q_{l+\frac{1}{2}} = \left\{ \frac{\partial(\bigcirc)_{l+\frac{1}{2}}}{\partial Q}\left[\frac{\partial(*)}{\partial k}\right]_{l+\frac{1}{2}} + (\bigcirc)_{l+\frac{1}{2}}\frac{\partial}{\partial k}\left[\frac{\partial(*)}{\partial Q}\right]_{l+\frac{1}{2}}\right\} \Delta Q_{l+\frac{1}{2}} . \tag{199}$$

Using the same differencing techniques given above and recalling the upwind discretization of the inviscid fluxes, Equation (199) can be discretized as follows

$$\left[\frac{\partial S_v(Q)}{\partial Q}\right]_{l+\frac{1}{2}} \Delta Q_{l+\frac{1}{2}} = \bar{S}_v^{+} \Delta Q_l + \bar{S}_v^{-} \Delta Q_{l+1} , \tag{200}$$

where

$$\bar{S}_v^{-} = \left\{ \frac{1}{2}\left[\frac{\partial(*)}{\partial k}\right]_{l+\frac{1}{2}}\left[\frac{\partial(\mathrm{O})}{\partial Q}\right]_{l+1} + (\mathrm{O})_{l+\frac{1}{2}}\left[\frac{\partial(*)}{\partial Q}\right]_{l+1} \right\} , \tag{201}$$

$$\bar{S}_v^{+} = \left\{ \frac{1}{2}\left[\frac{\partial(*)}{\partial k}\right]_{l+\frac{1}{2}}\left[\frac{\partial(\mathrm{O})}{\partial Q}\right]_{l} - (\mathrm{O})_{l+\frac{1}{2}}\left[\frac{\partial(*)}{\partial Q}\right]_{l} \right\} . \tag{202}$$

This is the same type of discretization used by Cinnella [Reference 40] in the development of the production code GASP (General Aerodynamic Simulation Program). The use of Equation (198) allows for the implicit treatment of the viscous fluxes while maintaining the efficiency of the LU decomposition. The discretized components of the viscous Jacobians are given in Appendix E.

c. TURBULENCE MODELING

The TLNS equations are applicable to both laminar and turbulent flows, provided that the turbulence model is based on eddy viscosity. The total viscosity and thermal conductivity are given as the sum of the laminar and turbulent contributions, as follows

$$\mu = \mu_l + \mu_t , \tag{203}$$

$$\mathcal{K} = \mathcal{K}_l + \mathcal{K}_t , \tag{204}$$

where subscripts l and t denote the laminar and turbulent values, respectively. The laminar viscosity and thermal conductivity are provided by the Black Box.

The turbulent viscosity is determined using the Baldwin and Lomax model [Reference 41]. A very good description of this model and its application is given by Chen [Reference 28] and the details are not repeated here. The turbulent thermal conductivity is computed by

$$\mathcal{K}_t = \frac{\tilde{c}_p \, \mu_t}{Pr_t} , \tag{205}$$

where $\tilde{c}_p$ is the frozen specific heat at constant pressure defined in Equation (19) and Pr_t is the turbulent Prandtl number. Since there are few turbulent studies for high enthalpy flows and no data as to what is a practical value for Pr_t, the standard value of $Pr_t = 0.90$ will be used in the calculations.

6. BOUNDARY CONDITIONS

Explicit boundary conditions are applied throughout using a first order extrapolation to a layer of phantom cells surrounding the computational domain. All inflow and outflow boundaries incorporate the characteristic variable boundary conditions, CVBC's, as developed by Janus [Reference 42], which allow flow information to be propagated in the direction of the characteristic wave speeds. CVBC's are also used at impermeable surfaces for inviscid computations. No–slip boundary conditions are used at impermeable surfaces for viscous computations along with a specified pressure gradient and either adiabatic wall or specified wall temperature.

Application of the boundary conditions for a real gas are the same as for a perfect gas, with the exception that the thermodynamic properties are obtained by means of the Black Box, as was stated previously in Section II. The known thermodynamic properties resulting from the enforcement of the CVBC subsonic inflow, outflow or impermeable surface boundary condition are pressure and density and therefore the complete thermodynamic system, CTS, is defined by using the "Black Box" as a function of pressure and density, $\mathrm{CTS} = f(p, \varrho)$. For the no slip boundary condition with specified temperature, pressure and temperature are the known properties and hence, $\mathrm{CTS} = f(p, T)$.

SECTION VIII

FLOW SOLVER RESULTS

Numerical results have been obtained using the methods proposed in the previous sections. As a means of validation, four test cases, two inviscid and two viscous, were examined. The inviscid computation involved hypersonic flow about a blunt 9° half-angle cone with a nose radius of 2.5 in. and the numerical simulation of the Space Shuttle Main Engine (SSME). The two viscous test cases include a standard flat plate computation, for code validation, and a hypersonic inlet. Also, a numerical study is made of the efficiency of the chemical equilibrium solver.

All of the solutions have been obtained using second order spatial accuracy, advancing the solution to its steady state by means of the Euler implicit scheme described in Section VII. The approximate Riemann solver of the Roe type, developed in Section VII, is used for all calculations and higher order accuracy is attained using the Van Leer limiter.

Characteristic variable boundary conditions are used wherever applicable, including the impermeable surface for inviscid computations. No–slip, adiabatic–wall, with zero pressure gradient boundary conditions are used for the viscous calculations.

The simple 5–Species Air Model is employed as the air chemistry model, along with the Consistent K_c. The thermodynamic model used is the Vibrational Model. Newton Limiter and Relative Limiter are used for corrections of the species densities and temperature updates, respectively. Transport properties are provided by the combination of Sutherland Model for the species values and Wilke's Rule for the mixture values.

1. INVISCID RESULTS

a. BLUNT CONE

The geometry of the blunt cone and the 71×26 grid used for the inviscid computations can be seen in Figure 38. The freestream conditions, corresponding to an altitude of 10 km, were: pressure $p_\infty = 26.5$ kPa, density $\rho_\infty = 0.414$ kg/m^3 and temperature $T_\infty = 223$ K. Computations were made at Mach number $M_\infty = 10$ and zero angle of attack using both the perfect gas model and the 5–Species Air Model.

The effects of a "real gas" are immediately apparent in Figure 39, where the temperature profiles along the stagnation streamline are plotted for both reactive and perfect gas computations. Shock standoff distance and temperature levels are strongly affected by the thermochemical model chosen. The reduced temperatures for the chemical equilibrium solution are due to the conversion of some of the kinetic energy to dissociation energy, where for a perfect gas all of the kinetic energy would go to thermal energy. Higher densities in the shock layer for the real gas solution, characteristic of reactive flows [Reference 44], are seen in Figure 40 where the density profiles along the stagnation streamline are plotted. Figure 41 depicts the temperature profiles along the body surface, where large temperature differences between the perfect gas and real gas solutions exist at the nose, but the solutions are in good agreement in the cooler regions, starting at the shoulder. The previous results correlate nicely with the plot of the mixture composition along the body surface seen in Figure 42. The plot indicates strong oxygen dissociation at the nose, but as the flow moves along the body and cools, recombination occurs. Figure 43 depicts the pressure coefficient along the body surface. It can be seen that pressure is not strongly affected by real gas effects, due to its "mechanical" nature [Reference 45].

b. SSME NOZZLE

The geometry of the SSME nozzle and the 88 x 31 grid used for the inviscid computations are shown in Figure 44. Combustion chamber conditions correspond to 100% power at sea level and were: mixture ratio of 6.0, Mach number $M_c = 0.2$, temperature $T_c = 3639.0$ K, and pressure $p_c = 20.24$ MPα. Computations were made using both the perfect gas model, with $\gamma = 1.18$, and Hydrogen–Oxygen Combustion Model.

Density profiles along the centerline and wall of the nozzle are given in Figure 45. In the following, the axial distances shown in the figures will be referenced to the throat position. The results show that there is little difference between the perfect gas and real gas solutions. A greater disparity is seen for the temperature profiles in Figure 46. Higher temperatures for the real gas solutions occur at a point just past the throat. The reason for this becomes apparent when looking at Figure 47, where the composition along the wall is given: as the flow expands on the downstream side of the throat, recombination reactions occur, which are exothermic in nature.

Similar computations were made by Wang and Chen [Reference 13], using a pressure-based flow solver and equilibrium chemistry. Comparisons of the real gas solutions obtained in the present study with the results obtained by Wang and Chen [Reference 13] are made in Figure 48 and Figure 49, where plots of Mach number profiles and pressure decays are given, respectively. The figures show excellent agreement between the two sets of results, with the exception being the throat region. The present study appears to do a better job of capturing the nozzle shock at the wall. The specific impulse of the SSME nozzle was computed to be 460.0 sec, which is also in excellent agreement with the value of 460.4 sec predicted by Wang and Chen [Reference 13].

2. VISCOUS RESULTS

a. FLAT PLATE

In order to validate the viscous capability of the code, solutions for the laminar and turbulent flow over a flat plate were obtained. The freestream conditions were: Mach number $M_\infty = 0.5$, temperature $T_\infty = 300$ K, and Reynolds numbers per unit length, Re/L, of $1.972\ 10^4$ and $1.972\ 10^6$, for the laminar and turbulent computations, respectively. The laminar results for both the perfect gas and 5-Species Air Model, presented in Figure 50, nicely reproduce the Blasius solution. Similarly, the turbulent results using the 5-Species Air Model, as given in Figure 51, are seen to be in excellent agreement with the law of the Wall results.

b. INLET

The hypersonic inlet is composed of a flat-surfaced cowl and a 10° ramp, with an inlet height D = 2 m and exit height of 0.5 D. The overall length is 4.25 D and the cowl length is 0.5 D. Conditions at the inlet are: Mach number $M_\infty = 10$, pressure $p_\infty = 1.015$ kPa, density $\varrho_\infty = 1.172\ 10^{-2}$ kg/m^3, temperature $T_\infty = 300$ K, and Reynolds number based on the inlet height $Re_D = 4.4\ 10^6$. Figure 52 depicts the inlet geometry and 111×61 grid used for the viscous calculations. Computations were made using the perfect gas model and the 5-Species Air Model. Grid packing at the wall resulted in y^+ values less than 1, which is considered more than adequate to define the viscous sub-layer.

Figure 53 depicts the temperature profiles along the top and bottom walls of the inlet. Two important points need to be made about this plot. The first is the gross overproduction of the temperature values by the perfect gas model. The second is the displaced location of the incident shock on the top wall; shock location for the real gas solution is slightly downstream of that for the perfect gas solution. The surface pressure distributions for the top and bottom walls are given in Figure 54. As was seen previously, pressure is not strongly affected by the inclusion of real gas effects. Similar results are seen in Figure 55, where the coefficient of skin friction is plotted. The primary difference in both plots is the displacement of the incident shock. The mixture composition along the bottom wall is given in Figure 56, where it can be seen that oxygen is almost entirely dissociated. Of particular interest is the slight decrease in the mole percentage of the monatomic species, which occurs before the ramp induced oblique shock. This correlates nicely with the slight drop in temperature seen in Figure 53. Opposite results occur for the expansion. Figure 57 depicts the Mach number, temperature and pressure profiles along the centerline. As can be seen, there is very little difference between the solutions for the two thermochemical models, other than the reduced shock angle. The real gas effects are local to the boundary layer and have the greatest impact on the surface temperatures.

3. PERFORMANCE

In order to determine the efficiency of the chemical equilibrium flow solver, a numerical study was made involving inviscid computations for the blunt cone geometry. CPU times and iteration counts obtained using the 5–Species Air Model were compared to those obtained using the perfect gas model. Several techniques for enhancing the efficiency of the solver were implemented and tested. All computations were made on a Silicon Graphics IRIS 4D–340VGX machine.

The techniques used to enhance the efficiency include the use of vector reduction and chemistry freezing, both of which have been described previously in Section IV. Five test cases were tried using the 5–Species Air Model and compared to the perfect gas solution. Case 1 represents the baseline computation, where no efficiency techniques are implemented. Vector reduction was implemented in Cases 2–5, and various freezing strategies were employed for Cases 3–5. The convergence strategy used for both perfect gas and real gas runs, as well as the efficiency strategies employed are summarized in Table 8.

The results for Cases 1–3 and the perfect gas run are given in Figure 58, where the normalized residuals versus CPU time are plotted. Each symbol on the plots corresponds to 100 cycles. The perfect gas computation achieves a residual reduction of almost five orders of magnitude in a little less than one CPU hour. The baseline real gas computation, Case 1, requires 20 CPU hours to attain a comparable residual reduction. It should be pointed out that the first 200 cycles accounts for nearly 30 percent of the total CPU time. Using vector reduction, a reduction in CPU time of almost one half is realized, as can be seen for Case 2. A more significant reduction is attained when the first freezing strategy, Case 3, is employed, resulting in a CPU time savings of about 85 percent over the baseline computation.

Slight improvements are still obtainable, as is seen in Figure 59, in which the results for Cases 3–5 are compared to the perfect gas result. The total CPU time required for Case 4 is just under three hours. However, CPU requirements appear to be little affected by the particular freezing strategy employed, provided that a freezing strategy is employed. The results for Case 5, where a marginal improvement over Case 4 can be seen for the first 200 cycles but no overall gain is achieved, confirm this conclusion. Again it should be pointed out that the beginning of the computation, when variations in flow conditions are significant, requires a large percentage of the overall CPU time.

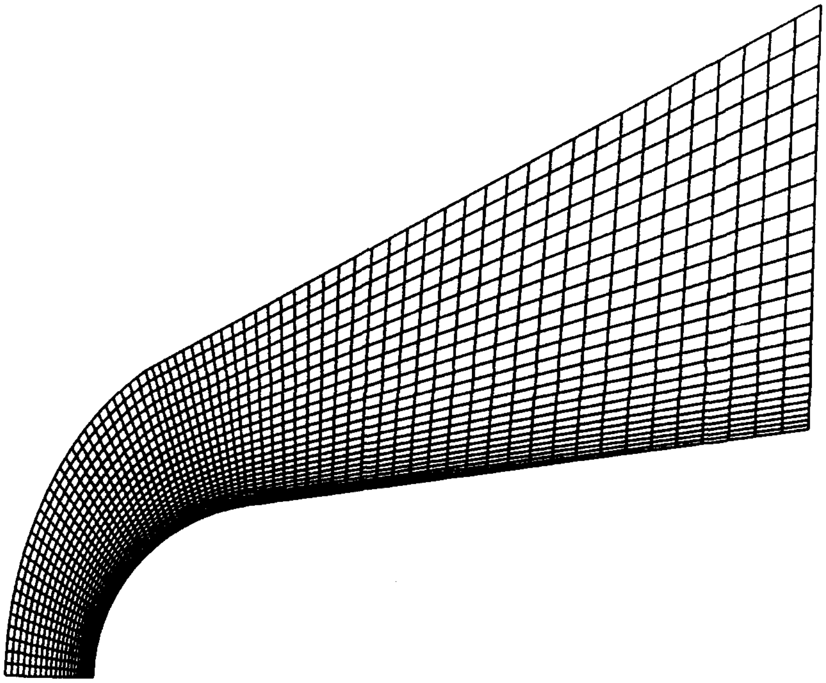

Figure 38 Blunt cone geometry and inviscid grid (71x26)

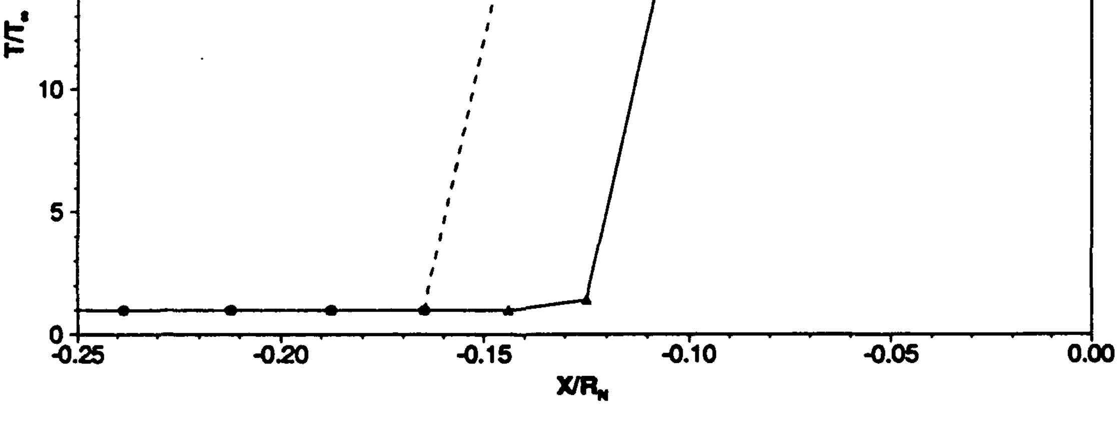

Figure 39 Temperature profiles along the stagnation streamline. Blunt cone, invisicid.

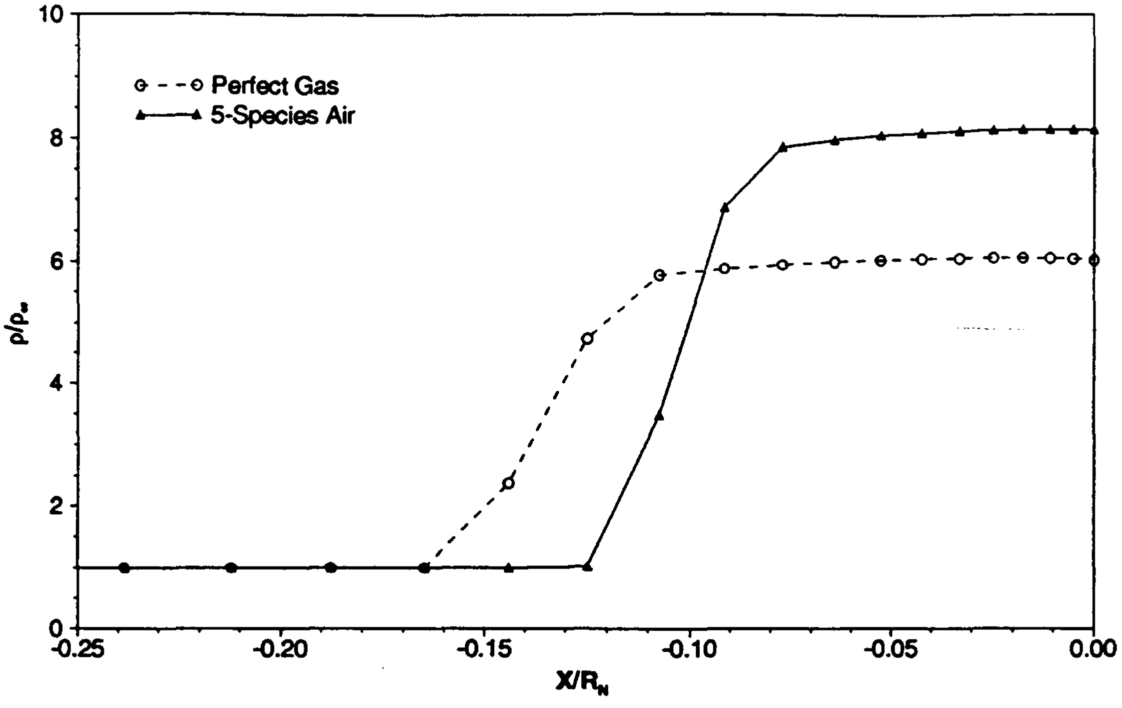

Figure 40 Density versus distance along the stagnation streamline. Blunt cone, inviscid.

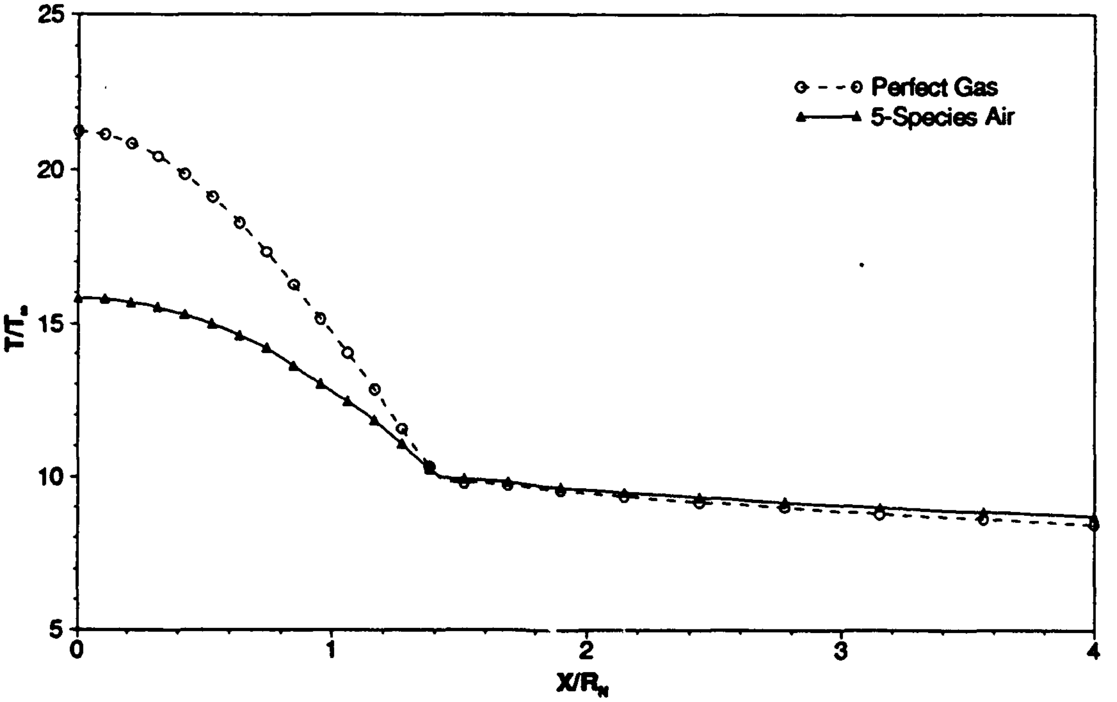

Figure 41 Temperature versus distance along the body surface. Blunt cone, inviscid.

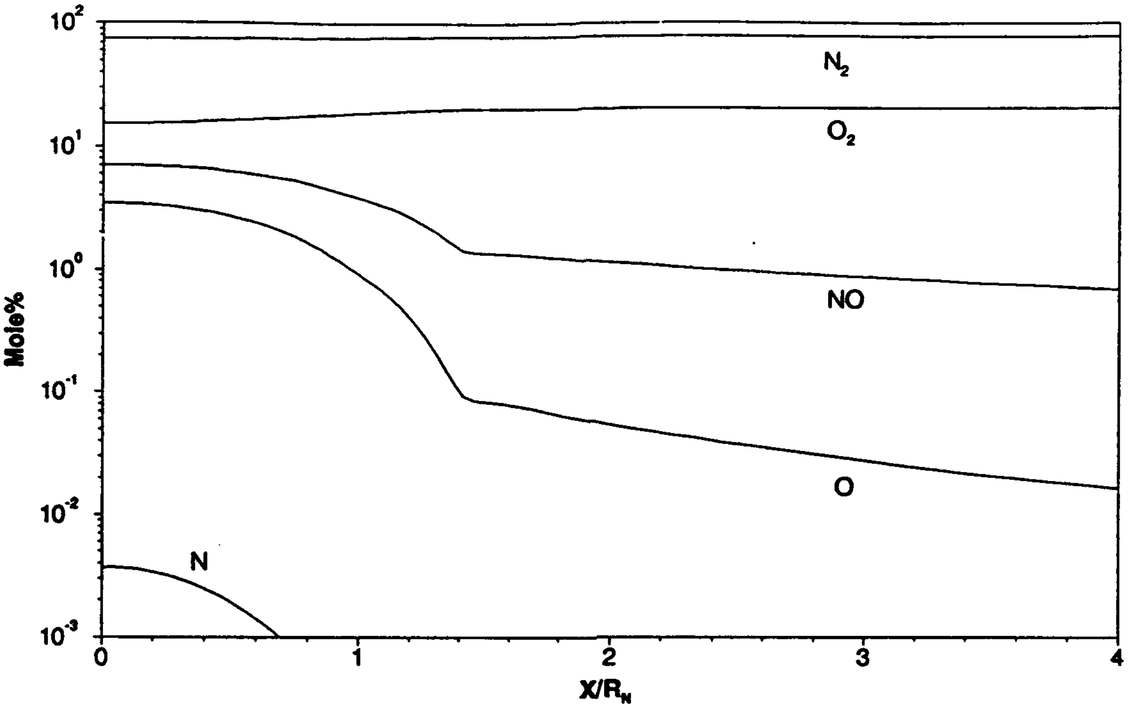

Figure 42 Mole fractions versus distance along the body surface. Blunt cone, inviscid

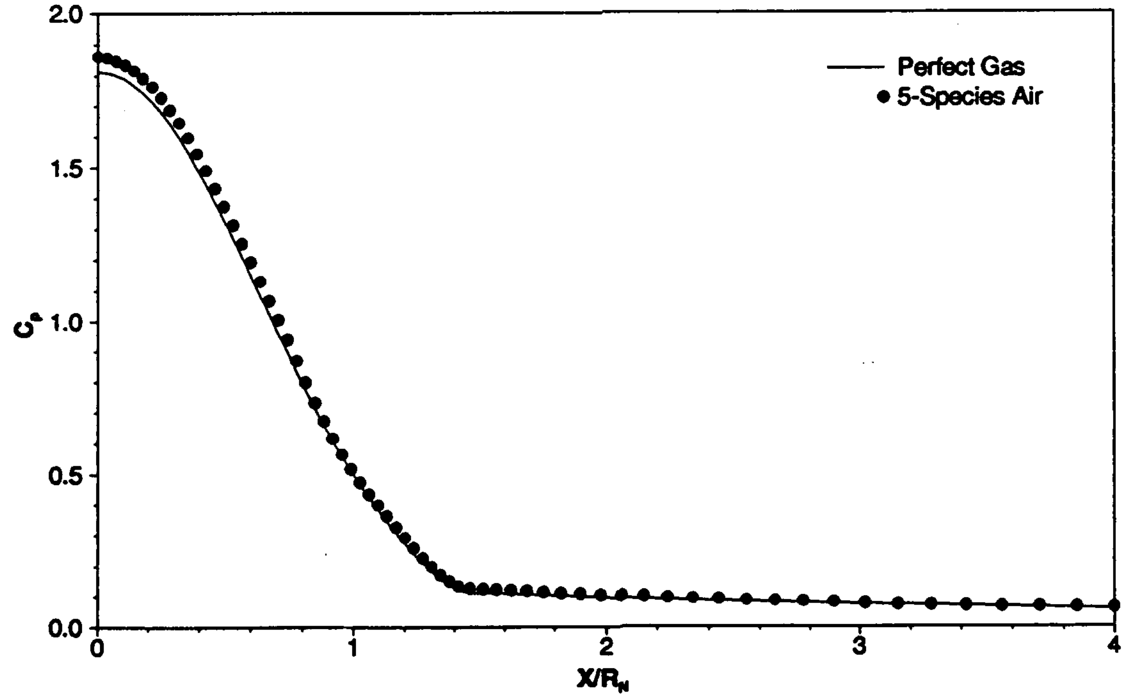

Figure 43 Pressure coefficient versus distance along the body surface.
Blunt cone, inviscid

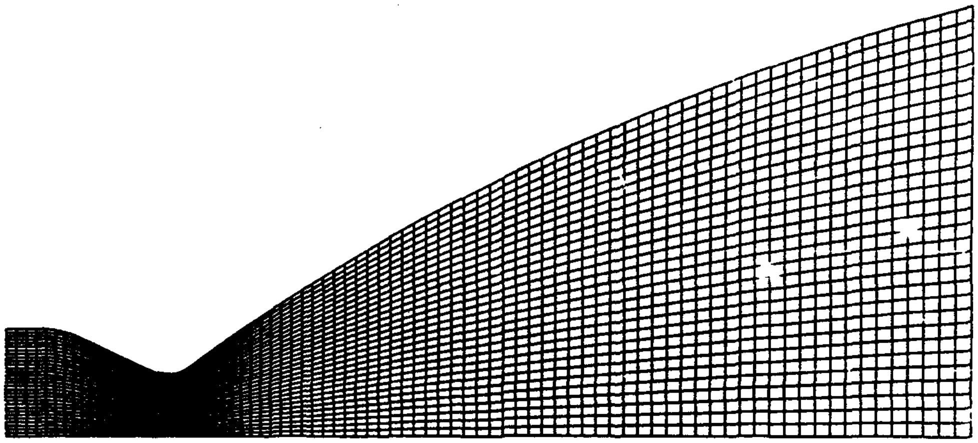

Figure 44 SSME nozzle geometry and inviscid grid (88x31)

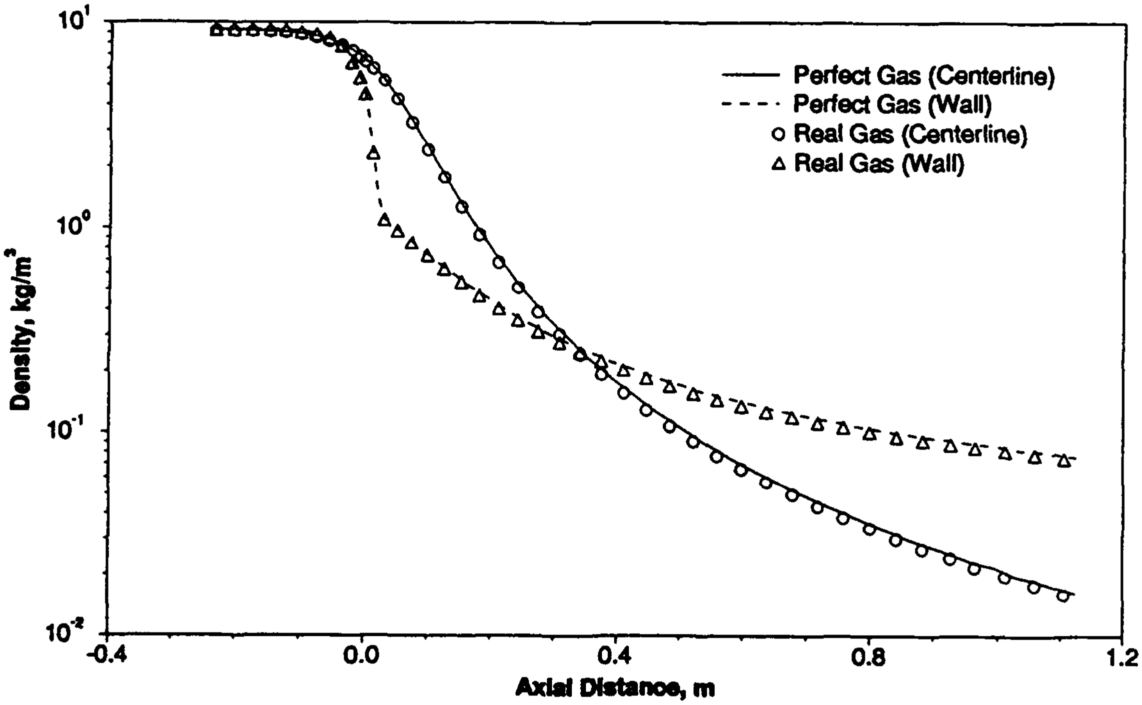

Figure 45 Comparison of density profiles. SSME nozzle.

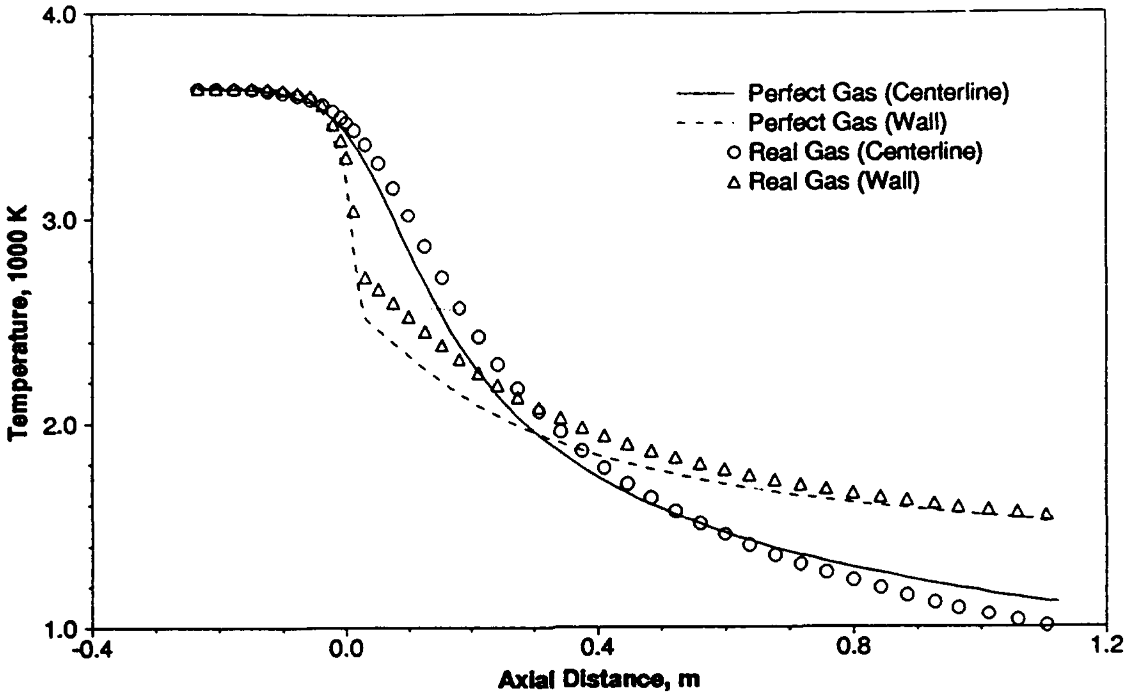

Figure 46 Comparison of temperature profiles. SSME nozzle.

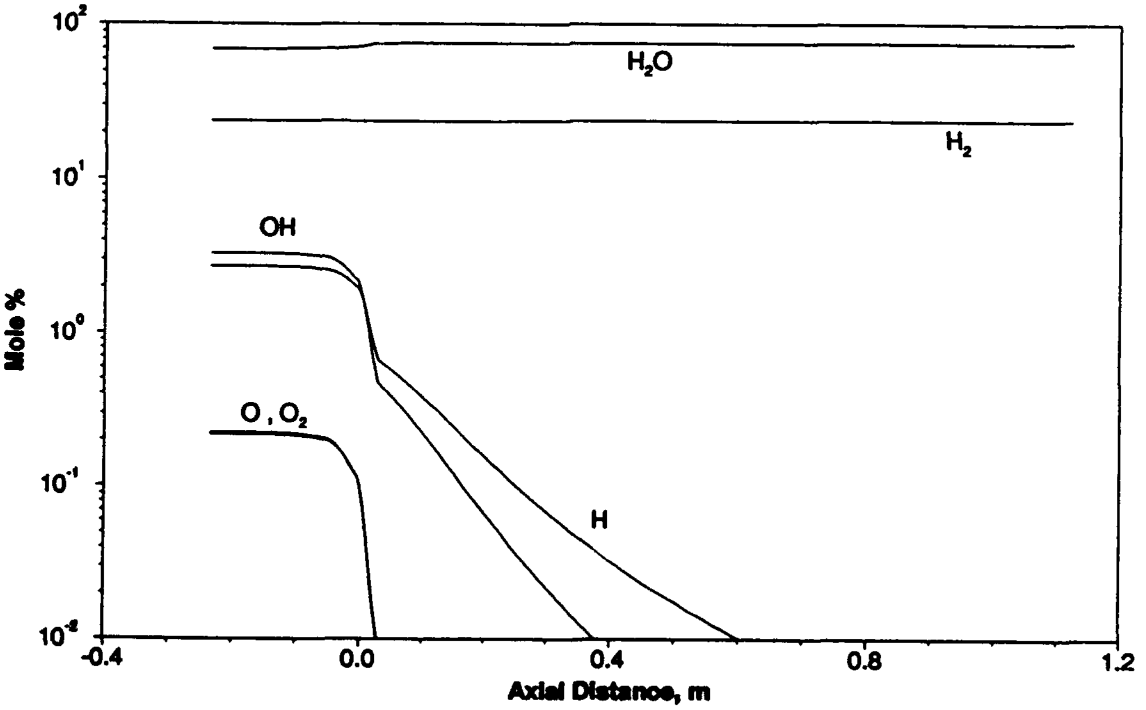

Figure 47 Composition along the wall. SSME nozzle.

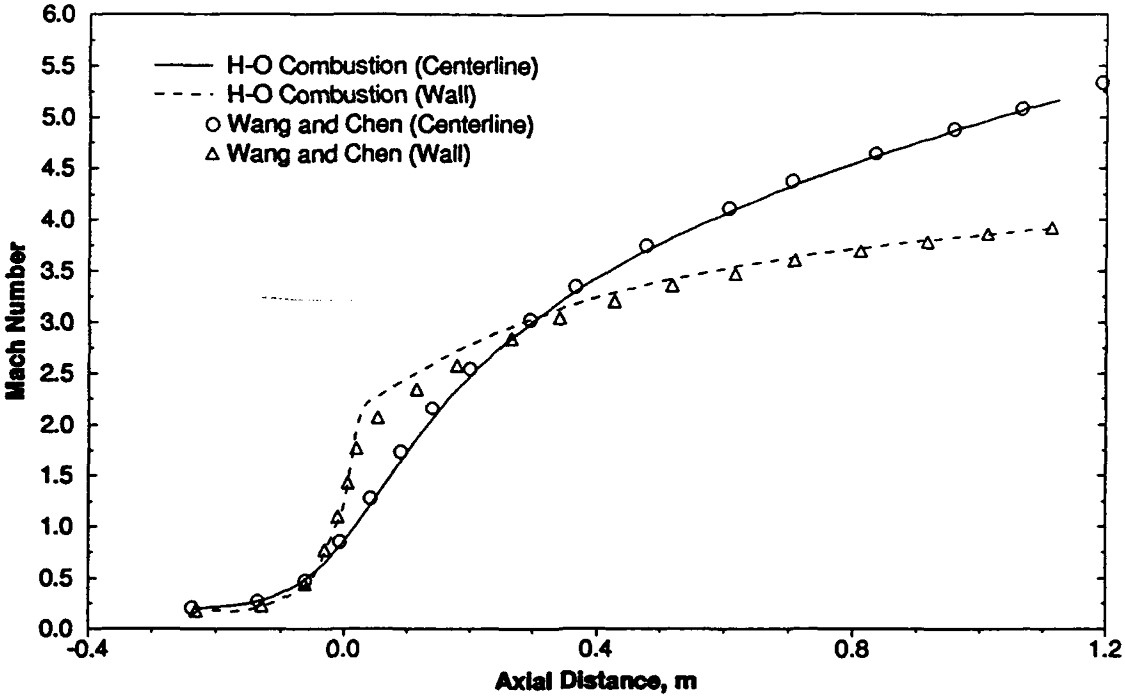

Figure 48 Comparison of Mach number distributions. SSME nozzle.

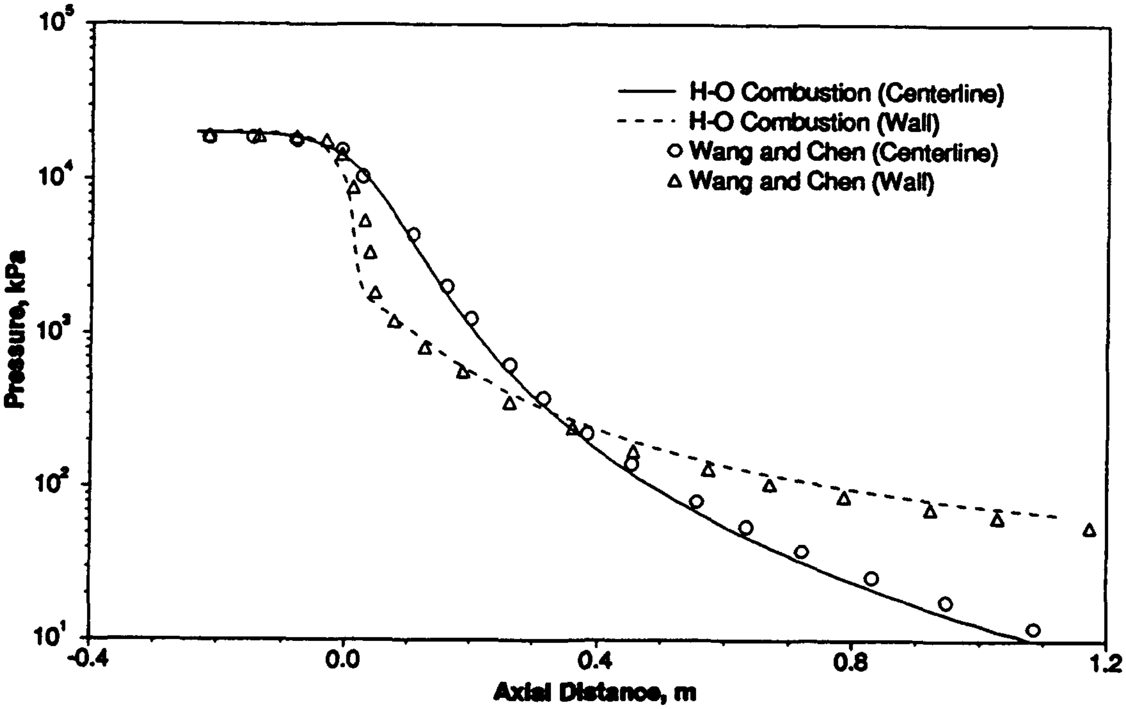

Figure 49 Comparison of pressure decays. SSME nozzle

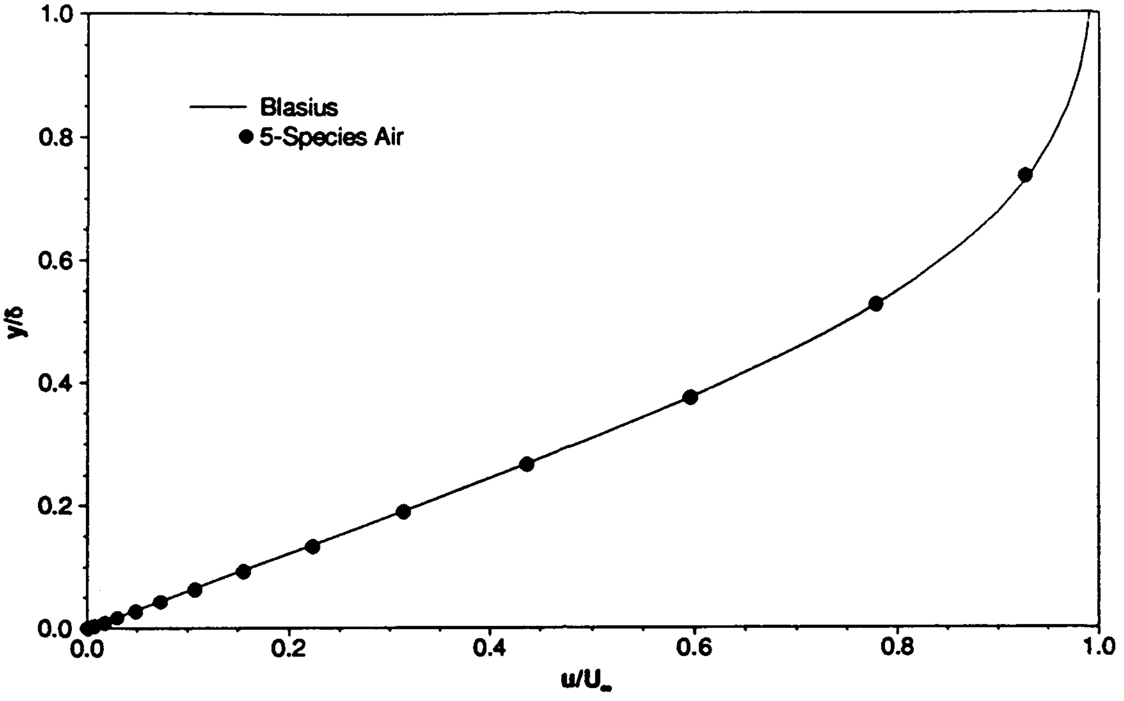

Figure 50 Laminar velocity profiles for the flat plate.

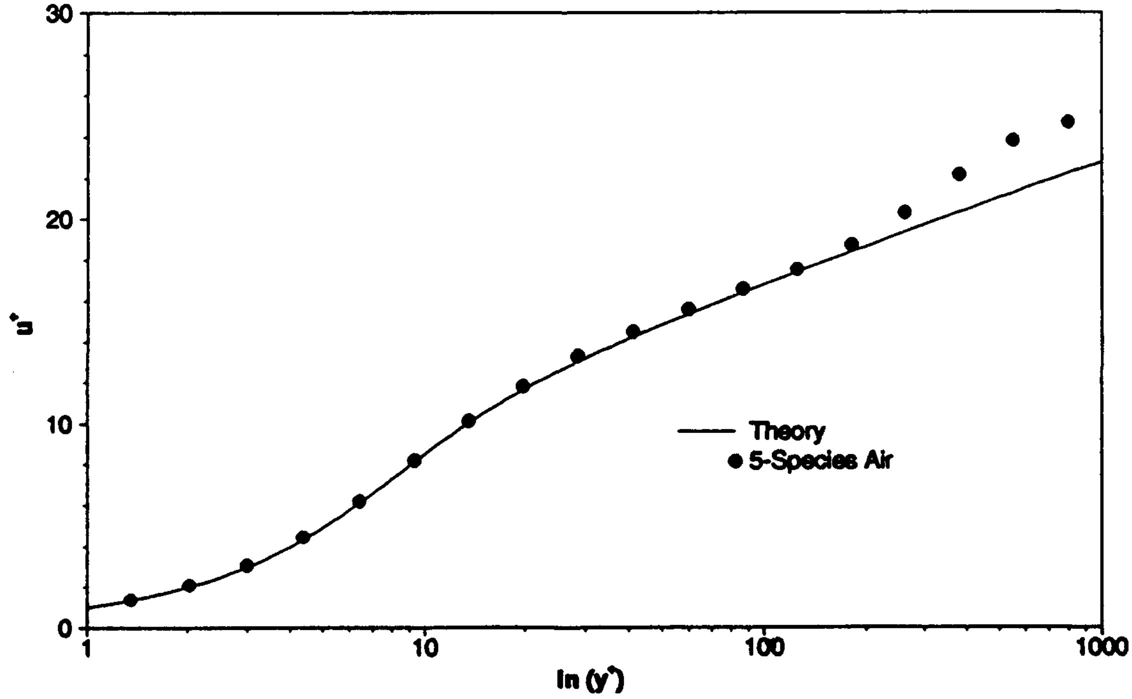

Figure 51 Turbulent velocity profiles for the flat plate.

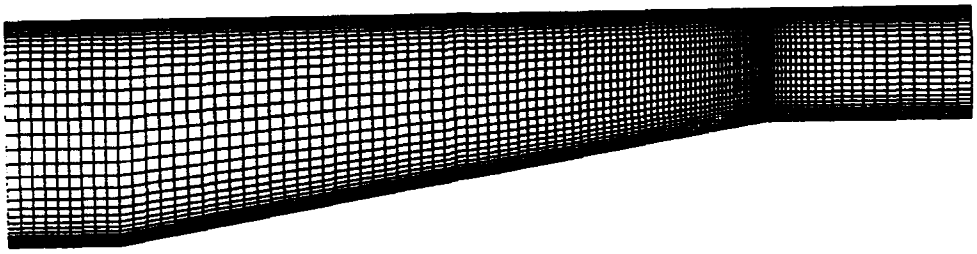

Figure 52 Inlet geometry and grid (111x61x2).

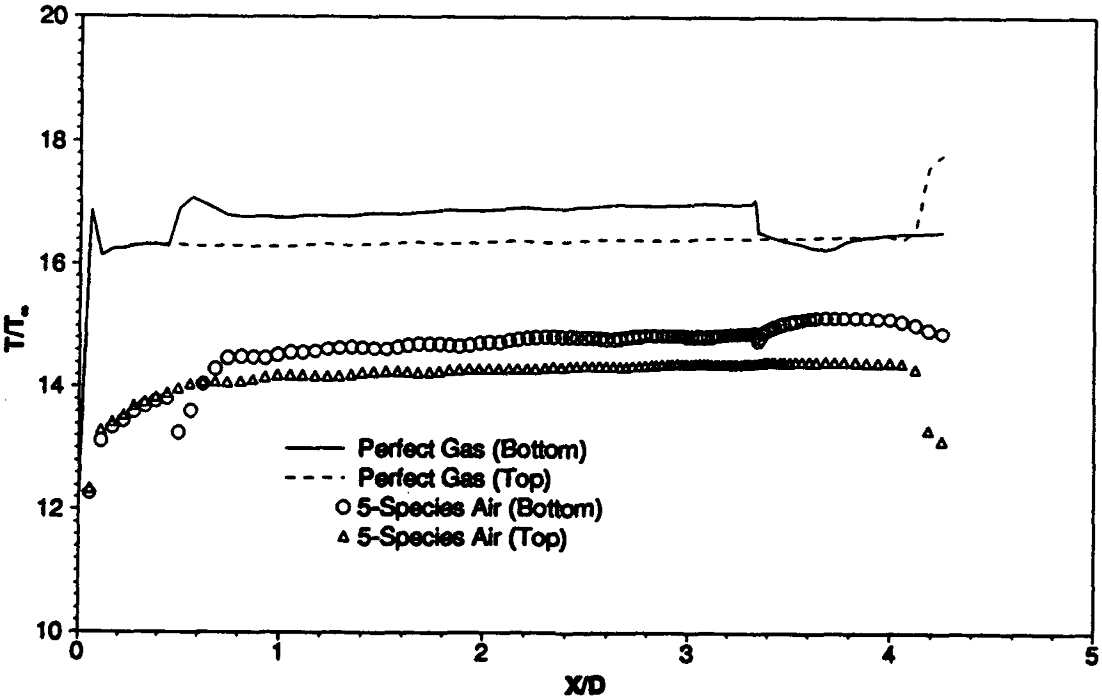

Figure 53 Temperature profiles along the walls. Inlet, viscous.

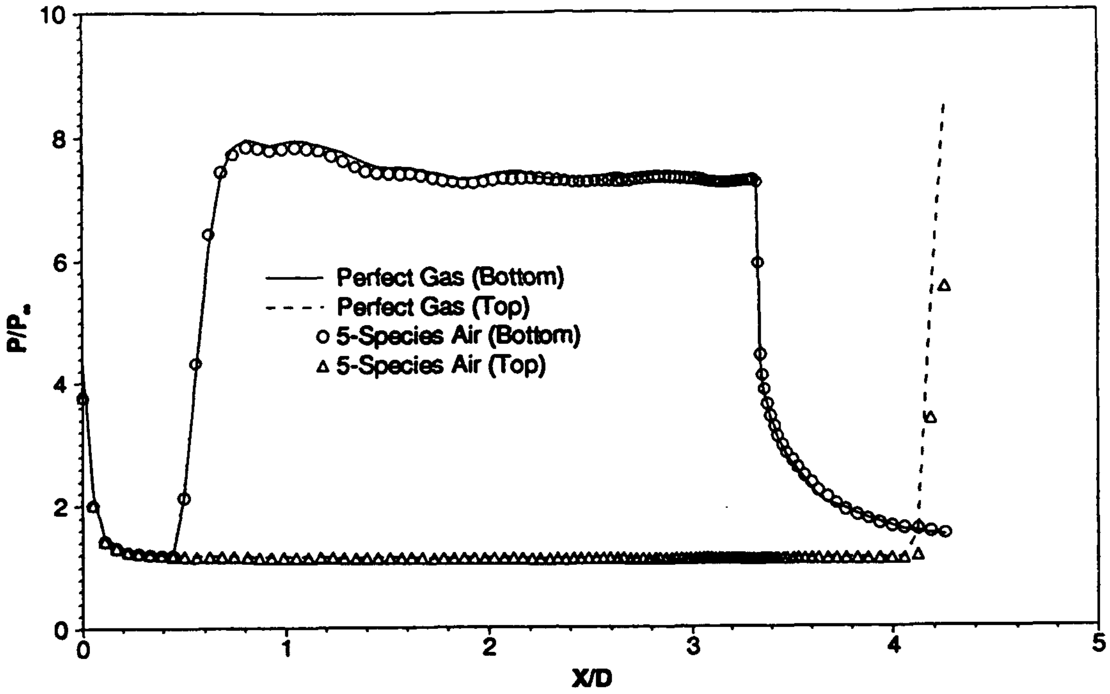

Figure 54 Pressure profiles along the walls. Inlet, viscous.

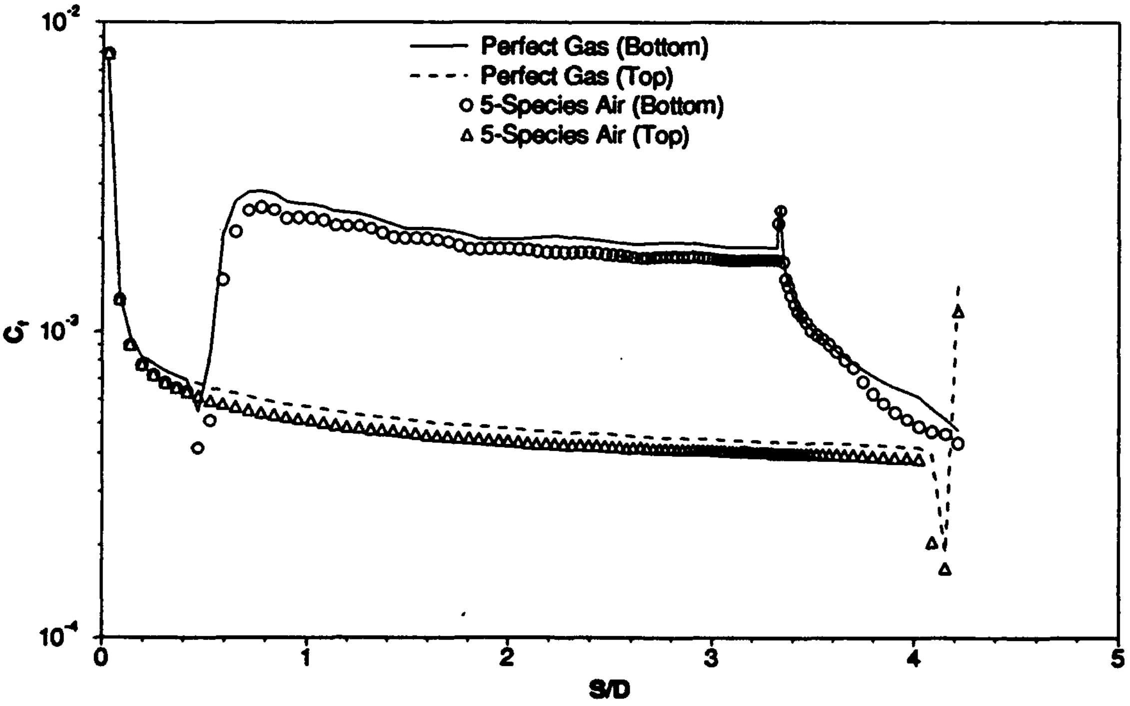

Figure 55 Skin friction coefficient profiles along the walls. Inlet, viscous.

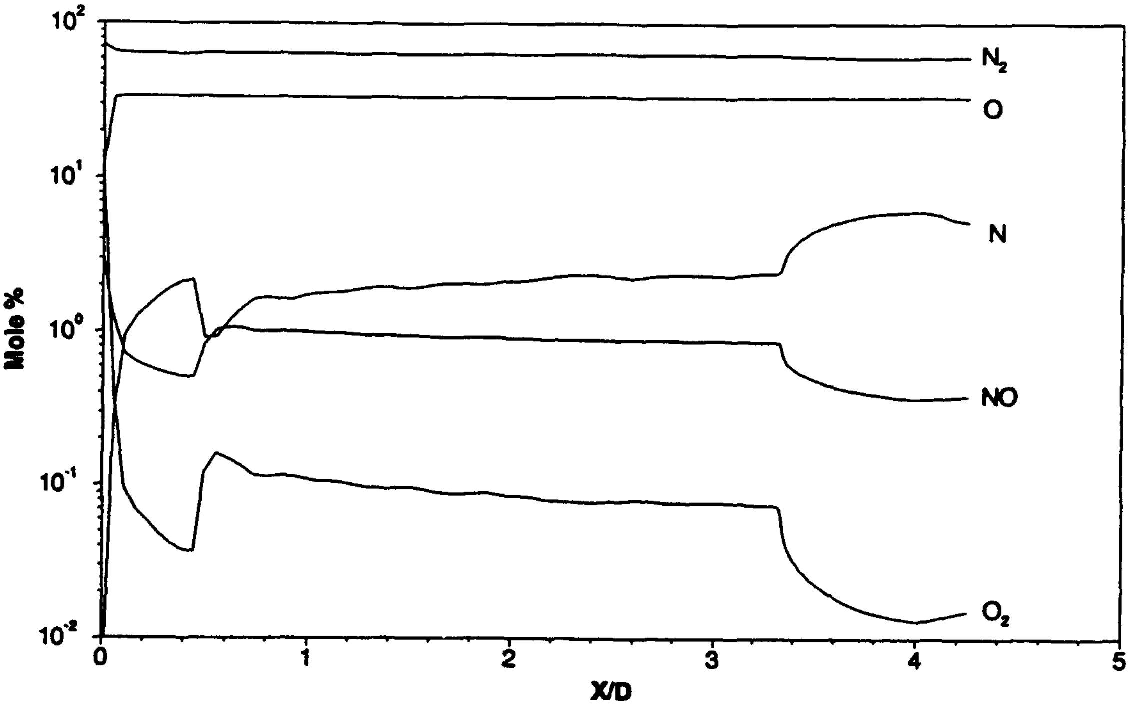

Figure 56 Composition along the bottom wall. Inlet, viscous.

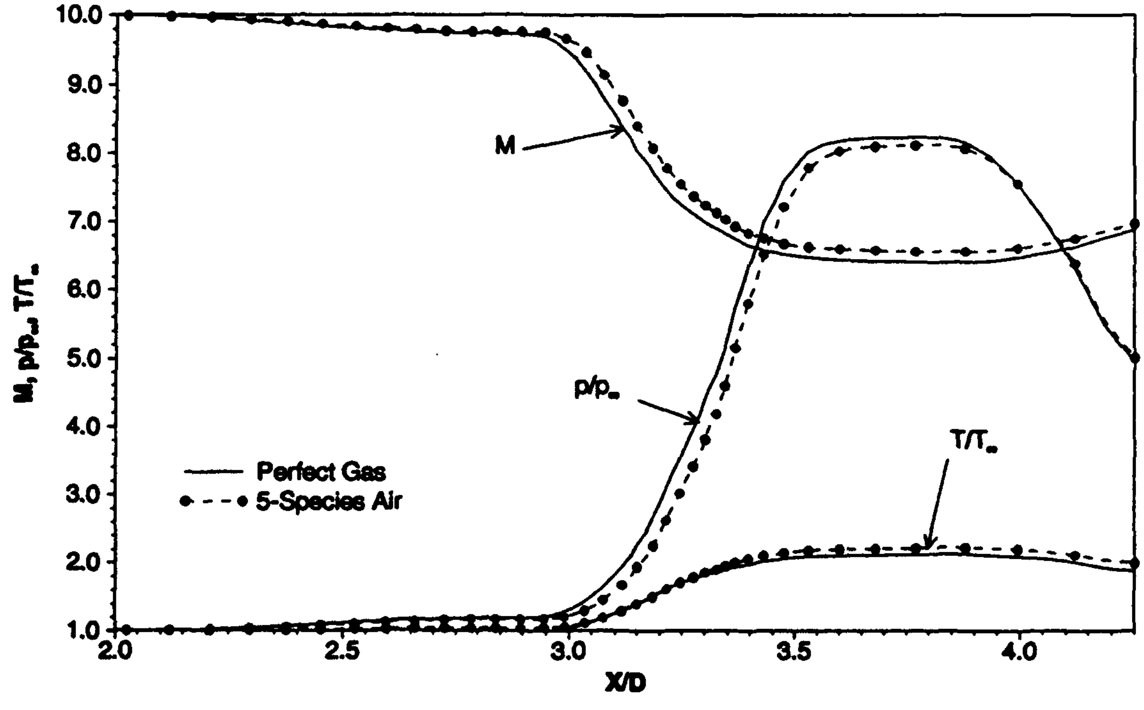

Figure 57 Mach number, pressure and temperature distributions along the centerline. Inlet, viscous.

Cycle	CFL #	Order	Vector Reduction / Number of Cycles Frozen				
			Case #1	Case #2	Case#3	Case #4	Case #5
0–100	0.5	1st	N / 0	Y / 0	Y / 5	Y / 10	Y / 20
100–200	1.0	2nd	N / 0	Y / 0	Y / 10	Y / 20	Y / 20
200–300	2.0	2nd	N / 0	Y / 0	Y / 10	Y / 20	Y / 50
300–400	4.0	2nd	N / 0	Y / 0	Y / 25	Y / 50	Y / 50
400–1000	4.0	2nd	N / 0	Y / 0	Y / 50	Y / 50	Y / 50

Table 8 Convergence and efficiency strategies.

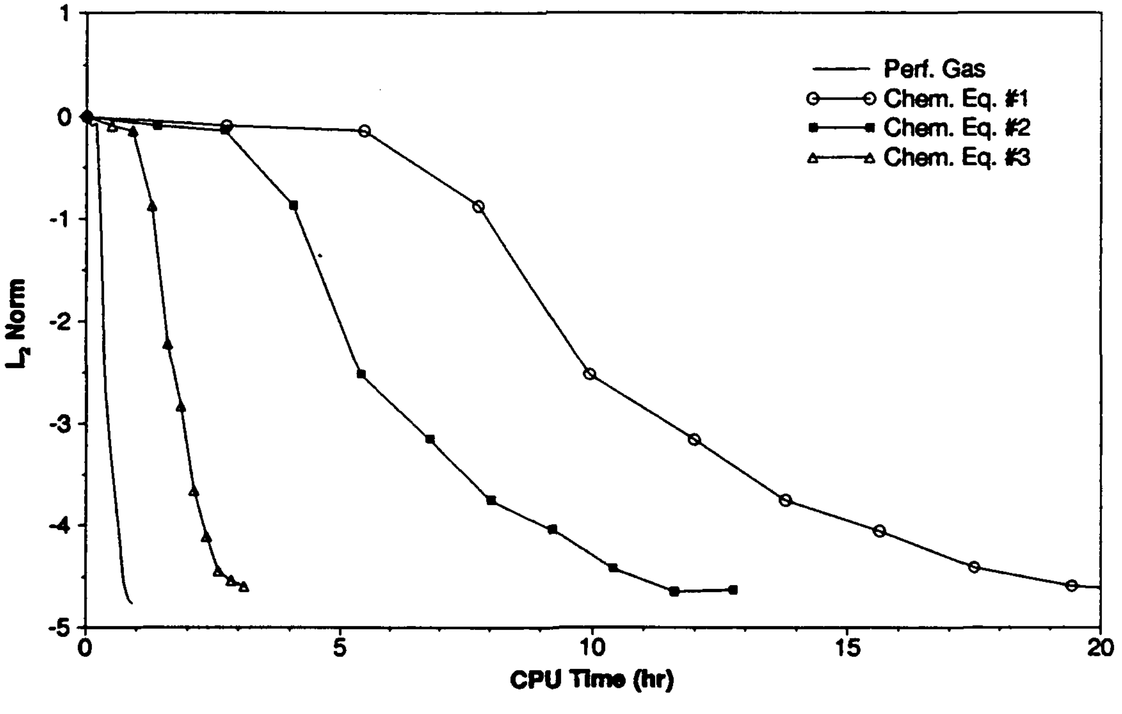

Figure 58 Comparison of residuals versus CPU time. Cases 1-3.

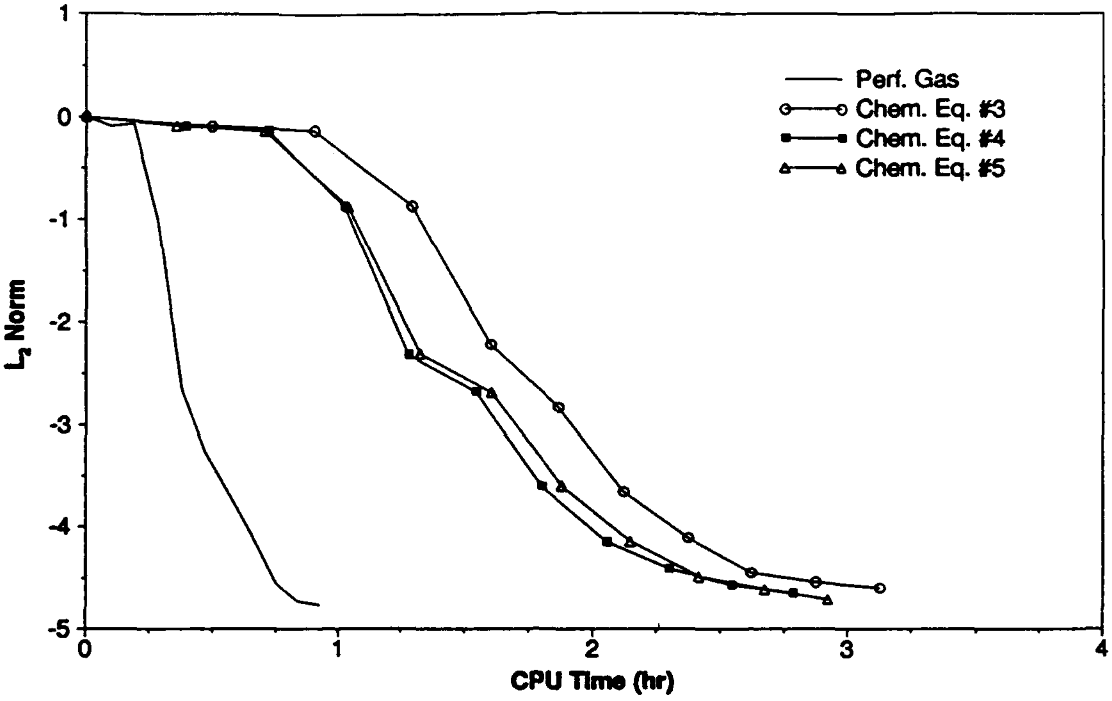

Figure 59 Comparison of residuals versus CPU time. Cases 3-5.

SECTION IX

SUMMARY AND CONCLUSIONS

The goal of the present study has been the development of an efficient solver for flows in local chemical equilibrium. The work has been carried out in two phases: the development of a "Black Box" solver for the determination of the equilibrium composition and thermodynamic properties; and the incorporation of this Black Box into a perfect gas flow solver that has been modified to include real gas effects. The end result is a numerical tool, whereby the solutions for high-temperature, high-speed flow fields can be efficiently obtained without the enormous computational cost associated with finite-rate chemistry.

A Black Box chemical equilibrium solver was developed for homogeneous mixtures of thermally perfect gases. Several practical chemistry models, describing air mixtures, combustion mixtures and a plasma, were implemented. The solver was written in a generic fashion, whereby the inclusion of additional chemistry models of interest is a relatively simple process. Two solution methods for the determination of the equilibrium composition were derived and implemented, the Mass Constraint Technique and the Degree of Advancement Technique. A third algorithm was explored briefly, but was found to be inadequate for the problem at hand, although further testing may be indicated. The Black Box provides the choice between two thermodynamic models, Vibrational Model and Curvefit Model, and two methods for the evaluation of the equilibrium constant, Curvefit K_c and Consistent K_c. For viscous computations, two procedures for the evaluation of the species transport properties were implemented, Sutherland Model and Gupta Model, and mixture values can be obtained with either Wilke Rule or Gupta Rule.

The Black Box was thoroughly tested for both efficiency and robustness. Although shortcomings were found in the basic algorithms, several efficiency saving and robustness enhancing techniques were implemented. The end result is a reliable solver for the determination of the composition and thermodynamic properties for an equilibrium gas mixture. The chemistry models that have been implemented were also tested on various conditions. The results show that the Black Box accurately predicts both composition and properties for a wide range of chemistry models, and illustrate the limitations of the perfect gas assumption.

The incorporation of "real gas" effects into an existing perfect gas flow solver posed an exciting challenge. Several modifications to the existing code were made, including the development of a new approximate Riemann solver for an arbitrary real gas. Real gas versions for the Steger-Warming flux-vector split scheme, split-flux Jacobians, and Roe-type flux-difference split scheme were derived and implemented. The real gas formulations were developed in a manner whereby they reduce to their perfect gas versions in a straightforward fashion.

Hypersonic flows, both inviscid and viscous, for a few test cases were investigated, as well as a validation computation using the ubiquitous flat plate. The results were encouraging, and demonstrated the fallacy of relying on the perfect gas assumption for high Mach number flows. The results for a hypersonic inlet also showed the importance of viscous effects in the study of real gas flows. Finally, an efficiency study was made of the chemical equilibrium flow solver. Techniques implemented to enhance efficiency worked very well. The results indicated that while the real gas computations are more expensive than comparable perfect gas computations, they are within reason and much more so than finite-rate computations.

Further work is necessary in several areas. Increasing the robustness of the Degree of Advancement Technique could also increase the efficiency of the flow solver, since this technique was found to be the more efficient of the "Black Box" algorithms. Further investigation of the chemical equilibrium solver developed by Meintjes and Morgan [Reference 4], might also prove profitable. An extended study of the effects of the number of species on flow solver efficiency is also warranted. In the present study, the "gamma" derivatives appearing in the split flux Jacobians were assumed to be zero, and the effects of this need to be ascertained. Numerical studies also need to be made of the transport property calculation procedures. The effects of using an improved initial guess for the Black Box computations, discussed in Section IV, also need to be investigated. Finally, multiblock capability needs to be added to the code, providing the ability to obtain solutions for more challenging geometries, such as the national aerospace plane (NASP), space shuttle and hypersonic vehicles with stores.

APPENDIX A
SPEED OF SOUND AND PRESSURE DERIVATIVES

1. SPEED OF SOUND

The speed of sound is defined by the relation

$$a^2 = \left(\frac{\partial p}{\partial \varrho}\right)_s . \tag{A.1}$$

Writing the combined 1st and 2nd Laws of Thermodynamics, for a gas in chemical equilibrium

$$Tds = de - \frac{p}{\varrho^2} d\varrho , \tag{A.2}$$

the partial derivative of internal energy with respect to density at constant entropy can be obtained as

$$\left(\frac{\partial e}{\partial \varrho}\right)_s = \frac{p}{\varrho^2} . \tag{A.3}$$

Expanding the partial derivative in Equation (A.1) and using the result from Equation (A.3), the equation for the speed of sound can be written in the following form

$$a^2 = \left(\frac{\partial p}{\partial \varrho}\right)_e + \frac{p}{\varrho^2}\left(\frac{\partial p}{\partial e}\right)_\varrho . \tag{A.4}$$

The thermal and caloric equations of state for an equilibrium mixture of thermally perfect gases can be written as

$$p = \varrho \tilde{R} T = \sum_{i=1}^{N} \varrho_i R_i T , \tag{A.5}$$

$$e = \sum_{i=1}^{N} Y_i e_i = = \sum_{i=1}^{N} Y_i \left[\int_{T_{ref}}^{T} c_{v_i} d\tau + h_{f_i} \right] . \tag{A.6}$$

The above equations can be cast in differential form, as follows

$$dp = \varrho \tilde{R} dT + \varrho T \sum_{i=1}^{N} R_i dT + \tilde{R} T d\varrho , \tag{A.7}$$

$$de = \tilde{c}_v dT + \sum_{i=1}^{N} e_i dY_i , \tag{A.8}$$

where the differential of the mass fractions is given by

$$dY_i = \left(\frac{\partial Y_i}{\partial \varrho}\right)_T d\varrho + \left(\frac{\partial Y_i}{\partial T}\right)_\varrho dT . \tag{A.9}$$

Substituting Equations (A.8) and (A.9) into Equation (A.7), the pressure differential can be written as

$$dp = \frac{\varrho\tilde{R} + \varrho T \sum_{i=1}^{N} R_i\left(\frac{\partial Y_i}{\partial T}\right)}{\tilde{c}_v + \sum_{i=1}^{N} e_i\left(\frac{\partial Y_i}{\partial T}\right)} \left[de - \sum_{i=1}^{N}\left(\frac{\partial Y_i}{\partial \varrho}\right)d\varrho\right] + \left[\tilde{R}T + \varrho T \sum_{i=1}^{N} R_i\left(\frac{\partial Y_i}{\partial \varrho}\right)\right]d\varrho \ . \tag{A.10}$$

Now the partial derivatives of pressure with respect to internal energy at constant density and with respect to density at constant internal energy can be easily obtained as

$$\left(\frac{\partial p}{\partial e}\right)_{\varrho} = \varrho \frac{\tilde{R} + T \sum_{i=1}^{N} R_i\left(\frac{\partial Y_i}{\partial T}\right)}{\tilde{c}_v + \sum_{i=1}^{N} e_i\left(\frac{\partial Y_i}{\partial T}\right)} \ , \tag{A.11}$$

$$\left(\frac{\partial p}{\partial \varrho}\right)_{e} = \tilde{R}T + \varrho T \sum_{i=1}^{N} R_i\left(\frac{\partial Y_i}{\partial \varrho}\right) - \varrho \sum_{i=1}^{N} e_i\left(\frac{\partial Y_i}{\partial \varrho}\right) \frac{\tilde{R} + T \sum_{i=1}^{N} R_i\left(\frac{\partial Y_i}{\partial T}\right)}{\tilde{c}_v + \sum_{i=1}^{N} e_i\left(\frac{\partial Y_i}{\partial T}\right)} \ . \tag{A.12}$$

Substituting these results into Equation (A.4) and after some algebra, the equation for the speed of sound can be written in the more familiar form

$$a^2 = \Gamma\frac{p}{\varrho} \ , \tag{A.13}$$

where the isentropic index is defined as

$$\Gamma = 1 + \frac{\tilde{R} + T\sum_{i=1}^{N} R_i\left(\frac{\partial Y_i}{\partial T}\right)}{\tilde{c}_v + \sum_{i=1}^{N} e_i\left(\frac{\partial Y_i}{\partial T}\right)} + \frac{\varrho}{\tilde{R}T}\sum_{i=1}^{N}\left(\frac{\partial Y_i}{\partial \varrho}\right)\left[R_iT - e_i\,\frac{\tilde{R} + T\sum_{i=1}^{N} R_i\left(\frac{\partial Y_i}{\partial T}\right)}{\tilde{c}_v + \sum_{i=1}^{N} e_i\left(\frac{\partial Y_i}{\partial T}\right)}\right] . \tag{A.14}$$

Defining γ to be the ratio of the enthalpy and internal energy derivatives at constant density, as follows

$$\bar{\gamma} = \frac{\left(\frac{\partial h}{\partial T}\right)_{\varrho}}{\left(\frac{\partial e}{\partial T}\right)_{\varrho}} = 1 + \frac{\left(\frac{\partial \tilde{R}T}{\partial T}\right)_{\varrho}}{\left(\frac{\partial e}{\partial T}\right)_{\varrho}} = 1 + \frac{\tilde{R} + T\sum_{i=1}^{N} R_i\left(\frac{\partial Y_i}{\partial T}\right)}{\tilde{c}_v + \sum_{i=1}^{N} e_i\left(\frac{\partial Y_i}{\partial T}\right)} , \tag{A.15}$$

and substituting this definition into Equation (A.14), the isentropic index can be rewritten as

$$\Gamma = \bar{\gamma} + \frac{\varrho}{\tilde{R}T}\sum_{i=1}^{N}\left(\frac{\partial Y_i}{\partial \varrho}\right)\left[R_iT - (\bar{\gamma} - 1)e_i\right] . \tag{A.16}$$

Similarly, the pressure derivatives defined in Equations (A.11) and (A.12), can be rewritten as

$$\left(\frac{\partial p}{\partial e}\right)_{\varrho} = \varrho(\bar{\gamma} - 1) , \tag{A.17}$$

$$\left(\frac{\partial p}{\partial \varrho}\right)_{e} = \tilde{R}T(1 + \Gamma - \bar{\gamma}) . \tag{A.18}$$

2. PRESSURE DERIVATIVES

A key part in the development of a flow solver for real gases is the evaluation of the pressure derivatives, specifically the partial derivatives of pressure with respect to the dependent variable vector, Q, as follows

$$\left(\frac{\partial p}{\partial Q}\right) = \left[\left(\frac{\partial p}{\partial \varrho}\right), \left(\frac{\partial p}{\partial \varrho u}\right), \left(\frac{\partial p}{\partial \varrho v}\right), \left(\frac{\partial p}{\partial \varrho w}\right), \left(\frac{\partial p}{\partial \varrho e_o}\right)\right]^T . \tag{A.19}$$

The pressure differential can be written as

$$
\begin{aligned}
dp &= \left(\frac{\partial p}{\partial \varrho}\right)_e d\varrho + \left(\frac{\partial p}{\partial e}\right)_\varrho de \\
&= \left(\frac{\partial p}{\partial \varrho}\right) d\varrho + \left(\frac{\partial p}{\partial \varrho u}\right) d\varrho u + \left(\frac{\partial p}{\partial \varrho v}\right) d\varrho v + \left(\frac{\partial p}{\partial \varrho w}\right) d\varrho w + \left(\frac{\partial p}{\partial \varrho e_o}\right) d\varrho e_o \ ,
\end{aligned}
\tag{A.20}
$$

and internal energy is given by

$$
e = \frac{\varrho e_o}{\varrho} - \frac{(\varrho u)^2 + (\varrho v)^2 + (\varrho w)^2}{2\varrho^2} \ . \tag{A.21}
$$

Differentiating Equation (A.21), and substituting the result into Equation (A.20), the following relations for the pressure derivatives are found

$$
\left(\frac{\partial p}{\partial \varrho}\right) = \left(\frac{\partial p}{\partial \varrho}\right)_e - \left(\frac{\partial p}{\partial e}\right)_\varrho \frac{e - \frac{q^2}{2}}{\varrho} = (\bar{\gamma} - 1)\left(\frac{q^2}{2} - h\right) + a^2 \ , \tag{A.22}
$$

$$
\left(\frac{\partial p}{\partial \varrho u}\right) = -\frac{u}{\varrho}\left(\frac{\partial p}{\partial e}\right)_\varrho = -u(\bar{\gamma} - 1) \ , \tag{A.23}
$$

$$
\left(\frac{\partial p}{\partial \varrho v}\right) = -\frac{v}{\varrho}\left(\frac{\partial p}{\partial e}\right)_\varrho = -v(\bar{\gamma} - 1) \ , \tag{A.24}
$$

$$
\left(\frac{\partial p}{\partial \varrho w}\right) = -\frac{w}{\varrho}\left(\frac{\partial p}{\partial e}\right)_\varrho = -w(\bar{\gamma} - 1) \ , \tag{A.25}
$$

$$
\left(\frac{\partial p}{\partial \varrho e_o}\right) = \frac{1}{\varrho}\left(\frac{\partial p}{\partial e}\right)_\varrho = \bar{\gamma} - 1 \ , \tag{A.26}
$$

where $q^2 = u^2 + v^2 + w^2$.

APPENDIX B
EIGENVALUES AND EIGENVECTORS OF THE INVISCID FLUX JACOBIANS

The following development parallels the work done by Janus [Reference 42] and therefore many steps will be intentionally left out. The primary focus is the extension of the previous work to real gases.

1. CONSERVATIVE VARIABLE JACOBIAN MATRIX

The inviscid flux Jacobians are given by

$$\bar{S} = \frac{\partial S}{\partial Q} \, , \tag{B.1}$$

where the dependent variable vector and generic flux vector are

$$Q = J \begin{bmatrix} \varrho \\ \varrho u \\ \varrho v \\ \varrho w \\ \varrho e_o \end{bmatrix} , \qquad S = J \begin{bmatrix} \varrho \beta_k \\ \varrho u \beta_k + p k_x \\ \varrho v \beta_k + p k_y \\ \varrho w \beta_k + p k_z \\ \beta_k(\varrho e_o + p) - p k_t \end{bmatrix} . \tag{B.2}$$

After differentiating, the components of the inviscid Jacobian matrix are given by rows as

$$\bar{S}_{11} = k_x \, , \quad \bar{S}_{12} = k_y \, , \quad \bar{S}_{13} = k_z \, , \quad \bar{S}_{14} = k_t \, , \quad \bar{S}_{15} = 0 \, , \tag{B.3}$$

$$\bar{S}_{21} = \left[\left(\frac{\partial p}{\partial \varrho} \right)_e - \left(\frac{\partial p}{\partial e} \right)_\varrho \left[\frac{e - \frac{q^2}{2}}{\varrho} \right] \right] k_x - u \theta_k \, ,$$

$$\bar{S}_{22} = \left[1 - \frac{1}{\varrho} \left(\frac{\partial p}{\partial e} \right)_\varrho \right] u k_x + \beta_k \, , \quad \bar{S}_{23} = - \frac{v}{\varrho} \left(\frac{\partial p}{\partial e} \right)_\varrho k_x + u k_y \, , \tag{B.4}$$

$$\bar{S}_{24} = - \frac{w}{\varrho} \left(\frac{\partial p}{\partial e} \right)_\varrho k_x + u k_z \, , \quad \bar{S}_{25} = - \frac{1}{\varrho} \left(\frac{\partial p}{\partial e} \right)_\varrho k_x \, ,$$

$$\bar{S}_{31} = \left[\left(\frac{\partial p}{\partial \varrho} \right)_e - \left(\frac{\partial p}{\partial e} \right)_\varrho \left[\frac{e - \frac{q^2}{2}}{\varrho} \right] \right] k_y - v \theta_k \, ,$$

$$\bar{S}_{32} = - \frac{u}{\varrho} \left(\frac{\partial p}{\partial e} \right)_\varrho k_y + v k_x \, , \quad \bar{S}_{33} = \left[1 - \frac{1}{\varrho} \left(\frac{\partial p}{\partial e} \right)_\varrho \right] v k_y + \beta_k \, , \tag{B.5}$$

$$\bar{S}_{34} = - \frac{w}{\varrho} \left(\frac{\partial p}{\partial e} \right)_\varrho k_y + v k_z \, , \quad \bar{S}_{35} = - \frac{1}{\varrho} \left(\frac{\partial p}{\partial e} \right)_\varrho k_y \, ,$$

$$\bar{S}_{41} = \left[\left(\frac{\partial p}{\partial \varrho}\right)_e - \left(\frac{\partial p}{\partial e}\right)_\varrho \left[\frac{e - \frac{q^2}{2}}{\varrho}\right]\right] k_z - w\theta_k \ ,$$

$$\bar{S}_{42} = -\frac{u}{\varrho}\left(\frac{\partial p}{\partial e}\right)_\varrho k_z + wk_x \ , \quad \bar{S}_{43} = -\frac{v}{\varrho}\left(\frac{\partial p}{\partial e}\right)_\varrho k_z + wk_y \ , \tag{B.6}$$

$$\bar{S}_{44} = \left[1 - \frac{1}{\varrho}\left(\frac{\partial p}{\partial e}\right)_\varrho\right] wk_z + \beta_k \ , \quad \bar{S}_{45} = -\frac{1}{\varrho}\left(\frac{\partial p}{\partial e}\right)_\varrho k_z \ ,$$

$$\bar{S}_{51} = \left\{\left[\left(\frac{\partial p}{\partial \varrho}\right)_e - \left(\frac{\partial p}{\partial e}\right)_\varrho \left[\frac{e - \frac{q^2}{2}}{\varrho}\right]\right] - h_o\right\}\theta_k \ ,$$

$$\bar{S}_{52} = h_o k_x - \frac{u}{\varrho}\left(\frac{\partial p}{\partial e}\right)_\varrho \theta_k \ , \quad \bar{S}_{53} = h_o k_y - \frac{v}{\varrho}\left(\frac{\partial p}{\partial e}\right)_\varrho \theta_k \ , \tag{B.7}$$

$$\bar{S}_{54} = h_o k_z - \frac{w}{\varrho}\left(\frac{\partial p}{\partial e}\right)_\varrho \theta_k \ , \quad \bar{S}_{55} = \left[1 - \frac{1}{\varrho}\left(\frac{\partial p}{\partial e}\right)_\varrho\right]\theta_k + k_t \ .$$

The main difference between the present formulation and the perfect gas formulation is the evaluation of the pressure derivatives. Substituting the relations for the pressure derivatives developed in Appendix A, the second through fifth row (Equations (B.4)–(B.7)) of the Jacobian matrix can now be rewritten as

$$\bar{S}_{21} = (\phi + \psi)k_x - u\theta_k \ ,$$

$$\bar{S}_{22} = (2 - \bar{\gamma})uk_x + \beta_k \ , \quad \bar{S}_{23} = -v(\bar{\gamma} - 1)k_x + uk_y \ , \tag{B.8}$$

$$\bar{S}_{24} = -w(\bar{\gamma} - 1)k_x + uk_z \ , \quad \bar{S}_{25} = (\bar{\gamma} - 1)k_x \ ,$$

$$\bar{S}_{31} = (\phi + \psi)k_y - v\theta_k \ ,$$

$$\bar{S}_{32} = -u(\bar{\gamma} - 1)k_y + vk_x \ , \quad \bar{S}_{33} = (2 - \bar{\gamma})vk_y + \beta_k \ , \tag{B.9}$$

$$\bar{S}_{34} = -w(\bar{\gamma} - 1)k_y + vk_z \ , \quad \bar{S}_{35} = (\bar{\gamma} - 1)k_y \ ,$$

$$\begin{aligned}
\overline{S}_{41} &= (\phi + \psi)k_z - w\theta_k \ , \\
\overline{S}_{42} &= -\,u(\overline{\gamma} - 1)k_z + wk_x \ , \quad \overline{S}_{43} = -\,v(\overline{\gamma} - 1)k_z + wk_y \ , \\
\overline{S}_{44} &= (2 - \overline{\gamma})wk_z + \beta_k \ , \quad \overline{S}_{45} = (\overline{\gamma} - 1)k_z \ ,
\end{aligned} \tag{B.10}$$

$$\begin{aligned}
\overline{S}_{51} &= \{(\phi + \psi) - h_o\}\theta_k \ , \\
\overline{S}_{52} &= h_o k_x - u(\overline{\gamma} - 1)\theta_k \ , \quad \overline{S}_{53} = h_o k_y - v(\overline{\gamma} - 1)\theta_k \ , \\
\overline{S}_{54} &= h_o k_z - w(\overline{\gamma} - 1)\theta_k \ , \quad \overline{S}_{55} = \beta_k + (\overline{\gamma} - 1)\theta_k \ ,
\end{aligned} \tag{B.11}$$

where

$$\begin{aligned}
\phi &= \frac{\overline{\gamma} - 1}{2}\left(u^2 + v^2 + w^2\right) \ , \\
\psi &= a^2 - h(\overline{\gamma} - 1) \ .
\end{aligned} \tag{B.12}$$

For a perfect gas, $\overline{\gamma}$ will be given by the "standard" ratio of specific heats γ, ψ will be identically zero, and the above real gas formulation will identically reduce to its perfect gas counterpart.

2. PRIMITIVE VARIABLE JACOBIAN MATRIX

In order to work with a more amiable eigensystem, the conservative variable system is converted to one based on the primitive variables, where $q = J[\varrho, u, v, w, p]^T$ is the vector of primitive variables. The transformation matrix M, given by $M = \partial Q/\partial q$, is

$$M = \begin{bmatrix}
1 & 0 & 0 & 0 & 0 \\
u & \varrho & 0 & 0 & 0 \\
v & 0 & \varrho & 0 & 0 \\
w & 0 & 0 & \varrho & 0 \\
\dfrac{\phi - \psi}{\overline{\gamma} - 1} & \varrho u & \varrho v & \varrho w & \dfrac{1}{\overline{\gamma} - 1}
\end{bmatrix} . \tag{B.13}$$

Using the similarity transformation, $\varkappa = M^{-1}\,\overline{S}\,M$, the primitive variable Jacobian matrix $\varkappa$ is given by

$$\varkappa = \begin{bmatrix} \beta_k & \varrho k_x & \varrho k_y & \varrho k_z & 0 \\ 0 & \beta_k & 0 & 0 & \frac{k_x}{\varrho} \\ 0 & 0 & \beta_k & 0 & \frac{k_y}{\varrho} \\ 0 & 0 & 0 & \beta_k & \frac{k_z}{\varrho} \\ 0 & \varrho a^2 k_x & \varrho a^2 k_y & \varrho a^2 k_z & \beta_k \end{bmatrix} . \qquad \text{(B.14)}$$

which is identical to the perfect gas formulation obtained by Janus [Reference 42].

The eigenvalues, obtained by solving the equation $|\varkappa - \lambda I| = 0$, are

$$\begin{aligned} \lambda_k^1 &= \lambda_k^2 = \lambda_k^3 = \beta_k , \\ \lambda_k^4 &= \beta_k + a|\Delta k| , \qquad \text{(B.15)} \\ \lambda_k^5 &= \beta_k - a|\Delta k| . \end{aligned}$$

Considering the equation $(\varkappa - \lambda I)r = 0$ (where r are the right eigenvectors), the right eigenvector matrix P_k for the primitive variable Jacobians is obtained as

$$P_k = \begin{bmatrix} \alpha\tilde{k}_x & \alpha\tilde{k}_y & \alpha\tilde{k}_z & \alpha & \alpha \\ \tilde{k}_z & -\tilde{k}_z & \tilde{k}_y & \frac{k_x}{\sqrt{2}} & -\frac{k_x}{\sqrt{2}} \\ -\tilde{k}_y & 0 & -\tilde{k}_x & \frac{k_y}{\sqrt{2}} & -\frac{k_y}{\sqrt{2}} \\ 0 & \tilde{k}_x & 0 & \frac{k_z}{\sqrt{2}} & -\frac{k_z}{\sqrt{2}} \\ 0 & 0 & 0 & a^2\alpha & a^2\alpha \end{bmatrix} , \qquad \text{(B.16)}$$

where $\alpha = \varrho / a\sqrt{2}$ and the right eigenvectors are given by columns. Similarly, the matrix of left eigenvectors, P_k^{-1}, can be obtained

$$
P_k^{-1} = \begin{bmatrix} \frac{\tilde{k}_x}{\alpha} & 0 & \tilde{k}_z & -\tilde{k}_y & -\frac{k_x}{\alpha a^2} \\ \frac{\tilde{k}_y}{\alpha} & -\tilde{k}_z & 0 & \tilde{k}_x & -\frac{k_y}{\alpha a^2} \\ \frac{\tilde{k}_z}{\alpha} & \tilde{k}_y & -\tilde{k}_x & 0 & -\frac{k_z}{\alpha a^2} \\ 0 & \frac{\tilde{k}_x}{\sqrt{2}} & \frac{\tilde{k}_y}{\sqrt{2}} & \frac{\tilde{k}_z}{\sqrt{2}} & \beta \\ 0 & -\frac{\tilde{k}_x}{\sqrt{2}} & -\frac{\tilde{k}_y}{\sqrt{2}} & -\frac{\tilde{k}_z}{\sqrt{2}} & \beta \end{bmatrix} , \qquad (B.17)
$$

where $\beta = 1/\varrho a\sqrt{2}$ and the left eigenvectors are given by rows. At this point, the eigenvector matrices for the conservative variable Jacobians are easily obtained from the following relations

$$
\begin{aligned} T_k &= MP_k , \\ T_k^{-1} &= P_k^{-1} M^{-1} , \end{aligned} \qquad (B.18)
$$

where T_k is the matrix whose columns are the right eigenvectors and T_k^{-1} is the matrix whose rows are the left eigenvectors. Performing the matrix multiplications, the right eigenvectors are found to be

$$
r_1 = \begin{bmatrix} \alpha\tilde{k}_x \\ \alpha u\tilde{k}_x \\ \alpha v\tilde{k}_x + \varrho\tilde{k}_z \\ \alpha w\tilde{k}_x - \varrho\tilde{k}_y \\ \alpha\tilde{k}_x\left(\frac{\phi - \psi}{\gamma - 1}\right) + \varrho(v\tilde{k}_z - w\tilde{k}_y) \end{bmatrix} ,
$$

$$
r_2 = \begin{bmatrix} \alpha\tilde{k}_y \\ \alpha u\tilde{k}_y - \varrho\tilde{k}_z \\ \alpha v\tilde{k}_y \\ \alpha w\tilde{k}_y + \varrho\tilde{k}_x \\ \alpha\tilde{k}_y\left(\frac{\phi - \psi}{\gamma - 1}\right) + \varrho(w\tilde{k}_x - u\tilde{k}_z) \end{bmatrix} ,
$$

$$r_3 = \begin{bmatrix} \alpha\tilde{k}_z \\ \alpha u\tilde{k}_z + \varrho\tilde{k}_y \\ \alpha v\tilde{k}_z - \varrho\tilde{k}_x \\ \alpha w\tilde{k}_z \\ \alpha\tilde{k}_z\left(\dfrac{\phi - \psi}{\bar{\gamma} - 1}\right) + \varrho(u\tilde{k}_y - v\tilde{k}_x) \end{bmatrix},$$

$$r_{4,5} = \alpha\begin{bmatrix} 1 \\ u \pm a\tilde{k}_x \\ v \pm a\tilde{k}_x \\ w \pm a\tilde{k}_z \\ \dfrac{\phi + a^2 - \psi}{\bar{\gamma} - 1} \pm a\tilde{\theta}_k \end{bmatrix}, \tag{B.19}$$

and the left eigenvectors are

$$l_1 = \begin{bmatrix} \dfrac{1}{\alpha}\left(1 - \dfrac{\phi + \psi}{\alpha a^2}\right)\tilde{k}_x + \dfrac{1}{\varrho}(w\tilde{k}_y - v\tilde{k}_z) \\ \dfrac{(\bar{\gamma} - 1)}{\alpha a^2}u\tilde{k}_x \\ \dfrac{(\bar{\gamma} - 1)}{\alpha a^2}v\tilde{k}_x + \dfrac{\tilde{k}_z}{\varrho} \\ \dfrac{(\bar{\gamma} - 1)}{\alpha a^2}w\tilde{k}_x - \dfrac{\tilde{k}_y}{\varrho} \\ -\dfrac{(\bar{\gamma} - 1)}{\alpha a^2}\tilde{k}_x \end{bmatrix},$$

$$l_2 = \begin{bmatrix} \dfrac{1}{\alpha}\left(1 - \dfrac{\phi + \psi}{\alpha a^2}\right)\tilde{k}_y + \dfrac{1}{\varrho}(u\tilde{k}_z - w\tilde{k}_x) \\ \dfrac{(\bar{\gamma} - 1)}{\alpha a^2}u\tilde{k}_y - \dfrac{\tilde{k}_z}{\varrho} \\ \dfrac{(\bar{\gamma} - 1)}{\alpha a^2}v\tilde{k}_y \\ \dfrac{(\bar{\gamma} - 1)}{\alpha a^2}w\tilde{k}_y + \dfrac{\tilde{k}_x}{\varrho} \\ -\dfrac{(\bar{\gamma} - 1)}{\alpha a^2}\tilde{k}_y \end{bmatrix},$$

$$
l_3 = \begin{bmatrix} \frac{1}{\alpha}\left(1 - \frac{\phi + \psi}{\alpha a^2}\right)\tilde{k}_z + \frac{1}{\varrho}(v\tilde{k}_x - u\tilde{k}_y) \\ \frac{(\bar{\gamma} - 1)}{\alpha a^2}u\tilde{k}_z + \frac{\tilde{k}_y}{\varrho} \\ \frac{(\bar{\gamma} - 1)}{\alpha a^2}v\tilde{k}_z - \frac{\tilde{k}_x}{\varrho} \\ \frac{(\bar{\gamma} - 1)}{\alpha a^2}w\tilde{k}_z \\ -\frac{(\bar{\gamma} - 1)}{\alpha a^2}\tilde{k}_z \end{bmatrix},
$$

$$
l_{4,5} = \beta \begin{bmatrix} \phi + \psi \mp a\tilde{\theta}_k \\ -u(\bar{\gamma} - 1) \pm a\tilde{k}_x \\ -v(\bar{\gamma} - 1) \pm a\tilde{k}_y \\ -w(\bar{\gamma} - 1) \pm a\tilde{k}_z \\ (\bar{\gamma} - 1) \end{bmatrix}. \tag{B.20}
$$

Similar to what was seen for the inviscid *Jacobians*, the eigenvectors will nicely reduce to their perfect gas formulation.

APPENDIX C
SPLUT FLUX JACOBIANS

The following derivation for the split flux Jacobians follows closely the perfect gas development given by Belk [Reference 35]. Therefore, only the steps needed to clarify the real gas extensions will be given.

1. "TRUE" JACOBIANS

The generalized Steger–Warming split flux vectors for an arbitrary gas, as developed by Vinokur and Montagné [Reference 33], are

$$K_1^{\pm} = \frac{\Gamma - 1}{\Gamma}\begin{bmatrix} \varrho \\ \varrho u \\ \varrho v \\ \varrho w \\ \varrho\left(h_o - \dfrac{a^2}{\Gamma - 1}\right) \end{bmatrix} \lambda_1^{(\pm)} ,$$

$$K_4^{\pm} = \frac{1}{2\Gamma}\begin{bmatrix} \varrho \\ \varrho(u + ak_x) \\ \varrho(v + ak_y) \\ \varrho(w + ak_z) \\ \varrho(h_o + a\tilde{\theta}_k) \end{bmatrix} \lambda_4^{(\pm)} , \qquad K_5^{\pm} = \frac{1}{2\Gamma}\begin{bmatrix} \varrho \\ \varrho(u - ak_x) \\ \varrho(v - ak_y) \\ \varrho(w - ak_z) \\ \varrho(h_o - a\tilde{\theta}_k) \end{bmatrix} \lambda_5^{(\pm)} , \tag{C.1}$$

where the eigenvalues can be written as

$$\lambda_1^{(\pm)} = J|\nabla k|\frac{\tilde{\beta}_k \pm |\tilde{\beta}_k|}{2} ,$$

$$\lambda_4^{(\pm)} = J|\nabla k|\frac{(\tilde{\beta}_k + a) \pm |\tilde{\beta}_k + a|}{2} ,$$

$$\lambda_5^{(\pm)} = J|\nabla k|\frac{(\tilde{\beta}_k - a) \pm |\tilde{\beta}_k - a|}{2} . \tag{C.2}$$

The "true" (analytical) Jacobian, denoted by $\overline{A}^{\pm}$, is given by

$$\overline{A}^{\pm} = \frac{\partial K^{\pm}}{\partial Q} , \tag{C.3}$$

or

$$\overline{A}^{\pm} = \sum_{i=1,4,5} \overline{A}_i^{\pm} = \sum_{i=1,4,5} \frac{\partial K_i^{\pm}}{\partial Q} . \tag{C.4}$$

The split flux vectors can be redefined as

$$K_i^{\pm} = \lambda_i^{(\pm)}\, g_i\, K_i^{*} , \tag{C.5}$$

where

$$g_1 = \frac{\Gamma - 1}{\Gamma}\,, \qquad g_4 = g_5 = \frac{1}{2\Gamma}\,, \tag{C.6}$$

$$K_1^* = \begin{bmatrix} \varrho \\ \varrho u \\ \varrho v \\ \varrho w \\ \varrho\left(h_o - \dfrac{a^2}{\Gamma - 1}\right) \end{bmatrix}, \qquad K_{4,5}^* = \begin{bmatrix} \varrho \\ \varrho(u \pm ak_x) \\ \varrho(v \pm ak_y) \\ \varrho(w \pm ak_z) \\ \varrho(h_o \pm a\tilde{\theta}_k) \end{bmatrix}. \tag{C.7}$$

Expanding the partial differentiation of Equation (C.4), the split flux Jacobians can be viewed as having three separate contributions, as follows

$$\overline{A}^{\pm} = \overline{A}_{\lambda}^{\pm} + \overline{A}_{\Gamma}^{\pm} + \overline{A}_{K^*}^{\pm}\,, \tag{C.8}$$

where

$$\overline{A}_{\lambda}^{\pm} = g_i\, K_i^*\, \frac{\partial \lambda_i^{(\pm)}}{\partial Q}\,, \tag{C.9}$$

$$\overline{A}_{\Gamma}^{\pm} = \lambda_i^{(\pm)}\, K_i^*\, \frac{\partial g_i}{\partial Q}\,, \tag{C.10}$$

$$\overline{A}_{K^*}^{\pm} = \lambda_i^{(\pm)}\, g_i\, \frac{\partial K_i^*}{\partial Q}\,. \tag{C.11}$$

2. "λ" CONTRIBUTIONS

The contributions to the split flux Jacobians arising from the partial differentiation of the eigenvalues can be written as

$$\overline{A}_{\lambda} = \varrho \begin{bmatrix} \dfrac{\Gamma - 1}{\Gamma}L_1 + \dfrac{1}{2\Gamma}\left[L_4 + L_5\right] \\ u\dfrac{\Gamma - 1}{\Gamma}L_1 + \dfrac{1}{2\Gamma}\left[(u + a\tilde{k}_x)L_4 + (u - a\tilde{k}_x)L_5\right] \\ v\dfrac{\Gamma - 1}{\Gamma}L_1 + \dfrac{1}{2\Gamma}\left[(v + a\tilde{k}_y)L_4 + (v - a\tilde{k}_y)L_5\right] \\ w\dfrac{\Gamma - 1}{\Gamma}L_1 + \dfrac{1}{2\Gamma}\left[(w + a\tilde{k}_z)L_4 + (w - a\tilde{k}_z)L_5\right] \\ \left(h_o - \dfrac{a^2}{\Gamma - 1}\right)\dfrac{\Gamma - 1}{\Gamma}L_1 + \dfrac{1}{2\Gamma}\left[(h_o + a\tilde{\theta}_k)L_4 + (h_o - a\tilde{\theta}_k)L_5\right] \end{bmatrix}. \tag{C.12}$$

In the above, the vectors L_1, L_4 and L_5, are the eigenvalue derivatives, which are found to be

$$\left(a_1^*\right)_{21} = 0\ ,\quad \left(a_1^*\right)_{22} = 1\ ,\quad \left(a_1^*\right)_{23} = 0\ ,\quad \left(a_1^*\right)_{24} = 0\ ,\quad \left(a_1^*\right)_{25} = 0\ , \tag{C.18}$$

$$\left(a_1^*\right)_{31} = 0\ ,\quad \left(a_1^*\right)_{32} = 0\ ,\quad \left(a_1^*\right)_{33} = 1\ ,\quad \left(a_1^*\right)_{34} = 0\ ,\quad \left(a_1^*\right)_{35} = 0\ , \tag{C.19}$$

$$\left(a_1^*\right)_{41} = 0\ ,\quad \left(a_1^*\right)_{42} = 0\ ,\quad \left(a_1^*\right)_{43} = 0\ ,\quad \left(a_1^*\right)_{44} = 1\ ,\quad \left(a_1^*\right)_{45} = 0\ , \tag{C.20}$$

$$\begin{aligned}
\left(a_1^*\right)_{51} &= \frac{\partial p}{\partial \varrho} - \frac{2\varrho a}{\Gamma - 1}\frac{\partial a}{\partial \varrho} + \frac{\varrho a^2}{(\Gamma - 1)^2}\frac{\partial \Gamma}{\partial \varrho} - \frac{a^2}{\Gamma - 1}\ ,\\
\left(a_1^*\right)_{52} &= \frac{\partial p}{\partial \varrho u} - \frac{2\varrho a}{\Gamma - 1}\frac{\partial a}{\partial \varrho u} + \frac{\varrho a^2}{(\Gamma - 1)^2}\frac{\partial \Gamma}{\partial \varrho u}\ ,\\
\left(a_1^*\right)_{53} &= \frac{\partial p}{\partial \varrho v} - \frac{2\varrho a}{\Gamma - 1}\frac{\partial a}{\partial \varrho v} + \frac{\varrho a^2}{(\Gamma - 1)^2}\frac{\partial \Gamma}{\partial \varrho v}\ ,\\
\left(a_1^*\right)_{54} &= \frac{\partial p}{\partial \varrho w} - \frac{2\varrho a}{\Gamma - 1}\frac{\partial a}{\partial \varrho w} + \frac{\varrho a^2}{(\Gamma - 1)^2}\frac{\partial \Gamma}{\partial \varrho w}\ ,\\
\left(a_1^*\right)_{55} &= \frac{\partial p}{\partial \varrho e_o} - \frac{2\varrho a}{\Gamma - 1}\frac{\partial a}{\partial \varrho e_o} + \frac{\varrho a^2}{(\Gamma - 1)^2}\frac{\partial \Gamma}{\partial \varrho e_o} + 1\ ,
\end{aligned} \tag{C.21}$$

and the components of the matrices, $A_{4,5}^* = \partial K_{4,5}^* / \partial Q$, are

$$\left(a_{4,5}^*\right)_{11} = 1,\quad \left(a_{4,5}^*\right)_{12} = 0,\quad \left(a_{4,5}^*\right)_{13} = 0,\quad \left(a_{4,5}^*\right)_{14} = 0,\quad \left(a_{4,5}^*\right)_{15} = 0, \tag{C.22}$$

$$\begin{aligned}
&\left(a_{4,5}^*\right)_{21} = \pm\, a\tilde{k}_x \pm \varrho\tilde{k}_x\frac{\partial a}{\partial \varrho}\ ,\\
&\left(a_{4,5}^*\right)_{22} = 1 \pm \varrho\tilde{k}_x\frac{\partial a}{\partial \varrho u}\ ,\qquad \left(a_{4,5}^*\right)_{23} = \pm\, \varrho\tilde{k}_x\frac{\partial a}{\partial \varrho v}\ ,\\
&\left(a_{4,5}^*\right)_{24} = \pm\, \varrho\tilde{k}_x\frac{\partial a}{\partial \varrho w}\ ,\qquad \left(a_{4,5}^*\right)_{25} = \pm\, \varrho\tilde{k}_x\frac{\partial a}{\partial \varrho e_o}\ ,
\end{aligned} \tag{C.23}$$

$$\begin{aligned}
&\left(a_{4,5}^*\right)_{31} = \pm\, a\tilde{k}_y \pm \varrho\tilde{k}_y\frac{\partial a}{\partial \varrho}\ ,\\
&\left(a_{4,5}^*\right)_{32} = \pm\, \varrho\tilde{k}_y\frac{\partial a}{\partial \varrho u}\ ,\qquad \left(a_{4,5}^*\right)_{33} = 1 \pm \varrho\tilde{k}_y\frac{\partial a}{\partial \varrho v}\ ,\\
&\left(a_{4,5}^*\right)_{34} = \pm\, \varrho\tilde{k}_y\frac{\partial a}{\partial \varrho w}\ ,\qquad \left(a_{4,5}^*\right)_{35} = \pm\, \varrho\tilde{k}_y\frac{\partial a}{\partial \varrho e_o}\ ,
\end{aligned} \tag{C.24}$$

$$\begin{aligned}
&\left(a_{4,5}^*\right)_{41} = \pm\, a\tilde{k}_z \pm \varrho\tilde{k}_z\frac{\partial a}{\partial \varrho}\ ,\\
&\left(a_{4,5}^*\right)_{42} = \pm\, \varrho\tilde{k}_z\frac{\partial a}{\partial \varrho u}\ ,\qquad \left(a_{4,5}^*\right)_{43} = \pm\, \varrho\tilde{k}_z\frac{\partial a}{\partial \varrho v}\ ,
\end{aligned}$$

$$\left(a^*_{4,5}\right)_{44} = 1 \pm \varrho\tilde{k}_z \frac{\partial a}{\partial \varrho w} \; , \qquad \left(a^*_{4,5}\right)_{45} = \pm \varrho\tilde{k}_z \frac{\partial a}{\partial \varrho e_o} \; , \tag{C.25}$$

$$\begin{aligned}
\left(a^*_{4,5}\right)_{51} &= \frac{\partial p}{\partial \varrho} \pm \varrho\tilde{\theta}_k \frac{\partial a}{\partial \varrho} \; , \\
\left(a^*_{4,5}\right)_{52} &= \frac{\partial p}{\partial \varrho u} \pm \varrho\tilde{\theta}_k \frac{\partial a}{\partial \varrho u} \pm a\tilde{k}_x \; , \\
\left(a^*_{4,5}\right)_{53} &= \frac{\partial p}{\partial \varrho v} \pm \varrho\tilde{\theta}_k \frac{\partial a}{\partial \varrho v} \pm a\tilde{k}_y \; , \\
\left(a^*_{4,5}\right)_{54} &= \frac{\partial p}{\partial \varrho w} \pm \varrho\tilde{\theta}_k \frac{\partial a}{\partial \varrho w} \pm a\tilde{k}_z \; , \\
\left(a^*_{4,5}\right)_{55} &= \frac{\partial p}{\partial \varrho e_o} \pm \varrho\tilde{\theta}_k \frac{\partial a}{\partial \varrho e_o} + 1 \; .
\end{aligned} \tag{C.26}$$

5. SPEED OF SOUND DERIVATIVES

Recalling the definition for the speed of sound

$$a^2 = \Gamma \frac{p}{\varrho} \; , \tag{C.27}$$

and differentiating, the following relation is obtained

$$\frac{\partial a}{\partial q_i} = \frac{a}{2\Gamma}\frac{\partial \Gamma}{\partial q_i} + \frac{\Gamma}{2\varrho a}\frac{\partial p}{\partial q_i} - \frac{a}{2\varrho}\frac{\partial \varrho}{\partial q_i} \; . \tag{C.28}$$

Using Equation (C.28), the speed of sound derivatives are found to be

$$\begin{aligned}
\frac{\partial a}{\partial \varrho} &= \frac{a}{2\Gamma}\frac{\partial \Gamma}{\partial \varrho} + \frac{\Gamma}{2\varrho a}\frac{\partial p}{\partial \varrho} - \frac{a}{2\varrho} \; , \\
\frac{\partial a}{\partial \varrho u} &= \frac{a}{2\Gamma}\frac{\partial \Gamma}{\partial \varrho u} + \frac{\Gamma}{2\varrho a}\frac{\partial p}{\partial \varrho u} \; , \\
\frac{\partial a}{\partial \varrho v} &= \frac{a}{2\Gamma}\frac{\partial \Gamma}{\partial \varrho v} + \frac{\Gamma}{2\varrho a}\frac{\partial p}{\partial \varrho v} \; , \\
\frac{\partial a}{\partial \varrho w} &= \frac{a}{2\Gamma}\frac{\partial \Gamma}{\partial \varrho w} + \frac{\Gamma}{2\varrho a}\frac{\partial p}{\partial \varrho w} \; , \\
\frac{\partial a}{\partial \varrho e_o} &= \frac{a}{2\Gamma}\frac{\partial \Gamma}{\partial \varrho e_o} + \frac{\Gamma}{2\varrho a}\frac{\partial p}{\partial \varrho e_o} \; .
\end{aligned} \tag{C.29}$$

6. SPLIT FLUX JACOBIAN MATRIX

The split flux Jacobian can be constructed by summing up the contributions already presented. The components of the split flux Jacobian matrix $\overline{A}^{\pm}$ are given below, where the following relations are used

$$I_1 = \hat{i}_1^{(\pm)} \ , \tag{C.30}$$

$$I_2 = \hat{i}_4^{(\pm)} - \hat{i}_5^{(\pm)} \ , \tag{C.31}$$

$$I_3 = \hat{i}_4^{(\pm)} + \hat{i}_5^{(\pm)} \ , \tag{C.32}$$

$$I_4 = \hat{i}_1^{(\pm)} - \frac{1}{2}\left(\hat{i}_4^{(\pm)} + \hat{i}_5^{(\pm)}\right) \ . \tag{C.33}$$

The components of the first row are

$$\bar{a}_{11} = \tilde{k}_t I_1 - \frac{\tilde{k}_t}{\Gamma} I_4 + \frac{a}{4\Gamma} I_2 + C_{1A}\frac{\partial p}{\partial \varrho} + C_{1B}\frac{\partial \Gamma}{\partial \varrho} \ ,$$

$$\bar{a}_{12} = \tilde{k}_x I_1 - \frac{\tilde{k}_x}{\Gamma} I_4 + C_{1A}\frac{\partial p}{\partial \varrho u} + C_{1B}\frac{\partial \Gamma}{\partial \varrho u} \ ,$$

$$\bar{a}_{13} = \tilde{k}_y I_1 - \frac{\tilde{k}_y}{\Gamma} I_4 + C_{1A}\frac{\partial p}{\partial \varrho v} + C_{1B}\frac{\partial \Gamma}{\partial \varrho v} \ ,$$

$$\bar{a}_{14} = \tilde{k}_z I_1 - \frac{\tilde{k}_z}{\Gamma} I_4 + C_{1A}\frac{\partial p}{\partial \varrho w} + C_{1B}\frac{\partial \Gamma}{\partial \varrho w} \ ,$$

$$\bar{a}_{11} = \tilde{k}_t I_1 - \frac{\tilde{k}_t}{\Gamma} I_4 + \frac{a}{4\Gamma} I_2 + C_{1A}\frac{\partial p}{\partial \varrho} + C_{1B}\frac{\partial \Gamma}{\partial \varrho} \ ,$$

$$\bar{a}_{12} = \tilde{k}_x I_1 - \frac{\tilde{k}_x}{\Gamma} I_4 + C_{1A}\frac{\partial p}{\partial \varrho u} + C_{1B}\frac{\partial \Gamma}{\partial \varrho u} \ ,$$

$$\bar{a}_{13} = \tilde{k}_y I_1 - \frac{\tilde{k}_y}{\Gamma} I_4 + C_{1A}\frac{\partial p}{\partial \varrho v} + C_{1B}\frac{\partial \Gamma}{\partial \varrho v} \ ,$$

$$\bar{a}_{14} = \tilde{k}_z I_1 - \frac{\tilde{k}_z}{\Gamma} I_4 + C_{1A}\frac{\partial p}{\partial \varrho w} + C_{1B}\frac{\partial \Gamma}{\partial \varrho w} \ ,$$

$$\bar{a}_{15} = C_{1A}\frac{\partial p}{\partial \varrho e_o} + C_{1B}\frac{\partial \Gamma}{\partial \varrho e_o} \ , \tag{C.34}$$

where

$$C_{1A} = \frac{1}{4a} I_2 \ , \tag{C.35}$$

$$C_{1B} = \frac{\varrho}{\Gamma^2}\left[\tilde{\beta}_k I_4 - \frac{a}{4} I_2\right] . \tag{C.36}$$

The components of the second row are

$$\begin{aligned}
\bar{a}_{21} &= -\, u\tilde{\theta}_k I_1 - \frac{u\tilde{\theta}_k}{\Gamma} I_4 - \frac{a}{4\Gamma}(u + \tilde{k}_x\tilde{\beta}_k) I_2 + \frac{a}{2\Gamma}\tilde{k}_x\tilde{k}_t I_2 + C_{2A}\frac{\partial p}{\partial \varrho} + C_{2B}\frac{\partial \Gamma}{\partial \varrho} , \\
\bar{a}_{22} &= (u\tilde{k}_x + \tilde{\beta}_k) I_1 - \frac{u\tilde{k}_x + \tilde{\beta}_k}{\Gamma} I_4 + \frac{a}{2\Gamma}(1 + \tilde{k}_x{}^2) I_2 + C_{2A}\frac{\partial p}{\partial \varrho u} + C_{2B}\frac{\partial \Gamma}{\partial \varrho u} , \\
\bar{a}_{23} &= u\tilde{k}_y I_1 - \frac{u\tilde{k}_y}{\Gamma} I_4 + \frac{a\tilde{k}_x\tilde{k}_y}{2\Gamma} I_2 + C_{2A}\frac{\partial p}{\partial \varrho v} + C_{2B}\frac{\partial \Gamma}{\partial \varrho v} , \\
\bar{a}_{24} &= u\tilde{k}_z I_1 - \frac{u\tilde{k}_z}{\Gamma} I_4 + \frac{a\tilde{k}_x\tilde{k}_z}{2\Gamma} I_2 + C_{2A}\frac{\partial p}{\partial \varrho w} + C_{2B}\frac{\partial \Gamma}{\partial \varrho w} , \\
\bar{a}_{25} &= C_{2A}\frac{\partial p}{\partial \varrho e_o} + C_{2B}\frac{\partial \Gamma}{\partial \varrho e_o} ,
\end{aligned} \tag{C.37}$$

where

$$C_{2A} = \frac{1}{4a}\left[\, (u + \tilde{k}_x\tilde{\beta}_k) I_3 + 2a\tilde{k}_x I_2\right] , \tag{C.38}$$

$$C_{2B} = \frac{\varrho}{\Gamma^2}\left[u\tilde{\beta}_k I_4 - \frac{a}{4}(u + \tilde{k}_x\tilde{\beta}_k) I_2\right] . \tag{C.39}$$

The components of the third row are

$$\begin{aligned}
\bar{a}_{31} &= -\, v\tilde{\theta}_k I_1 - \frac{v\tilde{\theta}_k}{\Gamma} I_4 - \frac{a}{4\Gamma}(v + \tilde{k}_y\tilde{\beta}_k) I_2 + \frac{a}{2\Gamma}\tilde{k}_y\tilde{k}_t I_2 + C_{3A}\frac{\partial p}{\partial \varrho} + C_{3B}\frac{\partial \Gamma}{\partial \varrho} , \\
\bar{a}_{32} &= v\tilde{k}_x I_1 - \frac{v\tilde{k}_x}{\Gamma} I_4 + \frac{a\tilde{k}_x\tilde{k}_y}{2\Gamma} I_2 + C_{3A}\frac{\partial p}{\partial \varrho u} + C_{3B}\frac{\partial \Gamma}{\partial \varrho u} , \\
\bar{a}_{33} &= (v\tilde{k}_y + \tilde{\beta}_k) I_1 - \frac{v\tilde{k}_y + \tilde{\beta}_k}{\Gamma} I_4 + \frac{a}{2\Gamma}(1 + \tilde{k}_y{}^2) I_2 + C_{3A}\frac{\partial p}{\partial \varrho v} + C_{3B}\frac{\partial \Gamma}{\partial \varrho v} , \\
\bar{a}_{34} &= v\tilde{k}_z I_1 - \frac{v\tilde{k}_z}{\Gamma} I_4 + \frac{a\tilde{k}_y\tilde{k}_z}{2\Gamma} I_2 + C_{3A}\frac{\partial p}{\partial \varrho w} + C_{3B}\frac{\partial \Gamma}{\partial \varrho w} , \\
\bar{a}_{35} &= C_{3A}\frac{\partial p}{\partial \varrho e_o} + C_{3B}\frac{\partial \Gamma}{\partial \varrho e_o} ,
\end{aligned} \tag{C.40}$$

where

$$C_{3A} = \frac{1}{4a}\left[\, (v + \tilde{k}_y\tilde{\beta}_k) I_3 + 2a\tilde{k}_y I_2\right] , \tag{C.41}$$

$$C_{3B} = \frac{\varrho}{\Gamma^2}\left[v\tilde{\beta}_k I_4 - \frac{a}{4}(v + \tilde{k}_y\tilde{\beta}_k) I_2\right] . \tag{C.42}$$

The components of the fourth row are

$$\begin{aligned}
\bar{a}_{41} &= -\,w\tilde{\theta}_k I_1 - \frac{w\tilde{\theta}_k}{\Gamma} I_4 - \frac{a}{4\Gamma}(w + \tilde{k}_z\tilde{\beta}_k) I_2 + \frac{a}{2\Gamma}\tilde{k}_z\tilde{k}_t I_2 + C_{4A}\frac{\partial p}{\partial \varrho} + C_{4B}\frac{\partial \Gamma}{\partial \varrho} \;, \\
\bar{a}_{42} &= w\tilde{k}_x I_1 - \frac{w\tilde{k}_x}{\Gamma} I_4 + \frac{a\tilde{k}_x\tilde{k}_z}{2\Gamma} I_2 + C_{4A}\frac{\partial p}{\partial \varrho u} + C_{4B}\frac{\partial \Gamma}{\partial \varrho u} \;, \\
\bar{a}_{43} &= w\tilde{k}_y I_1 - \frac{w\tilde{k}_y}{\Gamma} I_4 + \frac{a\tilde{k}_y\tilde{k}_z}{2\Gamma} I_2 + C_{4A}\frac{\partial p}{\partial \varrho v} + C_{4B}\frac{\partial \Gamma}{\partial \varrho v} \;, \\
\bar{a}_{44} &= (w\tilde{k}_z + \tilde{\beta}_k) I_1 - \frac{w\tilde{k}_z + \tilde{\beta}_k}{\Gamma} I_4 + \frac{a}{2\Gamma}(1 + \tilde{k}_z^{\,2}) I_2 + C_{4A}\frac{\partial p}{\partial \varrho w} + C_{4B}\frac{\partial \Gamma}{\partial \varrho w} \;, \\
\bar{a}_{45} &= C_{4A}\frac{\partial p}{\partial \varrho e_o} + C_{4B}\frac{\partial \Gamma}{\partial \varrho e_o} \;,
\end{aligned} \tag{C.43}$$

where

$$C_{4A} = \frac{1}{4a}\Big[\, (w + \tilde{k}_z\tilde{\beta}_k) I_3 + 2a\tilde{k}_z I_2 \Big] \;, \tag{C.44}$$

$$C_{4B} = \frac{\varrho}{\Gamma^2}\Big[w\tilde{\beta}_k I_4 - \frac{a}{4}(w + \tilde{k}_z\tilde{\beta}_k) I_2 \Big] \;. \tag{C.45}$$

The components of the fifth row are

$$\begin{aligned}
\bar{a}_{51} &= -\,h_o\tilde{\theta}_k I_1 + \frac{\tilde{\theta}_k(h_o + a^2)}{\Gamma} I_4 - \frac{a}{4\Gamma}(h_o + \tilde{\theta}_k\tilde{\beta}_k) I_2 - \frac{a\tilde{\theta}_k^{\,2}}{2\Gamma}\tilde{k}_x\tilde{k}_t I_2 \\
&\qquad - C_{5A}\frac{\partial p}{\partial \varrho} + C_{5B}\frac{\partial \Gamma}{\partial \varrho} \;, \\
\bar{a}_{52} &= h_o\tilde{k}_x I_1 - \frac{\tilde{k}_x(h_o + a^2)}{\Gamma} I_4 + \frac{a\tilde{k}_x}{2\Gamma}(\tilde{\theta}_k + \tilde{\beta}_k) I_2 - C_{5A}\frac{\partial p}{\partial \varrho u} + C_{5B}\frac{\partial \Gamma}{\partial \varrho u} \;, \\
\bar{a}_{53} &= h_o\tilde{k}_y I_1 - \frac{\tilde{k}_y(h_o + a^2)}{\Gamma} I_4 + \frac{a\tilde{k}_y}{2\Gamma}(\tilde{\theta}_k + \tilde{\beta}_k) I_2 - C_{5A}\frac{\partial p}{\partial \varrho v} + C_{5B}\frac{\partial \Gamma}{\partial \varrho v} \;, \\
\bar{a}_{54} &= h_o\tilde{k}_z I_1 - \frac{\tilde{k}_z(h_o + a^2)}{\Gamma} I_4 + \frac{a\tilde{k}_z}{2\Gamma}(\tilde{\theta}_k + \tilde{\beta}_k) I_2 - C_{5A}\frac{\partial p}{\partial \varrho w} + C_{5B}\frac{\partial \Gamma}{\partial \varrho w} \;, \\
\bar{a}_{55} &= \tilde{\beta}_k I_1 - \frac{\tilde{\beta}_k}{\Gamma} I_4 + \frac{a}{2\Gamma} I_2 - C_{5A}\frac{\partial p}{\partial \varrho e_o} + C_{5B}\frac{\partial \Gamma}{\partial \varrho e_o} \;,
\end{aligned} \tag{C.46}$$

where

$$C_{5A} = \frac{\tilde{\beta}_k}{\Gamma} I_4 + \frac{\tilde{\theta}_k}{2} I_3 + \frac{1}{4a}(h_o + \tilde{\theta}_k\tilde{\beta}_k) I_2 + \frac{a}{2\Gamma} I_2 \;, \tag{C.47}$$

$$C_{5B} = \frac{\varrho}{\Gamma^2}\Big[h_o\tilde{\beta}_k I_4 + \frac{a}{2}(h_o + \tilde{\theta}_k\tilde{\beta}_k) I_2 \Big] \;. \tag{C.48}$$

The pressure derivatives appearing in the above formulation are given by Equations (A.22) - (A.26) . In the present work, the “gamma” derivatives are assumed to be zero, since their determination is much involved and would necessitate the use of numerical Jacobians, either fully or in some form of hybrid scheme. The above formulation differs from the perfect gas formulation in the evaluation of the pressure derivatives, the use of the isentropic index Γ as opposed to the ratio of specific heats γ, and the appearance of the “gamma” derivatives. With these considerations in mind, the split flux Jacobian matrix for a gas in chemical equilibrium can be shown to reduce to its prefect gas counterpart.

APPENDIX D
ROE AVERAGED VARIABLES

1. JUMP CONDITIONS

The key step in the development of an approximate Riemann solver is to determine averages of eigenvalues, eigenvectors, and wave strengths such that the jump conditions

$$[\![Q]\!] = \sum_{i=1}^{5} \hat{\sigma}_i \, \hat{r}_i \, , \tag{D.1}$$

and

$$[\![S]\!] = \sum_{i=1}^{5} \hat{\sigma}_i \, \hat{\lambda}_i \, \hat{r}_i \, , \tag{D.2}$$

are satisfied. The averaged eigenvalues read

$$\begin{aligned} \hat{\lambda}_1 &= \hat{\lambda}_2 = \hat{\lambda}_3 = J|\nabla k|\hat{\beta}_k \, , \\ \hat{\lambda}_4 &= J|\nabla k|(\, \hat{\beta}_k + \hat{a} \,) \, , \\ \hat{\lambda}_5 &= J|\nabla k|(\, \hat{\beta}_k - \hat{a} \,) \, , \end{aligned} \tag{D.3}$$

where the directional subscript k has been dropped for clarity. The averaged eigenvectors read

$$\hat{r}_1 = \begin{bmatrix} \hat{\alpha}\tilde{k}_x \\ \hat{\alpha}\hat{u}\tilde{k}_x \\ \hat{\alpha}\hat{v}\tilde{k}_x + \hat{\varrho}\tilde{k}_z \\ \hat{\alpha}\hat{w}\tilde{k}_x - \hat{\varrho}\tilde{k}_y \\ \hat{\alpha}\tilde{k}_x\left(\hat{h}_o - \hat{a}^2/(\hat{\gamma} - 1)\right) + \hat{\varrho}(\hat{v}\tilde{k}_z - \hat{w}\tilde{k}_y) \end{bmatrix} ,$$

$$\hat{r}_2 = \begin{bmatrix} \hat{\alpha}\tilde{k}_y \\ \hat{\alpha}\hat{u}\tilde{k}_y - \hat{\varrho}\tilde{k}_z \\ \hat{\alpha}\hat{v}\tilde{k}_y \\ \hat{\alpha}\hat{w}\tilde{k}_y + \hat{\varrho}\tilde{k}_x \\ \hat{\alpha}\tilde{k}_y\left(\hat{h}_o - \hat{a}^2/(\hat{\gamma} - 1)\right) + \hat{\varrho}(\hat{w}\tilde{k}_x - \hat{u}\tilde{k}_z) \end{bmatrix} ,$$

$$\hat{r}_{4,5} = \hat{\alpha} \begin{bmatrix} 1 \\ \hat{u} \pm \hat{a}\tilde{k}_x \\ \hat{v} \pm \hat{a}\tilde{k}_x \\ \hat{w} \pm \hat{a}\tilde{k}_z \\ \hat{h}_o \pm \hat{a}\hat{\theta}_k \end{bmatrix} , \tag{D.4}$$

and the wave strengths read

$$\hat{\sigma}_1 = \frac{\tilde{k}_x}{\hat{\alpha}}\left(\llbracket \varrho \rrbracket - \frac{\llbracket p \rrbracket}{\hat{a}^2} \right) + \tilde{k}_z \llbracket v \rrbracket - \tilde{k}_y \llbracket w \rrbracket \ ,$$

$$\hat{\sigma}_2 = \frac{\tilde{k}_y}{\hat{\alpha}}\left(\llbracket \varrho \rrbracket - \frac{\llbracket p \rrbracket}{\hat{a}^2} \right) - \tilde{k}_z \llbracket u \rrbracket + \tilde{k}_x \llbracket w \rrbracket \ ,$$

$$\hat{\sigma}_3 = \frac{\tilde{k}_z}{\hat{\alpha}}\left(\llbracket \varrho \rrbracket - \frac{\llbracket p \rrbracket}{\hat{a}^2} \right) + \tilde{k}_y \llbracket u \rrbracket - \tilde{k}_z \llbracket v \rrbracket \ ,$$

$$\hat{\sigma}_{4,5} = \frac{1}{\sqrt{2}}\left(\frac{\llbracket p \rrbracket}{\hat{\varrho}\hat{a}} \pm \llbracket \tilde{\theta}_k \rrbracket \right) \ . \tag{D.5}$$

2. [[Q]] - EQUATIONS

The system given by Equation (D.1) can be written as

$$\llbracket \varrho \rrbracket = \llbracket \varrho \rrbracket \ , \tag{D.6}$$

$$\llbracket \varrho u \rrbracket = \hat{u}\llbracket \varrho \rrbracket + \hat{\varrho}\llbracket u \rrbracket \ , \tag{D.7}$$

$$\llbracket \varrho v \rrbracket = \hat{v}\llbracket \varrho \rrbracket + \hat{\varrho}\llbracket v \rrbracket \ , \tag{D.8}$$

$$\llbracket \varrho w \rrbracket = \hat{w}\llbracket \varrho \rrbracket + \hat{\varrho}\llbracket w \rrbracket \ , \tag{D.9}$$

$$\llbracket \varrho e_o \rrbracket = \frac{\hat{\phi} - \hat{\psi}}{\hat{\gamma} - 1}\llbracket \varrho \rrbracket + \frac{1}{\hat{\gamma} - 1}\llbracket p \rrbracket + \hat{\varrho}(\hat{u}\llbracket u \rrbracket + \hat{v}\llbracket v \rrbracket + \hat{w}\llbracket w \rrbracket) \ . \tag{D.10}$$

3. [[F]] - EQUATIONS

The system given by Equation (D.2) can be written as

$$\llbracket \varrho \tilde{\beta}_k \rrbracket = \hat{\beta}_k \llbracket \varrho \rrbracket + \hat{\varrho}\llbracket \tilde{\theta}_k \rrbracket \ , \tag{D.11}$$

$$\llbracket \varrho u \tilde{\beta}_k + p\tilde{k}_x \rrbracket = \hat{u}\hat{\beta}_k \llbracket \varrho \rrbracket + \hat{\varrho}\hat{\beta}_k \llbracket u \rrbracket + \hat{\varrho}\hat{u}\llbracket \tilde{\theta}_k \rrbracket + \tilde{k}_x \llbracket p \rrbracket \ , \tag{D.12}$$

$$\llbracket \varrho v\tilde{\beta}_k + p\tilde{k}_y \rrbracket = \hat{v}\hat{\beta}_k\llbracket \varrho \rrbracket + \hat{\varrho}\hat{\beta}_k\llbracket v \rrbracket + \hat{\varrho}\hat{v}\llbracket \tilde{\theta}_k \rrbracket + \tilde{k}_y\llbracket p \rrbracket \ , \tag{D.13}$$

$$\llbracket \varrho w\tilde{\beta}_k + p\tilde{k}_z \rrbracket = \hat{w}\hat{\beta}_k\llbracket \varrho \rrbracket + \hat{\varrho}\hat{\beta}_k\llbracket w \rrbracket + \hat{\varrho}\hat{w}\llbracket \tilde{\theta}_k \rrbracket + \tilde{k}_z\llbracket p \rrbracket \ , \tag{D.14}$$

$$\begin{aligned} \llbracket \varrho h_o\tilde{\beta}_k - p\tilde{k}_t \rrbracket = {} & \frac{\hat{\phi} - \hat{\psi}}{\hat{\gamma} - 1}\hat{\beta}_k\llbracket \varrho \rrbracket + \hat{\varrho}\hat{\beta}_k\big(\hat{u}\llbracket u \rrbracket + \hat{v}\llbracket v \rrbracket + \hat{w}\llbracket w \rrbracket\big) \\ & + \frac{\hat{\beta}_k}{\hat{\gamma} - 1}\llbracket p \rrbracket + \tilde{\theta}_k\llbracket p \rrbracket + \hat{\varrho}\frac{\hat{\phi} + \hat{a}^2 - \hat{\psi}}{\hat{\gamma} - 1}\llbracket \tilde{\theta}_k \rrbracket \ . \end{aligned} \tag{D.15}$$

Multiplying each $\llbracket Q \rrbracket$-momentum equation, Equations (D.7) - (D.9), by their corresponding directional metric, as follows

$$\tilde{k}_x\llbracket \varrho u \rrbracket = \hat{u}\tilde{k}_x\llbracket \varrho \rrbracket + \hat{\varrho}\tilde{k}_x\llbracket u \rrbracket \ , \tag{D.16}$$

$$\tilde{k}_y\llbracket \varrho v \rrbracket = \hat{v}\tilde{k}_y\llbracket \varrho \rrbracket + \hat{\varrho}\tilde{k}_y\llbracket v \rrbracket \ , \tag{D.17}$$

$$\tilde{k}_z\llbracket \varrho w \rrbracket = \hat{w}\tilde{k}_z\llbracket \varrho \rrbracket + \hat{\varrho}\tilde{k}_z\llbracket w \rrbracket \ , \tag{D.18}$$

and adding all three equations, the following is obtained

$$\begin{aligned} \llbracket \tilde{k}_x\varrho u \rrbracket + \llbracket \tilde{k}_y\varrho v \rrbracket + \llbracket \tilde{k}_z\varrho w \rrbracket = {} & \big(\hat{u}\tilde{k}_x + \hat{v}\tilde{k}_y + \hat{w}\tilde{k}_z\big)\llbracket \varrho \rrbracket \\ & + \hat{\varrho}\big(\llbracket u\tilde{k}_x + v\tilde{k}_y + w\tilde{k}_z \rrbracket\big) \ . \end{aligned} \tag{D.19}$$

Adding $\llbracket \varrho \rrbracket\tilde{k}_t$ to both sides and regrouping yields

$$\llbracket \varrho\tilde{\beta}_k \rrbracket = \hat{\beta}_k\llbracket \varrho \rrbracket + \hat{\varrho}\llbracket \tilde{\theta}_k \rrbracket \ , \tag{D.20}$$

which is identically Equation (D.11). Following the same procedure for the $\llbracket F \rrbracket$-momentum equations, Equations (D.12) - (D.14), and adding $\llbracket \varrho\tilde{\beta}_k \rrbracket\tilde{k}_t$ to both sides, the result is

$$\llbracket \varrho\tilde{\beta}_k^2 \rrbracket = \hat{\beta}_k^2\llbracket \varrho \rrbracket + 2\hat{\varrho}\hat{\beta}_k\llbracket \tilde{\theta}_k \rrbracket \ . \tag{D.21}$$

However, noting that the jump in the temporal metric is zero, the jump in the relative contravariant velocity can be written as

$$\llbracket \tilde{\beta}_k \rrbracket = \llbracket u\tilde{k}_x + v\tilde{k}_y + w\tilde{k}_z \rrbracket + \llbracket \tilde{k}_t \rrbracket = \llbracket \tilde{\theta}_k \rrbracket \ . \tag{D.22}$$

Now Equations (D.20) and (D.21) can be rewritten as

$$\llbracket \varrho\tilde{\beta}_k \rrbracket = \hat{\beta}_k\llbracket \varrho \rrbracket + \hat{\varrho}\llbracket \tilde{\beta}_k \rrbracket \ , \tag{D.23}$$

$$\llbracket \varrho \tilde{\beta}_k^2 \rrbracket = \hat{\beta}_k^2 \llbracket \varrho \rrbracket + 2\hat{\varrho}\hat{\beta}_k \llbracket \tilde{\beta}_k \rrbracket \ . \tag{D.24}$$

Solving for $\hat{\varrho}$ and $\hat{\beta}_k$, the following averages are obtained

$$\hat{\varrho} = \left\langle \sqrt{\varrho} \right\rangle^2 - \frac{1}{4} \llbracket \sqrt{\varrho} \rrbracket^2 = \sqrt{\varrho_r \, \varrho_l} \ , \tag{D.25}$$

$$\hat{\beta}_k = \frac{\left\langle \tilde{\beta}_k \sqrt{\varrho} \right\rangle}{\left\langle \sqrt{\varrho} \right\rangle} = \frac{(\tilde{\beta}_k)_r \sqrt{\varrho_r} + (\tilde{\beta}_k)_l \sqrt{\varrho_l}}{\sqrt{\varrho_r} + \sqrt{\varrho_l}} \ , \tag{D.26}$$

where the arithmetic average, $< \cdot > = [(\cdot)_r + (\cdot)_l]/2$, has been utilized. Similar to the result for the relative contravariant velocity, the averages for the absolute contravariant velocity and Cartesian velocities are given by

$$\hat{\theta}_k = \mathfrak{R}(\tilde{\theta}_k) \ , \quad \hat{u} = \mathfrak{R}(u) \ , \quad \hat{v} = \mathfrak{R}(v) \ , \quad \hat{w} = \mathfrak{R}(w) \ , \tag{D.27}$$

where $\mathfrak{R}$ denotes the "standard" Roe average

$$\mathfrak{R}(\cdot) = \frac{(\cdot)_r \sqrt{\varrho_r} + (\cdot)_l \sqrt{\varrho_l}}{\sqrt{\varrho_r} + \sqrt{\varrho_l}} \ . \tag{D.28}$$

Looking at the energy equations, Equations (D.10) and (D.15), multiplying the former by $\hat{\beta}_k$, and subtracting the result from the latter, the following is obtained

$$\llbracket \varrho h_o \tilde{\beta}_k - p \tilde{k}_t \rrbracket - \hat{\beta}_k \llbracket \varrho e_o \rrbracket = \tilde{\theta}_k \llbracket p \rrbracket + \hat{\varrho} \frac{\hat{\phi} + \hat{a}^2 - \hat{\psi}}{\hat{\gamma} - 1} \llbracket \tilde{\theta}_k \rrbracket \ . \tag{D.29}$$

Recalling that

$$\hat{\psi} = \hat{a}^2 - (\hat{\gamma} - 1)\hat{h} \ , \tag{D.30}$$

$$\hat{\phi} = \frac{\hat{\gamma} - 1}{2}\left(\hat{u}^2 + \hat{v}^2 + \hat{w}^2\right) , \tag{D.31}$$

$$\llbracket \tilde{\beta}_k \rrbracket = \llbracket \tilde{\theta}_k \rrbracket \ , \tag{D.32}$$

Equation (D.29) can be rewritten as

$$\llbracket \varrho h_o \tilde{\beta}_k \rrbracket = \hat{\varrho} \hat{h}_o \llbracket \tilde{\beta}_k \rrbracket + \hat{\beta}_k \llbracket \varrho h_o \rrbracket \ . \tag{D.33}$$

Solving the above results in the following average for the total enthalpy $\hat{h}_o$

$$\hat{h}_o = \mathcal{R}(h_o) \ . \tag{D.34}$$

Returning to Equation (D.10), and splitting the total energy into internal and kinetic contributions, results in the following

$$\llbracket \varrho e_o \rrbracket = \frac{\hat{\phi} - \hat{\psi}}{\hat{\gamma} - 1}\llbracket \varrho \rrbracket + \frac{1}{\hat{\gamma} - 1}\llbracket p \rrbracket + \hat{\varrho}\left(\hat{u}\llbracket u \rrbracket + \hat{v}\llbracket v \rrbracket + \hat{w}\llbracket w \rrbracket\right) , \tag{D.35}$$

From Equation (D.24) the following formulas for the Cartesian velocities can be obtained

$$\begin{aligned}
\llbracket \varrho u^2 \rrbracket &= \hat{u}^2\llbracket \varrho \rrbracket + 2\hat{\varrho}\hat{u}\llbracket u \rrbracket \ , \\
\llbracket \varrho v^2 \rrbracket &= \hat{v}^2\llbracket \varrho \rrbracket + 2\hat{\varrho}\hat{v}\llbracket v \rrbracket \ , \\
\llbracket \varrho w^2 \rrbracket &= \hat{w}^2\llbracket \varrho \rrbracket + 2\hat{\varrho}\hat{w}\llbracket w \rrbracket \ .
\end{aligned}$$

Substituting the above relations into Equation (D.35), the following formulation for the internal energy is obtained

$$\llbracket \varrho e \rrbracket = \frac{1}{\hat{\gamma} - 1}\llbracket p \rrbracket - \frac{\hat{\psi}}{\hat{\gamma} - 1}\llbracket \varrho \rrbracket \ , \tag{D.36}$$

In order to obtain all jumps in terms of ϱ and T, the following relations are introduced

$$\llbracket p \rrbracket = \hat{\varrho}\hat{R}\llbracket T \rrbracket + \hat{R}\hat{T}\llbracket \varrho \rrbracket + \hat{\varrho}\hat{T}\sum_{i=1}^{N} R_i \llbracket \frac{\varrho_i}{\varrho} \rrbracket \ , \tag{D.37}$$

$$\llbracket \varrho e \rrbracket = \hat{\varrho}\sum_{i=1}^{N}\widehat{\left(\frac{\varrho_i}{\varrho}\right)}\llbracket e_i \rrbracket + \hat{\varrho}\sum_{i=1}^{N}\hat{e}_i\llbracket \frac{\varrho_i}{\varrho} \rrbracket + \sum_{i=1}^{N}\widehat{\left(\frac{\varrho_i}{\varrho}\right)}e_i\llbracket \varrho \rrbracket \ . \tag{D.38}$$

In the above, averages for mixture gas constant, temperature, species internal energy and species mass fraction are given by the "standard" Roe formulas, as follows

$$\hat{R} = \mathcal{R}(\tilde{R}) \ , \quad \hat{T} = \mathcal{R}(T) \ , \quad \hat{e}_i = \mathcal{R}(e_i) \ , \quad \hat{Y}_i = \mathcal{R}(Y_i) \ . \tag{D.39}$$

The jump in species internal energy can be written as

$$\llbracket e_i \rrbracket = \bar{c}_{v_i}\llbracket T \rrbracket \ , \tag{D.40}$$

where $\bar{c}_{v_i}$ is an integral average

$$\bar{c}_{v_i} = \frac{1}{\llbracket T \rrbracket}\int_{T_l}^{T_r} c_{v_i}(\tau)d\tau \ . \tag{D.41}$$

The jump in the species mass fractions can be obtained as

$$\llbracket \frac{\varrho_i}{\varrho} \rrbracket = \int_l^r \left(\frac{\partial Y_i}{\partial \varrho}\right) d\varrho + \int_l^r \left(\frac{\partial Y_i}{\partial T}\right) dT \,, \tag{D.42}$$

and rewritten using integral averages as follows

$$\llbracket \frac{\varrho_i}{\varrho} \rrbracket = \left(\frac{\overline{\partial Y_i}}{\partial \varrho}\right) \llbracket \varrho \rrbracket + \left(\frac{\overline{\partial Y_i}}{\partial T}\right) \llbracket T \rrbracket \,. \tag{D.43}$$

Vinokur [Reference 7] developed a procedure that would identically satisfy Equation (D.43). However, this procedure is complicated and numerically expensive. The simplest approximation for the integral averages is the trapezoidal rule, i.e.

$$\left(\frac{\overline{\partial Y_i}}{\partial \varrho}\right) \llbracket \varrho \rrbracket = \frac{1}{2} \left[\left(\frac{\partial Y_i}{\partial \varrho}\right)_r + \left(\frac{\partial Y_i}{\partial \varrho}\right)_l \right] (\varrho_r - \varrho_l) \,. \tag{D.44}$$

which is the choice adopted in this work. Substituting Equations (D.37) – (D.43) into Equation (D.36) and combining terms, results in the following

$$\begin{aligned} &\left\{ \hat{\varrho} \sum_{i=1}^{N} \left(\widehat{\frac{\varrho_i}{\varrho}}\right) \bar{c}_{v_i} + \hat{\varrho} \sum_{i=1}^{N} \hat{e}_i \left(\frac{\overline{\partial Y_i}}{\partial T}\right) - \frac{\hat{\varrho}\hat{R}}{\hat{\gamma} - 1} - \frac{\hat{\varrho}\hat{T}}{\hat{\gamma} - 1} \sum_{i=1}^{N} R_i \left(\frac{\overline{\partial Y_i}}{\partial T}\right) \right\} \llbracket T \rrbracket \\ &+ \left\{ \sum_{i=1}^{N} \left(\widehat{\frac{\varrho_i}{\varrho}}\right) \hat{e}_i + \hat{\varrho} \sum_{i=1}^{N} \hat{e}_i \left(\frac{\overline{\partial Y_i}}{\partial \varrho}\right) + \frac{\hat{\psi} - \hat{R}\hat{T}}{\hat{\gamma} - 1} - \frac{\hat{\varrho}\hat{T}}{\hat{\gamma} - 1} \sum_{i=1}^{N} R_i \left(\frac{\overline{\partial Y_i}}{\partial \varrho}\right) \right\} \llbracket \varrho \rrbracket \\ &= 0 \,. \end{aligned} \tag{D.45}$$

In order for Equation (D.45) to be satisfied, both coefficients, denoted by { }, must be identically zero, thus giving the following two equations

$$\hat{\varrho} \sum_{i=1}^{N} \left(\widehat{\frac{\varrho_i}{\varrho}}\right) \bar{c}_{v_i} + \hat{\varrho} \sum_{i=1}^{N} \hat{e}_i \left(\frac{\overline{\partial Y_i}}{\partial T}\right) - \frac{\hat{\varrho}\hat{R}}{\hat{\gamma} - 1} - \frac{\hat{\varrho}\hat{T}}{\hat{\gamma} - 1} \sum_{i=1}^{N} R_i \left(\frac{\overline{\partial Y_i}}{\partial T}\right) = 0 \,, \tag{D.46}$$

$$\sum_{i=1}^{N} \left(\widehat{\frac{\varrho_i}{\varrho}}\right) \hat{e}_i + \hat{\varrho} \sum_{i=1}^{N} \hat{e}_i \left(\frac{\overline{\partial Y_i}}{\partial \varrho}\right) + \frac{\hat{\psi} - \hat{R}\hat{T}}{\hat{\gamma} - 1} - \frac{\hat{\varrho}\hat{T}}{\hat{\gamma} - 1} \sum_{i=1}^{N} R_i \left(\frac{\overline{\partial Y_i}}{\partial \varrho}\right) = 0 \,. \tag{D.47}$$

Solving Equation (D.46) results in the average for the ratio of enthalpy and internal energy derivatives, as follows

$$\hat{\gamma} = 1 + \frac{\hat{R} + \hat{\varrho}\hat{T}\sum_{i=1}^{N} R_i\left(\frac{\overline{\partial Y_i}}{\partial T}\right)}{\hat{c}_v + \sum_{i=1}^{N} \hat{e}_i\left(\frac{\overline{\partial Y_i}}{\partial T}\right)} , \tag{D.48}$$

where

$$\hat{c}_v = \sum_{i=1}^{N}\left(\frac{\hat{\varrho}_i}{\hat{\varrho}}\right)\bar{c}_{v_i} . \tag{D.49}$$

Equation (D.47) can be solved for $\hat{\psi}$, as follows

$$\hat{\psi} = \hat{\Gamma}\hat{R}\hat{T} + (\hat{\gamma} - 1)\left[\sum_{i=1}^{N}\left(\frac{\hat{\varrho}_i}{\hat{\varrho}}\right)\hat{e}_i + \hat{R}\hat{T}\right] , \tag{D.50}$$

where the average for the isentropic index is taken to have the same form as given in Equation (A.16), as follows

$$\hat{\Gamma} = \hat{\gamma} + \frac{\hat{\varrho}}{\hat{R}\hat{T}}\sum_{i=1}^{N}\left(\frac{\overline{\partial Y_i}}{\partial \varrho}\right)\left[R_i\hat{T} - (\hat{\gamma} - 1)\hat{e}_i\right] = 0 . \tag{D.51}$$

Substituting Equation (D.50) into Equation (D.30) results in the following average for the speed of sound

$$\hat{a}^2 = \hat{\Gamma}\hat{R}\hat{T} + (\hat{\gamma} - 1)\left[\hat{h}_o - \frac{\hat{q}^2}{2} - \sum_{i=1}^{N}\hat{Y}_i\hat{e}_i - \hat{R}\hat{T}\right] , \tag{D.52}$$

which can be rearranged in the form

$$\hat{a}^2 = (\hat{\gamma} - 1)\left[\hat{h}_o - \frac{\hat{q}^2}{2}\right] + \left\{(\hat{\Gamma} - \hat{\gamma} + 1)\hat{R}\hat{T} - (\hat{\gamma} - 1)\sum_{i=1}^{N}\hat{Y}_i\hat{e}_i\right\} , \tag{D.53}$$

where $\hat{q}^2 = \hat{u}^2 + \hat{v}^2 + \hat{w}^2$. For a perfect gas, where $\hat{\Gamma} = \hat{\gamma} = \gamma$, the averages for the Cartesian velocity components and total enthalpy are the same, and

$$\sum_{i=1}^{N}\hat{Y}_i\hat{e}_i = \frac{R}{\gamma - 1}\hat{T} . \tag{D.54}$$

Consequently, the term in braces in Equation (D.53) will be identically zero, and the relation for the averaged speed of sound will reduce to

$$\hat{a}^2 = (\gamma - 1)\left[\hat{h}_o - \frac{\hat{q}^2}{2}\right] , \qquad \text{(D.55)}$$

which is the original formula developed by Roe [Reference 34].

APPENDIX E
DISCRETIZED VISCOUS JACOBIANS

1. DISCRETIZATION OF VISCOUS JACOBIANS

The following are the components of the discretized viscous Jacobian matrix, taken at cell face l + 1/2

$$\left(\bar{s}_v^{\pm}\right)_{11} = \left(\bar{s}_v^{\pm}\right)_{12} = \left(\bar{s}_v^{\pm}\right)_{13} = \left(\bar{s}_v^{\pm}\right)_{14} = \left(\bar{s}_v^{\pm}\right)_{15} = 0 \,, \tag{E.1}$$

$$\left(\bar{s}_v^{\pm}\right)_{21} = \pm\, |\Delta k| \left\{ (\mu)_{l+\frac{1}{2}} \left(\frac{u}{\varrho}\right)_{l\pm} + \left[\frac{\mu}{3}\tilde{k}_x\tilde{\theta}_k\right]_{l+\frac{1}{2}} \left(\frac{1}{\varrho}\right)_{l\pm} \right\} - \frac{1}{2}|\Delta k| \left[\frac{\mu}{3}\tilde{k}_x V^*\right]_{l+\frac{1}{2}} \left(\frac{1}{\varrho}\right)_{l\pm} ,$$

$$\left(\bar{s}_v^{\pm}\right)_{22} = \mp\, |\Delta k| \left\{ \left[\mu + \frac{\mu}{3}\tilde{k}_x^{\,2}\right]_{l+\frac{1}{2}} \left(\frac{1}{\varrho}\right)_{l\pm} \right\} ,$$

$$\left(\bar{s}_v^{\pm}\right)_{23} = \mp\, |\Delta k| \left\{ \left[\frac{\mu}{3}\tilde{k}_x\tilde{k}_y\right]_{l+\frac{1}{2}} \left(\frac{1}{\varrho}\right)_{l\pm} \right\} ,$$

$$\left(\bar{s}_v^{\pm}\right)_{24} = \mp\, |\Delta k| \left\{ \left[\frac{\mu}{3}\tilde{k}_x\tilde{k}_z\right]_{l+\frac{1}{2}} \left(\frac{1}{\varrho}\right)_{l\pm} \right\} ,$$

$$\left(\bar{s}_v^{\pm}\right)_{25} = 0 \,, \tag{E.2}$$

$$\left(\bar{s}_v^{\pm}\right)_{31} = \pm\, |\Delta k| \left\{ (\mu)_{l+\frac{1}{2}} \left(\frac{v}{\varrho}\right)_{l\pm} + \left[\frac{\mu}{3}\tilde{k}_y\tilde{\theta}_k\right]_{l+\frac{1}{2}} \left(\frac{1}{\varrho}\right)_{l\pm} \right\} - \frac{1}{2}|\Delta k| \left[\frac{\mu}{3}\tilde{k}_y V^*\right]_{l+\frac{1}{2}} \left(\frac{1}{\varrho}\right)_{l\pm} ,$$

$$\left(\bar{s}_v^{\pm}\right)_{32} = \mp\, |\Delta k| \left\{ \left[\frac{\mu}{3}\tilde{k}_x\tilde{k}_y\right]_{l+\frac{1}{2}} \left(\frac{1}{\varrho}\right)_{l\pm} \right\} ,$$

$$\left(\bar{s}_v^{\pm}\right)_{33} = \mp\, |\Delta k| \left\{ \left[\mu + \frac{\mu}{3}\tilde{k}_y^{\,2}\right]_{l+\frac{1}{2}} \left(\frac{1}{\varrho}\right)_{l\pm} \right\} ,$$

$$\left(\bar{s}_v^{\pm}\right)_{34} = \mp\, |\Delta k| \left\{ \left[\frac{\mu}{3}\tilde{k}_y\tilde{k}_z\right]_{l+\frac{1}{2}} \left(\frac{1}{\varrho}\right)_{l\pm} \right\} ,$$

$$\left(\bar{s}_v^{\pm}\right)_{35} = 0\ , \tag{E.3}$$

$$\left(\bar{s}_v^{\pm}\right)_{41} = \pm\ |\Delta k| \left\{ (\mu)_{l+\frac{1}{2}} \left(\frac{w}{\varrho}\right)_{l^\pm} + \left[\frac{\mu}{3}\tilde{k}_z\tilde{\theta}_k\right]_{l+\frac{1}{2}} \left(\frac{1}{\varrho}\right)_{l^\pm} \right\}$$

$$- \frac{1}{2}|\Delta k| \left[\frac{\mu}{3}\tilde{k}_z V^*\right]_{l+\frac{1}{2}} \left(\frac{1}{\varrho}\right)_{l^\pm}\ ,$$

$$\left(\bar{s}_v^{\pm}\right)_{42} = \mp\ |\Delta k| \left\{ \left[\frac{\mu}{3}\tilde{k}_x\tilde{k}_z\right]_{l+\frac{1}{2}} \left(\frac{1}{\varrho}\right)_{l^\pm} \right\}\ ,$$

$$\left(\bar{s}_v^{\pm}\right)_{43} = \mp\ |\Delta k| \left\{ \left[\frac{\mu}{3}\tilde{k}_y\tilde{k}_z\right]_{l+\frac{1}{2}} \left(\frac{1}{\varrho}\right)_{l^\pm} \right\}\ ,$$

$$\left(\bar{s}_v^{\pm}\right)_{44} = \mp\ |\Delta k| \left\{ \left[\mu + \frac{\mu}{3}\tilde{k}_z^{\ 2}\right]_{l+\frac{1}{2}} \left(\frac{1}{\varrho}\right)_{l^\pm} \right\}\ ,$$

$$\left(\bar{s}_v^{\pm}\right)_{45} = 0\ , \tag{E.4}$$

$$\left(\bar{s}_v^{\pm}\right)_{51} = \mp\ |\Delta k| \left\{ (\mathcal{K})_{l+\frac{1}{2}} \left(\frac{\partial T}{\partial \varrho}\right)_{l^\pm} - (\mu)_{l+\frac{1}{2}} \left(\frac{q^2}{\varrho}\right)_{l^\pm} - \left[\frac{\mu}{3}\tilde{\theta}_k\right]_{l+\frac{1}{2}} \left(\frac{\tilde{\theta}_k}{\varrho}\right)_{l^\pm} \right\}$$

$$- |\Delta k| \left[\frac{\mu}{3} V^*\right]_{l+\frac{1}{2}} \left(\frac{\tilde{\theta}_k}{\varrho}\right)_{l^\pm}\ ,$$

$$\left(\bar{s}_v^{\pm}\right)_{52} = \mp\ |\Delta k| \left\{ (\mathcal{K})_{l+\frac{1}{2}} \left(\frac{\partial T}{\partial \varrho u}\right)_{l^\pm} + (\mu)_{l+\frac{1}{2}} \left(\frac{u}{\varrho}\right)_{l^\pm} + \left[\frac{\mu}{3}\tilde{k}_x\tilde{\theta}_k\right]_{l+\frac{1}{2}} \left(\frac{1}{\varrho}\right)_{l^\pm} \right\}$$

$$+ \frac{1}{2}|\Delta k| \left[\frac{\mu}{3}\tilde{k}_x V^*\right]_{l+\frac{1}{2}} \left(\frac{1}{\varrho}\right)_{l^\pm}\ ,$$

$$\left(\bar{s}_v^{\pm}\right)_{53} = \mp\ |\Delta k| \left\{ (\mathcal{K})_{l+\frac{1}{2}} \left(\frac{\partial T}{\partial \varrho v}\right)_{l^\pm} + (\mu)_{l+\frac{1}{2}} \left(\frac{v}{\varrho}\right)_{l^\pm} + \left[\frac{\mu}{3}\tilde{k}_y\tilde{\theta}_k\right]_{l+\frac{1}{2}} \left(\frac{1}{\varrho}\right)_{l^\pm} \right\}$$

$$+ \frac{1}{2}|\Delta k| \left[\frac{\mu}{3}\tilde{k}_y V^*\right]_{l+\frac{1}{2}} \left(\frac{1}{\varrho}\right)_{l^\pm}\ ,$$

$$\left(\bar{s}_v^{\pm}\right)_{54} = \mp\ |\Delta k| \left\{ (\mathcal{K})_{l+\frac{1}{2}} \left(\frac{\partial T}{\partial \varrho w}\right)_{l\pm} + (\mu)_{l+\frac{1}{2}} \left(\frac{w}{\varrho}\right)_{l\pm} + \left[\frac{\mu}{3}\tilde{k}_z \tilde{\theta}_k\right]_{l+\frac{1}{2}} \left(\frac{1}{\varrho}\right)_{l\pm} \right\}$$

$$+ \frac{1}{2}|\Delta k| \left[\frac{\mu}{3}\tilde{k}_z V^*\right]_{l+\frac{1}{2}} \left(\frac{1}{\varrho}\right)_{l\pm} ,$$

$$\left(\bar{s}_v^{\pm}\right)_{55} = \mp\ |\Delta k| \left\{ (\mathcal{K})_{l+\frac{1}{2}} \left(\frac{\partial T}{\partial \varrho e_o}\right)_{l\pm} \right\} . \qquad \text{(E.5)}$$

In the above,

$$V^* = \tilde{k}_x \frac{\partial u}{\partial k} + \tilde{k}_y \frac{\partial v}{\partial k} + \tilde{k}_z \frac{\partial w}{\partial k} , \qquad \text{(E.6)}$$

$$q^2 = u^2 + v^2 + w^2 , \qquad \text{(E.7)}$$

and

$$(\cdot)_{l+} = (\cdot)_l , \qquad (\cdot)_{l-} = (\cdot)_{l+1} . \qquad \text{(E.8)}$$

The temperature derivatives can be derived in a similar fashion as the pressure derivatives, see Appendix A. The final results read

$$\left(\frac{\partial T}{\partial e}\right)_{\varrho} = \frac{1}{\tilde{c}_v + \sum\limits_{i=1}^{N} e_i \left(\frac{\partial Y_i}{\partial T}\right)} = \frac{1}{c_v} , \qquad \text{(E.9)}$$

$$\left(\frac{\partial T}{\partial \varrho}\right)_e = -\frac{1}{c_v} \sum_{i=1}^{N} e_i \left(\frac{\partial Y_i}{\partial \varrho}\right) , \qquad \text{(E.10)}$$

$$\left(\frac{\partial T}{\partial \varrho}\right) = \left(\frac{\partial T}{\partial \varrho}\right)_e - \left(\frac{\partial T}{\partial e}\right)_{\varrho} \frac{e - \frac{q^2}{2}}{\varrho} = -\frac{1}{c_v}\left[\sum_{i=1}^{N} e_i \left(\frac{\partial Y_i}{\partial \varrho}\right) + \frac{e - \frac{q^2}{2}}{\varrho}\right] , \qquad \text{(E.11)}$$

$$\left(\frac{\partial T}{\partial \varrho u}\right) = -\frac{u}{\varrho}\left(\frac{\partial T}{\partial e}\right)_{\varrho} = -\frac{u}{\varrho c_v} , \qquad \text{(E.12)}$$

$$\left(\frac{\partial T}{\partial \varrho v}\right) = -\frac{v}{\varrho}\left(\frac{\partial T}{\partial e}\right)_{\varrho} = -\frac{v}{\varrho c_v} , \qquad \text{(E.13)}$$

$$\left(\frac{\partial T}{\partial \varrho w}\right) = -\frac{w}{\varrho}\left(\frac{\partial T}{\partial e}\right)_{\varrho} = -\frac{w}{\varrho c_v} , \qquad \text{(E.14)}$$

$$\left(\frac{\partial T}{\partial \varrho e_o}\right) = \frac{1}{\varrho}\left(\frac{\partial T}{\partial e}\right)_{\varrho} = \frac{1}{\varrho c_v} . \qquad \text{(E.15)}$$

REFERENCES

1. G. V. Candler and R. W. MacCormack, "The Computation of Hypersonic Ionized Flows in Chemical and Thermal Nonequilibrium", AIAA Paper No. 88-0511, 1988.

2. R. W. Walters, P. Cinnella, D. C. Slack and D. Halt, "Characteristic-Based Algorithms for Flows in Thermo-Chemical Nonequilibrium", AIAA Journal, Vol. 30, No. 5, pp. 1304-1313, 1992.

3. Y. Liu and M. Vinokur, "Equilibrium Gas Flow Computations. I. Accurate and Efficient Calculation of Equilibrium Gas Properties", AIAA Paper No. 89-1736, 1989.

4. K. Meintjes and A. P. Morgan, "Element Variables and the Solution of Complex Chemical Equilibrium Problems", Combustion Science and Technology, Vol. 68, 1989.

5. M. S. Liou, B. van Leer and J. -S. Shuen, "Splitting of Inviscid Fluxes for Real Gases," NASA TM-100856, 1988.

6. R. Abgrall, "An Extension of Roe's Upwind Scheme to Algebraic Equilibrium Real Gas Models", Computers and Fluids, Vol. 19, No. 2, pp. 171-182, 1991.

7. M. Vinokur, "Flux Jacobian Matrices and Generalized Roe Average for an Equilibrium Real Gas", NASA CR 177512, 1988.

8. P. Glaister, "An Approximate Linearised Riemann Solver for the Euler Equations for Real Gases", Journal of Computational Physics, Vol. 77, pp. 361-383, 1988.

9. B. Grossman and R. W. Walters, "Flux-Split Algorithms for the Multi-Dimensional Euler Equations with Real Gases", Computers and Fluids, Vol. 17, No. 1, pp. 99-112, 1989.

10. P. Cinnella and C. F. Cox, "Robust Algorithms for the Thermo-Chemical Properties of Real Gases", 4th International Symposium on Computational Fluid Dynamics, September 1991.

11. J. A. Désidéri, N. Glinsky, and E. Hettena, "Hypersonic Reactive Flow Computations", Computers and Fluids, Vol. 18, No. 2, pp. 151-182, 1990.

12. W. C. Davy, C. K. Lombard and M. J. Green, "Forebody and Base Region Real-Gas Flow in Severe Planetary Entry by a Factored Implicit Numerical Method-Part II: Equilibrium Reactive Gas", AIAA Paper No. 81-0282, 1981.

13. T. Wang and Y. Chen, "A Unified Navier-Stokes Flowfield and Performance Analysis of Liquid Rocket Engines", AIAA Paper No. 90-2494, 1990.

14. W. C. Vincenti and C. H. Kruger, Introduction to Physical Gas Dynamics, Krieger, Florida, 1986.

15. B. J. McBride, S. Heimel, J. G. Ehlers, and S. Gordon, "Thermodynamic Properties to 6000 K for 210 Substances Involving the First 18 Elements", NASA SP-3001, 1963.

16. D. D. Esch, A. Siripong, R. W. Pike, "Thermodynamic Properties in Polynomial Form for Carbon, Hydrogen, Nitrogen, and Oxygen Systems from 300 to 15000 K", NASA RFL-TR-70-3, 1970.

17. R. N. Gupta, J. M. Yos, R. A. Thompson, and K. P. Lee, "A Review of Reaction Rates and Thermodynamic Properties for an 11-Species Air Model for Chemical and Thermal Nonequilibrium Calculations to 30 000 K", NASA RP-1232, 1990.

18. H. W. Lieppman and A. Roshko, Elements of Gasdynamics, Wiley, New York, 1957.

19. M. C. Dunn and S. W. Kang, "Theoretical and Experimental Studies of Reentry Plasmas", NASA CR-2232, 1973.

20. R. C. Rogers and W. Chinitz, "Using a Global Hydrogen-Air Combustion Model in Turbulent Reacting Flow Calculations", AIAA Journal, Vol. 21, No. 4, 1983.

21. I. I. Glass and A. Takano, "Nonequilibrium Expansion Flows of Dissociated Oxygen and Ionized Argon Around a Corner", Progress in Aerospace Sciences, Vol. 6, 1965.

22. D. R. Stull and H. Prophet, (Project Directors), JANAF Thermochemical Tables (Second Edition), National Standard Reference Data System NBS 37, 1971.

23. J. D. Anderson, Jr., Modern Compressible Flow - With Historical Perspective, McGraw-Hill, New York, 1982.

24. J. Hilsenrath, M. Klein and H. W. Wooley, "Tables of Thermodynamic Properties of Air Including Dissociation and Ionization from 1,500 K to 15,000 K", AEDC Technical Report No. TR-59-20, 1959.

25. P. Cinnella and C. F. Cox, "An Efficient 'Black Box' Solver for the Equilibrium Composition of Real Gases", AIAA Paper No. 91-3322, 1991.

26. B. Gatlin, "An Implicit, Upwind Method for Obtaining Symbiotic Solutions to the Thin-Layer Navier-Stokes Equations", Ph.D. Dissertation, Mississippi State University, Mississippi, August 1987.

27. B. Simpson, "Unsteady Three-Dimensional Thin-Layer Navier-Stokes Solutions on Dynamic Blocked Grids", Ph.D. Dissertation, Mississippi State University, Mississippi, December 1988.

28. J. P. Chen, "Unsteady Three-Dimensional Thin-Layer Navier-Stokes Solutions for Turbomachinery in Transonic Flow", Ph.D. Dissertation, Mississippi State University, Mississippi, December 1988.

29. D. A. Anderson, J. C. Tannehill and R. H. Pletcher, Computational Fluid Mechanics and Heat Transfer, Hemisphere Publishing Corp., New York, 1984.

30. R. M. Beam and R. F. Warming, "An Implicit Finite-Difference Algorithm for Hyperbolic Systems in Conservation-Law Form," Journal of Computational Physics, Vol. 22, pp. 87-110, 1976.

31. W. R. Briley and H. McDonald, "On the Structure and Use of Linearized Block Implicit Schemes," Journal of Computational Physics, Vol. 34, pp. 54-73, 1980.

32. J. L. Steger and R. F. Warming, "Flux Vector Splitting of the Inviscid Gasdynamic Equations with Applications to Finite-Difference Methods," Journal of Computational Physics, Vol. 40, 1981.

33. M. Vinokur and J.-L. Montagné, "Generalized Flux-Vector Splitting for an Equilibrium Real Gas," NASA CR 177513, 1988.

34. P. L. Roe, "Approximate Riemann Solvers, Parameter Vectors, and Difference Schemes," Journal of Computational Physics, Vol. 43, 1981.

35. D. M. Belk, "Unsteady Three-Dimensional Euler Equations Solutions on Dynamic Blocked Grids," Ph.D. Dissertation, Mississippi State University, Mississippi, August 1986.

36. B. Van Leer, J. L. Thomas, P. L. Roe, and R. W. Newsome, "A Comparison of Numerical Flux Formulas for the Euler and Navier-Stokes Equations", AIAA Paper No. 87-1104-CP, 1987.

37. D. L. Whitfield and J. M. Janus, "Three-Dimensional Unsteady Euler Equations Solution Using Flux Vector Splitting," AIAA Paper No. 84-1552, 1984.

38. P. L. Roe, "Characteristic-Based Schemes for the Euler Equations", Annual Review of Fluid Mechanics, Vol. 18, pp 337-365, 1986.

39. D. L. Whitfield, J. M. Janus and L. B. Simpson, "Implicit Finite Volume High Resolution Wave-Split Scheme for Solving the Unsteady Three-Dimensional Euler and Navier-Stokes Equations on Stationary or Dynamic Grids", MSSU-EIRS-ASE-88-2, Mississippi State University, 1988.

40. P. Cinnella, "Flux-Split Algorithms for Flows with Non-Equilibrium Chemistry and Thermodynamics", PhD Dissertation, Virginia Polytechnic Institute and State University, Virginia, December 1989.

41. B. S. Baldwin and H. Lomax, "Thin Layer Approximation and Algebraic Model for Separated Turbulent Flows", AIAA Paper No. 78-257, 1978.

42. J. M. Janus, "The Development of a Three-Dimensional Split Flux Vector Euler Solver with Dynamic Grid Applications", Masters Thesis, Mississippi State University, Mississippi, August 1984.

43. D. L. Whitfield, "Newton-Relaxation Schemes for Nonlinear Hyperbolic Systems", MSSU-EIRS-ASE-90-3, Mississippi State University, 1990.

44. J. D. Anderson, Jr., Hypersonic and High Temperature Gas Dynamics, McGraw-Hill, New York, 1989.

45. C. F. Cox and P. Cinnella, "An Approximate Riemann Solver for Arbitrary Real Gas Mixtures", AIAA Paper No. 93-0892, 1993.

DISTRIBUTION
(WL-TR-92-7044)

Defense Technical Info. Center
Attn: DTIC/DDAC
Cameron Station 2
Alexandria VA 22304-6145

AFSAA/SAI
The Pentagon, Rm 1D363 1
Washington DC 20330-5420

AUL/LSE 1
Maxwell AFB AL 36112-5564

Eglin AFB offices:

WL/CA-N 1
WL/MNOI (Scientific and Tech. Info. Facility) 1

HQ USAFE/INATW 1
APO NY 09012-5001

WL/FIES/SURVIAC 1
Wright-Patterson AFB OH 45433-6553

HQ ACC/XP-JSG 1
Langley AFB VA 23665-5000

Eglin AFB offices:

ASC/XRC 1
WL/MNSI 1
WL/MNAG 1
WL/MNM 1
WL/MNAV 1
WL/MNPX 1
WL/MNAA 4
AFDTC/PA 1

Commander 1
U.S. Army Missile Command
Redstone Sci. Info. Center
Attn: AMSMI-RD-CS-R/Documents
Redstone Arsenal AL 35898-5241

Commander 1
Naval Weapons Center (Code 3431)
Attn: Technical Library
China Lake CA 93555-6001

ASC/ENSTA 1
Wright-Patterson AFB OH 45433-6503

ASC/XRH 1
Wright-Patterson AFB OH 45433-6503

Wright-Patterson AFB OH 45433-6553

WL/CA-F 1
WL/FIM 1
WL/FIB 1
WL/FIGX 1
WL/FIGCC 1

WL/TXA . 1
Wright-Patterson AFB OH 45433-6523

AFIA/INT 1
Bolling AFB DC 20332-5000

EOARD/LDV
Box 14 1
FPO NY 09510-0200

NASA Langley Research Center 1
Technical Library - MS 185
Attn: Document Cataloging
Hampton VA 23665-5225